FUEL-EFFICIENT EMISSIONS REDUCTION FROM DIESEL ENGINES VIA ADVANCED GAS-EXCHANGE MANAGEMENT

A Dissertation

Submitted to the Faculty

of

Purdue University

by

Dheeraj Bharadwaj Gosala

In Partial Fulfillment of the

Requirements for the Degree

of

Doctor of Philosophy

December 2018

Purdue University

West Lafayette, Indiana

THE PURDUE UNIVERSITY GRADUATE SCHOOL
STATEMENT OF DISSERTATION APPROVAL

Dr. Gregory Shaver, Chair

School of Mechanical Engineering

Dr. Peter Meckl

School of Mechanical Engineering

Dr. Amy Marconnet

School of Mechanical Engineering

Dr. John Lumkes

School of Agricultural and Biological Engineering

Approved by:

Dr. Jay Gore

Head of the School Graduate Program

Dedicated to my family

for their constant and unwavering support throughout this incredible journey

ACKNOWLEDGMENTS

I could not have asked for anything better from my four years at Purdue. For sure, there have been numerous ups and downs, but I am happy to have enjoyed the journey, and learned a great deal from it. This would not have been possible without the immense help and support from my advisor, colleagues, friends and family.

I would like to extend my heartfelt gratitude and thanks to my advisor Prof. Greg Shaver, who has been a wonderful mentor, teacher, boss and friend. Not only has he helped me learn how to perform effective independent research, but also taught me how best to disseminate my research to make it more relevant to the industry and to the society. The freedom he has consistently extended to work on new (sometimes crazy) ideas has been great motivation for me. I am indebted to him for all the career advice and recommendations, and for the numerous opportunities he has given me to hone my various skills, especially with research presentation, classroom teaching and research mentoring.

I would like to thank Eric Holloway for being an awesome manager, and for keeping our project running like a well-oiled machine. I very much enjoyed working with him, and am grateful to him for helping me learn how to set realistic project targets and goals, and how they can effectively be divided and conquered by a team. Special thanks to David Meyer and Ryan Thayer for helping me work hands-on in the test cell without breaking any million-dollar equipment. It is difficult to imagine the engine and test cell operating so smoothly without their constant support. Shout out to Bob Brown, Frank Lee, Ron Evans and Charlie Baxter for their watchful eye, and for ensuring that we stuck to safe practices in the lab and test cell. I would like to also thank our points of contact at Eaton and Cummins - Jim McCarthy, Dale Stretch, Lisa Farrell, Tim Lutz, Ed Koeberlein and Akash Desai for all the intellectually stimulating discussions during our face-to-face meetings, and for helping

ask the right questions to answer. Special thanks to Jim for sparing his time helping me prepare myself better for life after graduate school, and valuable career advice.

I am fortunate to have extremely motivated and helpful colleagues, who have immensely helped me during my time at Purdue. Thanks to Cody for being a dependable colleague and wonderful friend, and for all the professional advice he gave me. I will miss the intense technical, non-technical and sometimes, nonsensical discussions with Cody and Aswin. A big thanks to them, Soumya and Dave for being very patient in helping me learn the nitty-gritties of the VVA, test cell and the Simulink code, and for keeping a cool mind when things did not always go right in the test cell! It was great working with Mrunal, an ever-reliable engine-run partner with super-contagious enthusiasm! I also greatly enjoyed working with Sharon, Kalen, Alex, Troy, Matt, Hari and Sirish, each of whom I had an opportunity of working with, on at least one major project, and I cannot overstate how much I have learned from each of them. I also enjoyed working with Ife, Jon, John, Vaishnavi, Shveta, Miles, Xing, Ashish, Harsha, Tridib, Sylvia, Lucius and Mayura during my tenure at Purdue.

A big thanks to all my friends at Purdue, who I am very grateful to, for all their help, support and advice. My sincerest thanks to Vasu, Pramod, Yeshaswi, Akash, Chaitu, Neeraj, Amar, Soumya and Mukta for all the help and support and they have extended during the course of my PhD. I would also like to acknowledge all my teammates at AeroAssault and PUCC cricket teams, whom it was great fun to play with, and I share some very valuable memories from all the cricket leagues we played together.

I am very grateful to Vaidehi for being such a strong source of support, for standing by me through thick and thin, and for always helping me bring out my best. My parents Anuradha and Venu Gopal, and brother Nikhil, have constantly been my pillars of strength, and have always motivated me to ‘shoot for the stars’. They have always given me the best they could and helped me in all my decisions, and it is only with their blessings and love that I pursue all my endeavors in life.

TABLE OF CONTENTS

LIST OF TABLES

LIST OF FIGURES

Figure Page

Figure Page

SYMBOLS

m	mass
v	velocity
$\dot{W}_{brake}$	Brake power developed by the engine
$\dot{Q}_{exh}$	Rate of heat transfer to the exhaust stream
$\dot{Q}_{loss}$	Rate of energy loss
T_{brake}	Brake torque produced by the engine
N	Engine speed (RPM)
$\dot{m}_{air}$	Mass flow rate of fresh air entering the engine
$\dot{m}_{fuel}$	Mass flow rate of fuel entering the engine
$\dot{m}_{exh}$	Mass flow rate of exhaust gas leaving from the engine
TOT	Turbine outlet temperature
T_{ref}	Reference temperature, taken as 25°C
T_{cat}	Lumped aftertreatment catalyst temperature
T_{amb}	Ambient air temperature
$C_{p,exh}$	Specific heat constant of exhaust gas
$C_{p,air}$	Specific heat constant of fresh air
LHV_{fuel}	Lower heating value of the fuel (diesel)
V_d	Displaced volume

ABBREVIATIONS

AFR	Air-to-Fuel Ratio
BMEP	Brake Mean Effective Pressure
BSFC	Break Specic Fuel Consumption
BTE	Brake Thermal Efficiency
CAC	Charge Air Cooler
CAD	Crank Angle Degrees
CCE	Closed Cycle Efficiency
CDA	Cylinder Deactivation
DCA	Dynamic Cylinder Activation
DEF	Diesel Exhaust Fluid
DOC	Diesel Oxidation Catalyst
DPF	Diesel Particulate Filter
ECM	Engine Control Module
EEVO	Early Exhaust Valve Opening
EGR	Exhaust Gas Recirculation
EPA	Environmental Protection Agency
EVC	Exhaust Valve Closing
EVL	Exhaust Valve Lift
EVO	Exhaust Valve Opening
FE Baseline	Fuel efficiency based baseline operation
ft-lbs	Foot-pounds (unit of Torque)
FTP	Federal Testing Procedure
GHG	Green House Gases
GIMEP	Gross Indicated Mean Effective Pressure
HC	Hydrocarbon

HD-FTP	Heavy Duty Federal Test Procedure
iEGR	Internal Exhaust Gas Recirculation
IVC	Intake Valve Closing
IVL	Intake Valve Lift
IVO	Intake Valve Opening
LHV	Lower Heating Value
LIVC	Late Intake Valve Closure
ME	Mechanical Efficiency
NIMEP	Net Indicated Mean Effective Pressure
NOx	Oxides of Nitrogen
NVO	Negative Valve Overlap
OCE	Open Cycle Efficiency
PM	Particulate Matter
PMEP	Pumping Mean Effective Pressure
RPM	Revolutions Per Minute
SCR	Selective Catalytic Reduction
TDC	Top Dead Center
TM Baseline	Thermal management based baseline operation
TOT	Turbine Outlet Temperature
UHC	Unburnt Hydrocarbons
VCC	Ventilated Cylinder Cutout
VGT	Variable Geometry Turbine
VVA	Variable Valve Actuation

ABSTRACT

Gosala, Dheeraj B. Ph.D., Purdue University, December 2018. Fuel-Efficient Emissions Reduction from Diesel Engines via Advanced Gas-Exchange Management. Major Professor: Gregory M. Shaver, School of Mechanical Engineering.

Strict emissions regulations are mandated by the environmental protection agency (EPA) to reduce emission of greenhouse gases and criteria air pollutants from diesel engines, which are widely used in commercial vehicles. A ten-fold reduction in allowable heavy-duty on-road oxides of nitrogen (NOx) emissions are projected to be enforced by 2024. The need to meet these emission regulations, along with consumer demand for better fuel efficiency, has resulted in greater effort towards cleaner and more efficient diesel engines.

Diesel engine aftertreatment systems are effective in reducing engine-out emissions, but only at catalyst bed temperatures above 200°C. The aftertreatment system needs to be quickly warmed up to its efficient operating temperatures, and maintain elevated temperatures in a fuel-efficient manner, which is a challenge using conventional engine strategies. This study details the use of advanced gas-exchange management, via variable valve actuation, to improve both 'warm-up' and 'stay-warm' aftertreatment thermal management.

Fast initial warm-up of the aftertreatment system, following a cold engine start, is enabled by strategies such as early exhaust valve opening (EEVO), internal exhaust gas recirculation (iEGR) and late intake valve closure (LIVC). Steady state and drive cycle results of a combination of EEVO and iEGR at idle operation, and a combination of EEVO and LIVC at off-idle conditions below 7.6 bar BMEP, are presented. It is demonstrated that $\sim$ 150°C higher steady state temperatures are achieved at idle, and up to 10.1% reduction in predicted tailpipe-out NOx is achieved at 3.1% fuel penalty over the heavy-duty federal test procedure (HD-FTP) drive cycle.

Fuel-efficient 'stay-warm' aftertreatment thermal management is demonstrated to be effectively achieved via cylinder deactivation (CDA), to reduce fuel consumption, elevate engine-outlet temperatures and reduce exhaust flow rates at idle and low load engine operation. Implementation of CDA at idle and low loads below 3 bar BMEP is demonstrated to achieve fuel savings of 4% over the HD-FTP drive cycle, while maintaining similar levels of tailpipe-out NOx emissions. It is demonstrated that lower airflow during CDA at, and near, idle operation does not compromise the transient torque/power capabilities of the engine- a key finding in enabling the practical implementation of CDA in diesel engines.

Some of the practical challenges expected with CDA are studied in detail, and alternate strategies addressing the challenges are introduced. Dynamic cylinder activation (DCA) is introduced as a means to enable greater control over the torsional vibration characteristics of the engine, via selection of appropriate firing patterns, while maintaining similar performance and emissions as fixed CDA. A generic strategy to use CDA and an appropriate DCA strategy to operate away from driveline resonant frequencies at different engine speeds is described. Ventilated cylinder cutout (VCC) is introduced as a means to potentially mitigate oil accumulation concerns during CDA, by ventilating the non-firing cylinders to the intake/exhaust manifold(s) by opening the intake/exhaust valves during all the four strokes of the engine cycle. The fuel efficiency and thermal management performance of VCC is assessed for different ventilation configurations and compared with CDA and baseline engine operation.

1. INTRODUCTION

1.1 Motivation

Air pollution is a cause of major concern as it poses serious health risks and hazards to humans, and has been identified as the world's largest single environmental health risk by the World Health Organization (WHO) [1]. Particulate matter (PM), oxides of nitrogen (NOx), oxides of sulphur (SOx), carbon monoxide (CO), ground-level ozone and lead have been identified as common toxic pollutants (also known as "criteria air pollutants"), found all over the U.S. with potential to harm human, plant and animal life. The transportation sector is a major contributor to criteria pollutants, being responsible for 56%, 90% and 21% of the global emissions of NOx, PM and SOx, respectively [2].

Besides air pollution, global warming is another major environmental problem today, with the average surface temperature of the earth having increased by 1° C over the last century [3], as shown in Figure 1.1. The increase in temperature has been studied to correlate with the increase in atmospheric greenhouse gas (GHG) emission levels, especially in the post industrial revolution era. CO_2 makes up for 82% of the total GHG inventory, and is predominantly a product of combustion of fossil fuels [4]. The transportation sector accounts for approximately 27% of the global GHG emissions today, with light-, medium- and heavy-duty trucks contributing to 41% of the transportation GHGs, as shown in Figure 1.2. As the CO_2 footprint from the transportation sector directly corresponds to the fuel consumed, there is a major drive to improve the fuel efficiency of vehicles.

In order to reduce/eliminate the emission of criteria air pollutants and greenhouse gases, stringent regulations on CO_2, NOx and PM are enforced on the transportation sector by the Environmental Protection Agency (EPA). Figure 1.3 shows that up to

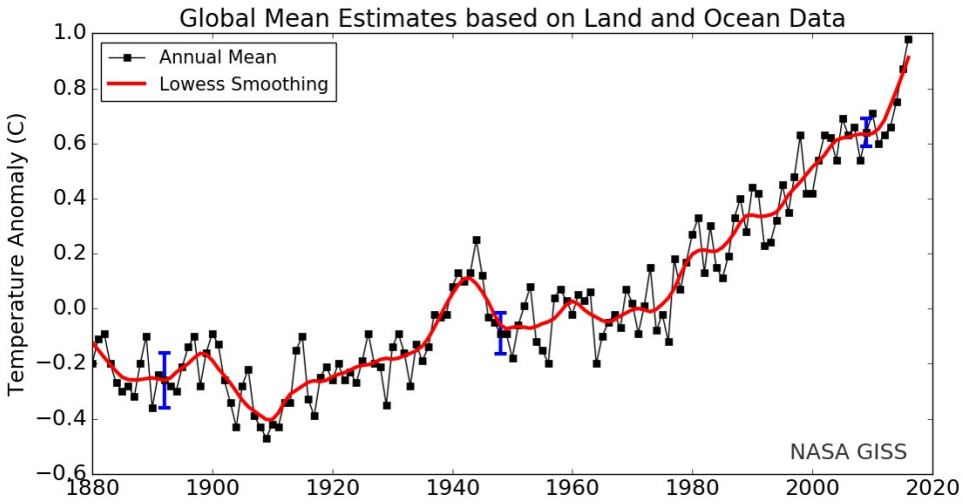

Figure 1.1. Increase in surface temperature of the earth over the last century (adopted from [3]).

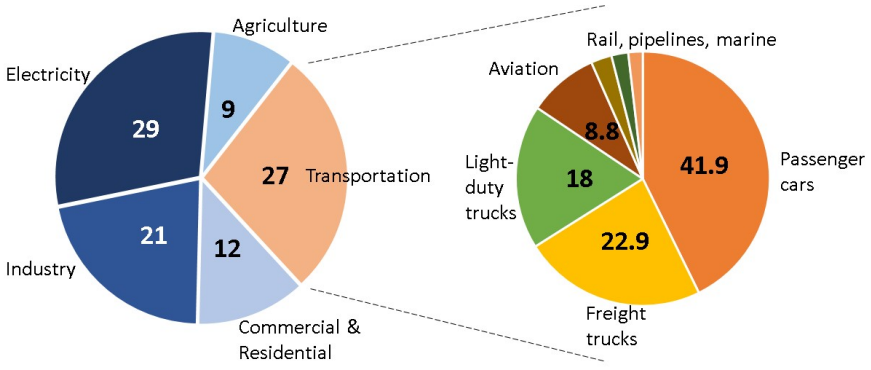

Figure 1.2. Greenhouse gas sources by economic sector, and within transportation sector [4].

40% reductions in CO_2 emissions are sought over the next 15 years from various classes of heavy-duty vehicles [5, 6]. The regulations over PM and NOx are more stringent, with a ten-fold reduction in heavy-duty NOx emissions planned to be enforced around 2024. As shown in Figure 1.4, the ten-fold reduction in NOx is already an optional standard in California.

Engine and truck manufacturing companies are therefore pursuing advanced technologies in diesel engines to meet GHG and air pollutant regulations. Major technologies being pursued in medium- and heavy-duty vehicles to meet emission regulations are shown in Figure 1.5 [7]. The objective of this dissertation is to characterize the GHG and air pollutant-reduction potential of advanced gas exchange strategies in diesel engines.

A reduction in fuel consumption in heavy-duty vehicles is also sought by customers for financial reasons. Fuel and oil contribute to approximately 30% of the total costs for operation of a truck, and is the largest variable [8]. An improvement of 1 mile per gallon over the existing average fuel economy of 6 miles per gallon can bring down the annual operating costs by around $12,000 per truck. Fleet owners and operators are usually very quick to adapt to new engine technologies that show fuel savings potential.

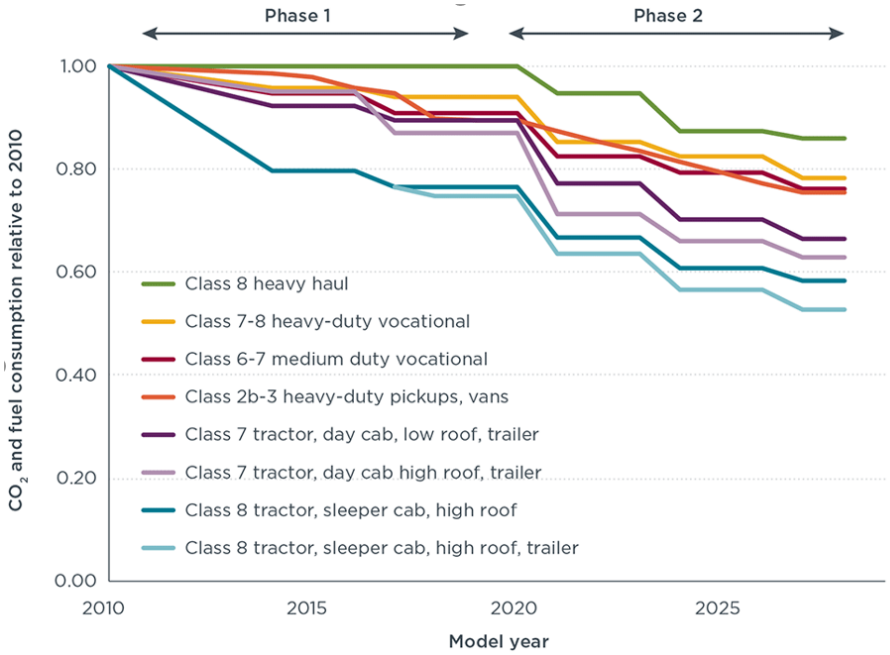

Figure 1.3. Summary of CO_2 and fuel consumption reduction standards in heavy-duty vehicles.

Year	CO	HC[a]	HC[a]+NOx	NO_x	PM	
					General	Urban Bus
1974	40	-	16	-	-	
1979	25	1.5	10	-	-	
1985	15.5	1.3	-	10.7	-	
1987	15.5	1.3	-	10.7[d]	0.60[f]	
1988	15.5	1.3[b]	-	10.7[d]	0.60	
1990	15.5	1.3[b]	-	6.0	0.60	
1991	15.5	1.3[c]	-	5.0	0.25	0.25[g]
1993	15.5	1.3[c]	-	5.0	0.25	0.10
1994	15.5	1.3[c]	-	5.0	0.10	0.07
1996	15.5	1.3[c]	-	5.0[e]	0.10	0.05[h]
1998	15.5	1.3	-	4.0	0.10	0.05[h]
2004[j]	15.5	-	2.4[i]	-	0.10	0.05[h]
2007	15.5	0.14[k]	-	0.20[k]	0.01	
2015	15.5	0.14	-	0.02[l]	0.01	

Figure 1.4. US EPA regulation showing the limits for CO, HC, NOx and PM over the years.

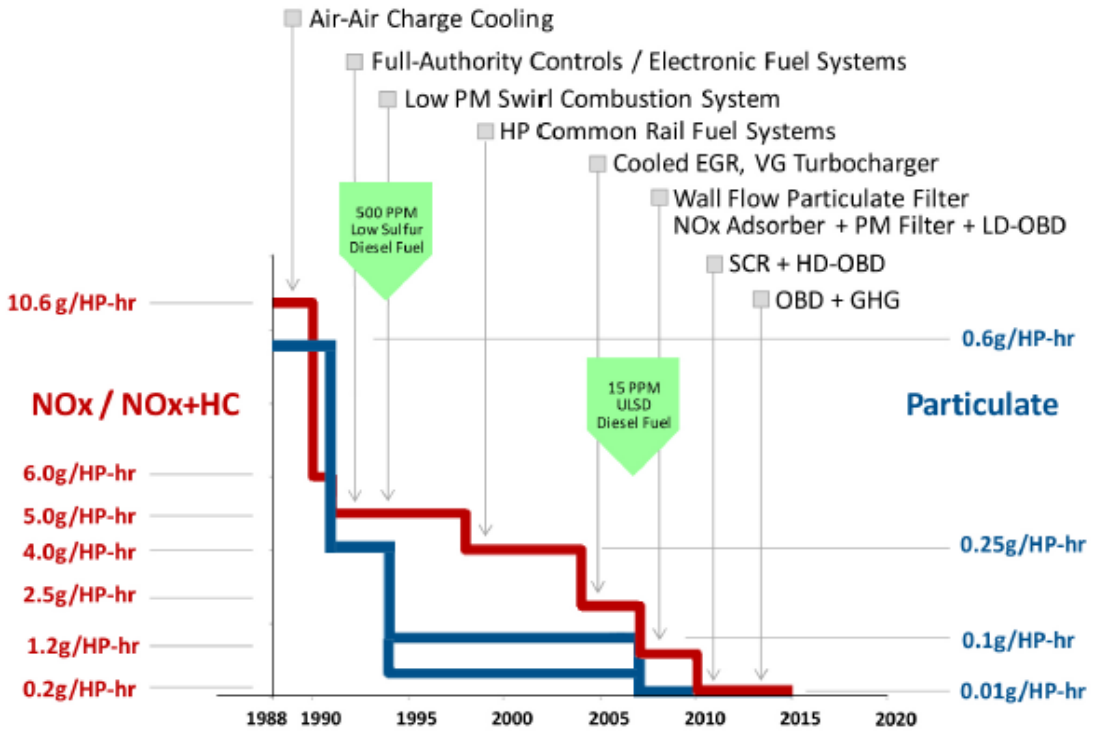

Figure 1.5. Evolution of diesel engine and aftertreatment technologies to meet emissions regulations. [9]

1.2 Literature Review

Diesel engines dominate the medium- and heavy-duty transportation industry due to their higher power and superior fuel efficiency. However, they emit harmful criteria pollutants including oxides of nitrogen (NOx), particulate matter (PM) and unburnt hydrocarbons (UHC). Diesel engines, in order to meet the EPA emissions criteria, therefore use an aftertreatment system to process and reduce engine-out emissions before releasing them into the atmosphere through the vehicle tailpipe.

1.2.1 Aftertreatment Thermal Management

Diesel engine aftertreatment systems typically include a diesel oxidation catalyst (DOC), diesel particulate filter (DPF) and selective catalytic reduction (SCR) system, in that order, as shown in Figure 1.6. The DOC converts UHC emissions to carbon dioxide and water, and 'lights off' at catalyst temperatures of around 200°C [10, 11]. Besides UHC, the DOC also oxidizes NO to NO_2, and CO to CO_2. The exothermic nature of the oxidation reaction typically helps in warm-up of the catalysts downstream of the DOC. The DPF is a filter that traps particulate matter, and requires periodic 'regeneration' to clean the filter, a process by which the accumulated PM is oxidized to CO_2. Temperatures in excess of 500°C are required for 'active' regeneration [12], where the oxygen in the exhaust stream reacts with the carbon in PM to form CO_2. 'Passive' regeneration occurs between 400 and 450°C, where the NO_2 emissions react with carbon in the particulate matter to form NO and CO_2 [13, 14]. The SCR reduces NOx emissions in the exhaust gases to N_2 through a reaction with ammonia, which is injected into the aftertreatment system as Diesel Exhaust Fluid (DEF). The SCR requires temperatures above 250°C for efficient NOx conversion [7, 15–18].

Thermal management of the aftertreatment system is therefore of paramount concern in modern diesel engine systems, as it is desired that the aftertreatment components stay within the desired temperature band during engine operation [20, 21].

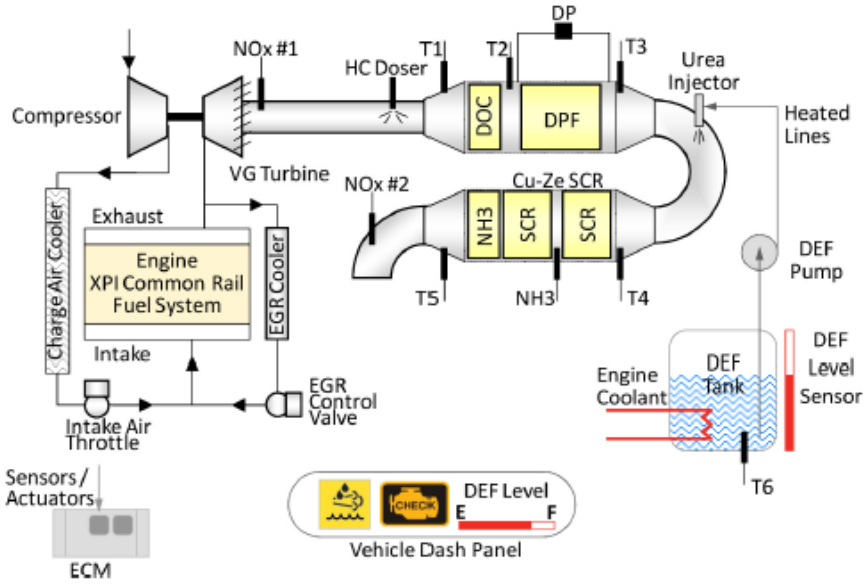

Figure 1.6. Aftertreatment system architecture in 2013 on-highway vehicle applications [9].

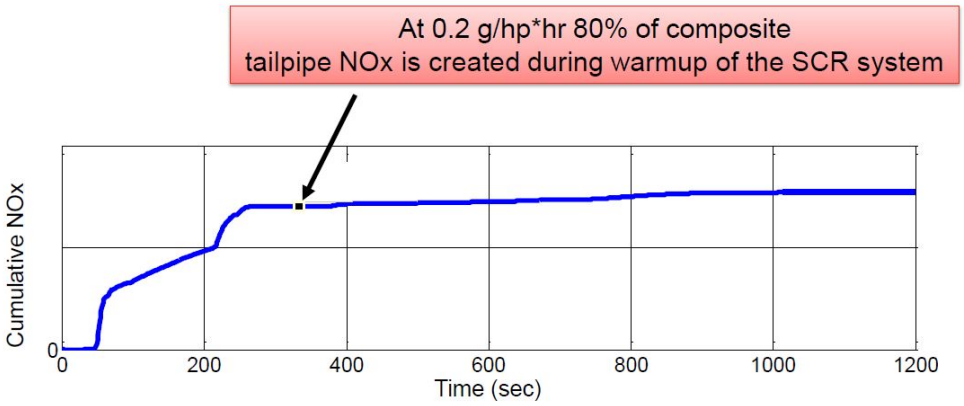

Figure 1.7. Approximately 80% of cumulative tailpipe-out NOx occurs during SCR warm-up (adopted from [19].)

Aftertreatment thermal management is categorized into two phases- the 'warm-up' phase and the 'stay-warm' phase.

The 'warm-up' phase involves bringing the aftertreatment components to their effective operating temperatures when starting from ambient temperatures (cold start). Approximately 80% of the cumulative tailpipe-out NOx emissions over the emissions

certification cycle occur during the initial catalyst warm-up phase while the SCR is below its optimum temperatures [19], as shown in Figure 1.7, and therefore, accelerated catalyst warm-up is desired. High turbine-outlet temperatures and exhaust flow rates are desirable from warm-up strategies. A fuel penalty is expected and perhaps inevitable during this phase, however, as faster aftertreatment warm-up enables the use of more fuel-efficient strategies later in the drive cycle, the initial fuel penalty is acceptable.

'Stay-warm' aftertreatment thermal management follows the aftertreatment warm-up, and aims at maintaining elevated aftertreatment component temperatures with the lowest possible fuel consumption. A significant portion of engine operation occurs at low-load operation where the turbine-outlet temperatures are below 250°C, as shown in Figure 1.8, which results in low SCR conversion efficiency. Stay-warm strategies are generally characterized by high TOT, to maintain elevated aftertreatment temperatures, and low exhaust flow rates to minimize the cool-down of the catalysts when the exhaust gas temperature falls lower than the catalyst bed temperature. Engines used in mid-range and heavy-duty vehicles used in stop and go applications spend a sizable amount of time at low-load conditions, and therefore, fuel savings are highly desirable for stay-warm strategies.

Aftertreatment thermal management strategies can be classified as air path strategies and fuel path strategies [22]. Mayer et al. [23] highlighted the role of excess airflow in reducing engine-outlet gas temperatures at low loads - an undesirable result for thermal management.

Air path strategies achieve higher temperatures by reducing airflow through the engine. Several authors in the research community have demonstrated that airflow reductions via cylinder deactivation (CDA) can result in improved aftertreatment thermal management, in addition to reduction in fuel consumption [24–29]. Garg et al. [28] demonstrated up to 50°C higher engine-outlet temperature via intake valve modulation at 1200 RPM, 2.5 bar BMEP, also via a reduction in airflow. Bouchez and

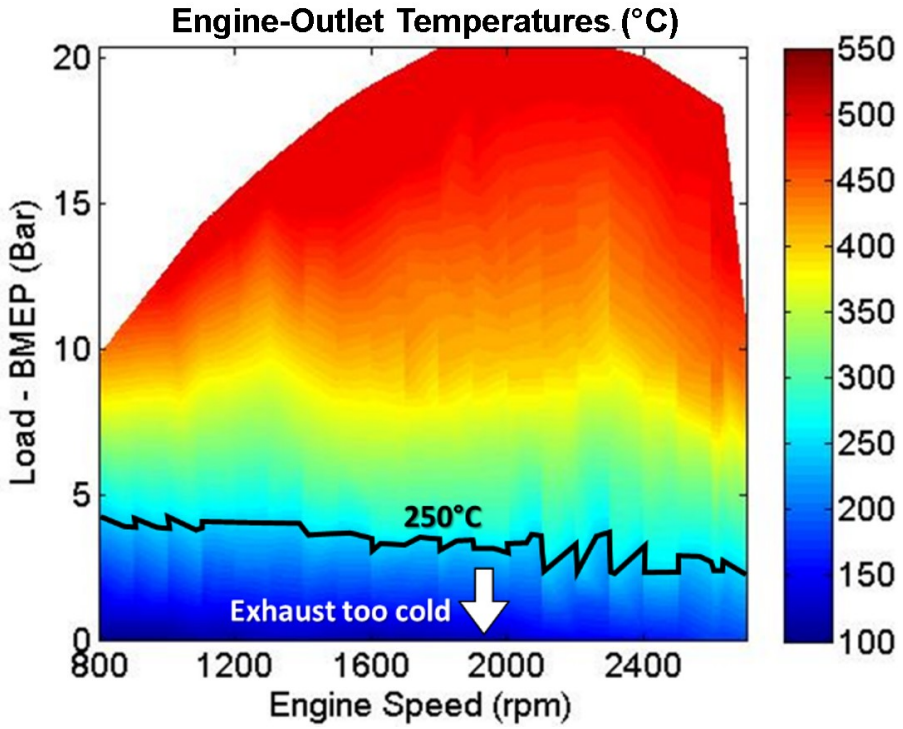

Figure 1.8. Exhaust gas temperature contours at various operating conditions.

Dementhon [30] observed a 150°C increase in engine-outlet temperature by opening the turbocharger wastegate to reduce air-to-fuel ratio.

Fuel path strategies, on the other hand, achieve aftertreatment thermal management through reductions in engine efficiency. Parks et al. [31] highlighted the influence of fuel injection timing on engine-outlet gas temperature via injection of additional fuel early in the cycle, late in the cycle, and increasing fueling in only one cylinder. Hydrocarbon dosers can also be used to inject fuel upstream of the DOC [32, 33].

Although the air path strategies generally show lower fuel consumption and better DOC warm-up through lower air-to-fuel ratios, these strategies are not as effective in warming up the SCR system. This is the result of the SCR system typically being the last component before the tailpipe [7], which results in the preference for both elevated engine-outlet temperatures and flow rates for accelerated warm-up. Therefore, fuel-

path approaches are typically pursued during the 'warm-up' phase, while the air path approaches are used during the 'stay-warm' phase.

The gas exchange process in the engine, which includes the charge intake from the intake manifold and exhaust of combustion products to the exhaust manifold, plays an important role in diesel engine fuel efficiency and emissions. The gas exchange process can be made to affect not only the pumping work, but also the compression and expansion work through flexible actuation of the intake and exhaust valves.

1.2.2 Early Exhaust Valve Opening

Early exhaust valve opening (EEVO) is a fuel path thermal management strategy that shows potential to increase the engine-outlet temperatures at the cost of higher fuel consumption. Early opening of the exhaust valve reduces expansion work because of early blow-down of high pressure combustion gases, and therefore makes engine operation less efficient. Roberts et al. [34] experimentally observed a 30°C to 80°C increase in engine-outlet temperatures via EEVO, and predicted up to a 100°C increase, at the cost of reduced brake thermal efficiency (BTE). They also predicted that the engine-outlet temperatures of many low-load operating conditions can be increased above 250°C. Bharath et al. [35] concluded from simulations that EEVO and exhaust cam phasing yield higher DOC conversion efficiencies with a deterioration in fuel economy.

1.2.3 Internal Exhaust Gas Recirculation

Exhaust gas recirculation (EGR) is used in modern diesel engines for reduction of engine-out NOx emissions, by reducing peak cylinder temperatures. Conventional engine hardware typically has an EGR loop that passes through an intercooler to cool the hot exhaust gases before recirculating them into the intake manifold. As hot gases in the intake manifold reduce the density of intake charge, the EGR cooler is useful during high power engine operation where high volumetric efficiency is desired.

At low loads, internal EGR (iEGR) can be used as an alternative to conventional EGR for NOx mitigation, while avoiding heat loss from the exhaust gas to the EGR cooler. In addition, iEGR avoids the need to maintain a pressure difference between the exhaust and intake manifolds, thus improving gas exchange efficiency. iEGR is typically achieved via a secondary opening of the exhaust valve during the intake stroke, where gases from both intake and exhaust manifolds are inducted into the cylinder, or using early exhaust valve closing (EEVC) which traps a fraction of the exhaust gas in the cylinder during the exhaust stroke. Blumenröder et al. [36] determined that iEGR via re-induction of exhaust gas yielded higher engine-outlet temperatures.

1.2.4 Cylinder Deactivation

Cylinder deactivation (CDA) is a technique in multi-cylinder engines where a combination of cylinders are motored with or without their valves closed, effectively reducing the engine's displacement. CDA has been extensively studied and implemented in production gasoline engines as a means to improve fuel economy by allowing stoichiometric conditions to be maintained with less intake throttling [29,37,38]. Heywood and Welling [38] concluded that between 2000 and 2008, 6% of the light-duty gasoline engines use CDA. Leone and Pozar [29] predicted that CDA in gasoline engines gives between 6-11% fuel economy benefit over the EPA metro/highway test cycle for various V8 and V10 passenger car and light truck applications. Recent implementation of CDA on production V6 engines by GM has shown up to 9% fuel economy benefit, while up to 6% benefit was achieved on 3 and 4 cylinder engines by Ford and Volkswagen ([39]).

CDA, however, has not been implemented in production on any transportation-based diesel engine. Ding et al. [26] and Ramesh et al. [40] experimentally demonstrated that CDA, when combined with other VVA strategies, including late intake valve closing (LIVC) and internal EGR (iEGR), shows a better trade-off between fuel

economy and thermal management than conventional operation at lightly-loaded, highly-loaded idle and high-speed low-load operating conditions. Lu et al. [41] concluded that implementation of CDA at highway cruise conditions enables active diesel particulate filter (DPF) regeneration without the presence of a hydrocarbon doser ahead of the diesel oxidation catalyst (DOC), by elevating the exhaust gas temperatures by 170-220°C.

Kitabatake et al. [42] predicted that running CDA at low loads over a JE05 drive cycle would allow an 8.9% improvement in fuel economy, and attributed this to reduction in heat loss. Bharath et al. [35] determined from simulations that better fuel economy and DOC conversion efficiency was achieved with CDA due to higher exhaust gas temperature and lower flow rate. Yang et al. [43] observed that cylinder cutout (strategy where only fuel injection is stopped in the non-firing cylinders) yielded a 11-13% improvement in fuel efficiency compared to baseline engine operation.

1.2.5 Torsional Vibration during CDA

CDA leads to lower-order torsional vibrations of higher amplitude as combustion of a greater quantity of fuel occurs in a fewer number of cylinders than conventional operation [44, 45]. Firing frequencies are proportional to engine speed, therefore, the lowest firing frequencies occur at idle engine operation, where studies have shown major benefit of CDA in diesel engines, as described above. The forcing frequencies vary depending on the number of active cylinders and the order in which cylinders are fired.

Low-frequency high-amplitude torsional vibration is a challenge for practical implementation, especially at low-speed operating conditions, where (i) firing frequencies lie closer to typical drivetrain resonance frequencies and (ii) humans are more likely to be bothered by any resulting vehicle vibration [44]. Figure 1.9 shows that vehicle and powertrain rigid body modes are typically excited between 1 Hz and 20 Hz.

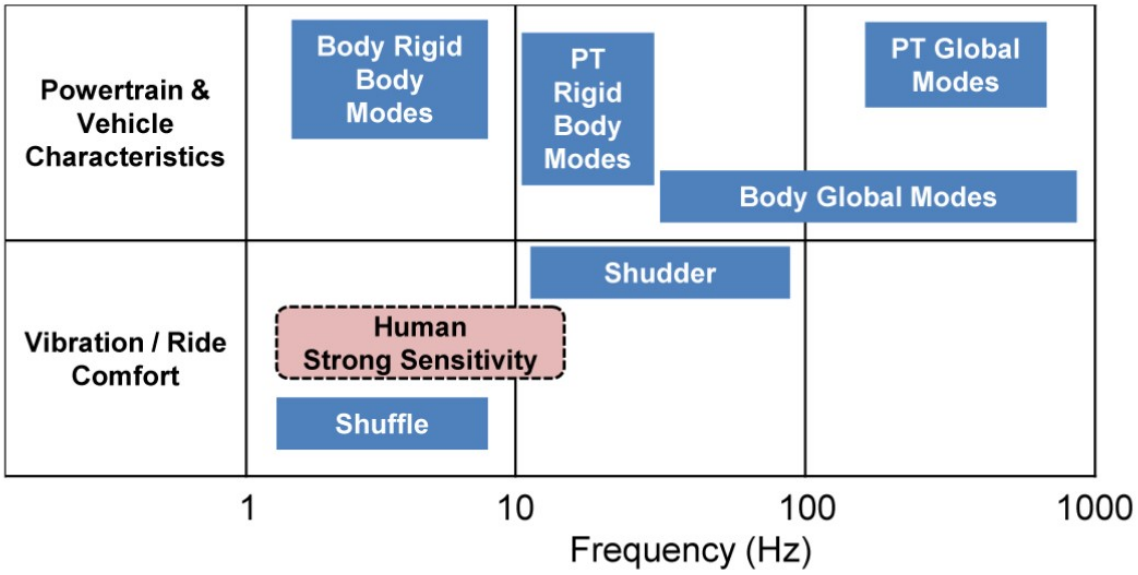

Figure 1.9. Drivetrain modal characteristics and human ride comfort in typical vehicles (adopted from [44]).

Archer and McCarthy, Jr., [46] studied the torsional vibration characteristics of CDA at various engine speeds, and observed resonance upon implementation of particular modes of CDA at certain speeds. The authors propose that CDA with different number of active cylinders must be implemented at different engine speeds to avoid resonance. However, the effects of using a non-optimal mode of CDA at a given engine operating condition are not discussed.

1.2.6 Oil Accumulation during CDA

Deactivation of a cylinder results in a gas spring of trapped gases, occurring twice each engine cycle, in the non-firing cylinders. Allen et al. [47] observed a decay in in-cylinder pressure during the first few cycles immediately following deactivation via blowby through the piston rings and heat loss, and indicated that a vacuum is created in the cylinder. Ma [48] indicated that low gas pressures in the deactivated cylinders aid oil transport from the crankcase to the cylinders. Halbe et al. [49] observed that longer periods of cylinder deactivation led to greater oil accumulation,

although not severe enough to cause any problems with first fire readiness. Oil consumption leads to higher unburnt hydrocarbon and particulate emissions, and would require more frequent oil changes by the end user. Gottschalk et al. [50] proposed periodic recharge of the deactivated cylinders to maintain the cylinder pressure above a minimum threshold, however, a tradeoff had to be made between minimum cylinder pressure and efficiency. General Motors, in their gasoline CDA system known as "Active Fuel Management (AFM)", avoid running AFM for more than ten minutes at a time, with the engine switching back to conventional operation for at least 60 seconds before re-entering AFM [51].

1.3 Contributions

1.3.1 DOC Thermal Modeling

The author led an effort, with additional guidance from Dr. Amy Marconnet, to develop a detailed thermal model of the diesel oxidation catalyst (DOC), using a finite element model, to capture the axial temperature variation in the DOC. The aim of this project was to compare the time taken by the DOC to reach light-off temperatures during CDA and six-cylinder operation. It was observed that the upstream-end of the DOC warmed up to light-off temperatures faster for CDA than six-cylinder operation as a result of higher engine-outlet temperatures, but the downstream-end warmed up at a slower rate because of lower flow rates associated with CDA. Details of this effort are not included in this dissertation.

1.3.2 GT-Power Study of Aggressive Valve Profiles

The author co-led a GT-Power-based study, with Aswin Ramesh and Mrunal Joshi, to assess the volumetric efficiency benefits and fuel savings achievable when valve profiles with more aggressive opening and closing ramp rates are implemented. Simulations, which were run at 1200 rpm, 3.8 bar BMEP, predicted 11.7% fuel savings with 10.8% lower airflow, and 2.2% fuel savings with a 1.4% higher airflow than baseline six-cylinder operation. Details of this effort are not included in this dissertation.

1.3.3 Transient Engine Operation with VVA

The author led the effort, with help from Aswin Ramesh and Cody Allen, to enable transient engine operation with VVA, as a part of upgrading the experimental facilities to evaluate advanced gas exchange strategies over drive cycle operation. Instantaneous transition between different VVA strategies (for example, between six-cylinder and CDA operation) was achieved, while achieving perfect coordination between the air handling controller, fuel handling controller and the VVA system. This

effort lay the foundation for all subsequent transient drive cycle experiments with VVA, including the results presented in Chapters 3 and 4 of this dissertation.

1.3.4 Study of Aftertreatment Warm-up Strategies

The author led an effort, with assistance from Aswin Ramesh, Cody Allen and Mrunal Joshi, to identify valve strategies that can expedite aftertreatment warm-up following cold start engine operation. Steady state tests were performed to identify strategies yielding elevated engine-outlet temperatures and exhaust flow rates, followed by implementation of the 'favorable' strategies over the HD-FTP drive cycle. A combination of early exhaust valve opening (EEVO) and internal EGR (iEGR) was identified to be the most favorable warm-up strategy at idle operation. EEVO and late intake valve closure (LIVC) was implemented at off-idle operation to further expedite aftertreatment warm-up. A major portion of this effort is outlined in Chapter 3 of this dissertation.

The aftertreatment warm-up characteristics of exhaust cam phasing, which is a production-viable variant of EEVO and iEGR, were analyzed. This study was conducted at low-load operating conditions at various speeds. Experiments were performed with a fixed VGT position to emulate a fixed geometry turbocharger, with no external EGR. Results indicate that exhaust cam phasing results in elevated engine outlet temperatures, higher fuel consumption, lower exhaust flow rates, lower NOx emissions and higher PM emissions. Details of this effort are not presented in this dissertation.

The author mentored Harikrishnan Raghukumar, an undergraduate student from IIT Madras, India, to perform a GT-power-based study on the aftertreatment warm-up potential of dual exhaust valve lifts, where an early first exhaust valve event is followed by a late second exhaust valve event, at idle operation. Results predicted that dual exhaust valve lift results in higher turbine-outlet temperatures than the

regular EEVO strategy at similar exhaust flow rates and higher fuel consumption. Details of this effort are not presented in this dissertation.

Assistance was given to Mrunal Joshi and Kalen Vos to characterize the warm-up potential of late exhaust valve opening (exhaust valve throttling), motivated by some of the results observed from the aforementioned GT-power study on dual exhaust valve lifts at idle operation. LEVO was also studied under fixed geometry turbocharger conditions to assess the warm-up benefits achievable without using a variable geometry turbine turbocharger. Details of this effort are not presented in this dissertation.

1.3.5 Characterization of Cylinder Deactivation as an Aftertreatment 'Stay-Warm' Strategy

The author co-led an effort with Mrunal Joshi, Kalen Vos and Cody Allen to characterize the fuel efficiency and aftertreatment thermal management benefits of CDA at steady state curb idle operation (800 rpm, 1.3 bar BMEP), and upon implementation of this strategy at low loads and idle regions of the HD-FTP drive cycle. Chapter 4 of this dissertation describes the results obtained from this work in greater detail.

The author also co-led an effort to assess the impact of various modes of CDA, when implemented over extended idle, and below 3 bar BMEP during predominantly low-load drive cycles such as heavy heavy-duty diesel truck (HHDDT) creep cycle, over extended periods. Results from this effort are not presented in this dissertation.

Transient response of the engine upon implementation of low load- and idle-CDA were studied, with assistance from Cody Allen and Aswin Ramesh. Specifically, the transient response of the engine, when different modes of CDA are implemented at unloaded idle, loaded idle and motoring operation, during select aggressive transient sections of the heavy-duty federal test procedure (HD-FTP) are analyzed. As will be described in Chapter 4 of this dissertation in greater detail, it was demonstrated

that implementation of CDA at and near idle operation does not affect the transient response of the engine.

The author mentored Sirish Srinivasan, an undergraduate student from IIT Madras, India, in predicting the fuel efficiency benefits of CDA when implemented at all loads below 3 bar BMEP during the "stay-warm" portions of real world drive cycles such as Orange County Bus Cycle and NREL Port Drayage drive cycle. While the results obtained are not detailed in this dissertation, they have been presented in reference [52].

Assistance was given to Cody Allen to study the differences between two CDA charge trapping strategies, namely, fresh charge trapping and combusted charge trapping, at 800 rpm, 1.3 bar BMEP and 2200 rpm, 1.3 bar BMEP. It was observed that there was no significant difference between the two charge trapping strategies, with the in-cylinder pressures in the non-firing cylinders decaying and converging within 0.8 seconds after transition to CDA. While the results obtained are not detailed in this dissertation, they have been presented in reference [47].

1.3.6 Dynamic Cylinder Activation

The author implemented and characterized dynamic cylinder activation (DCA) in diesel engines, the first known effort of its kind, with assistance from Cody Allen. This study showed that DCA can enable greater control over torsional vibration of the engine, while achieving similar fuel consumption and aftertreatment thermal management benefits as fixed CDA. This effort, and the resulting insights, are described in greater detail in Chapter 5 of this dissertation.

A firing pattern selection algorithm was developed by the author to choose the appropriate sequence of firing events during DCA, given a desired firing density and a range of 'unfavorable' forcing frequencies, so as to not excite the driveline resonant frequencies. This effort is not detailed in the dissertation.

1.3.7 Ventilation Strategies

New valvetrain strategies to 'ventilate the non-firing cylinders to the intake/exhaust manifolds, during CDA-like operation, were experimentally studied by the author. Results indicate that similar performance and emissions as fixed CDA can be achieved while maintaining in-cylinder pressures of the non-firing cylinders close to manifold pressures. This work, and the associated results, are described in greater detail in Chapter 6 of this dissertation.

Additional work was also performed on investigation of 'partial' ventilation strategies involving production-viable dual independent cam phasing in the non-firing cylinders, which is not presented in this dissertation.

1.3.8 Torsional and Linear Vibration of Advanced VVA Strategies

The author co-led an effort with Cody Allen, Matthew Pieczko (Eaton) and Akibi Archer (Eaton) to characterize the torsional and linear vibration of various VVA strategies, including fixed CDA, DCA, cylinder cutout, reverse breathing and VCC strategies. Vibration characteristics of various fixed CDA configurations were assessed below 3 bar BMEP at all engine speeds. The vibration characteristics of DCA (implemented with various firing densities and firing patterns), VCC and reverse breathing were studied at loads below 3 bar BMEP at 800 rpm. The results from these experiments are not detailed in this dissertation.

1.3.9 High BMEP Gasoline Engine Controls

The author co-led an effort with Xu (Sharon) Zhang to perform an air handling control analysis of a medium-duty high BMEP gasoline engine, as a part of the CERC-TRUCK consortium, in collaboration with US Department of Energy, Cummins and Argonne National Labs. A control-oriented model of a gasoline engine was developed in Simulink, and an observability-based analysis was carried out to develop a frame-

work to optimize air handling sensor selection, for accurate estimation of fresh air and EGR in the intake manifold. Assistance was given to Sean Franiak to accurately model condensation in the air handling path of the engine, to ultimately be able to detect and control condensation using conventional sensors and actuators. This dissertation does not describe this effort in further detail.

1.4 Outline of this Dissertation

1. This chapter **(Chapter 1)** motivates the need for reduction of greenhouse gas emissions from medium- and heavy-duty engines and presents the relevance of the study. The need for diesel engine aftertreatment thermal management and the role of gas exchange processes via variable valve actuation in improving thermal management is described. Finally, the contributions of the author to this project are presented.

2. **Chapter 2** broadly presents the 'resources, tools and procedures' used in this study. The experimental setup available for engine testing at Herrick laboratories is described in Section 2.1. The chapter also presents various techniques for data analysis which are extensively used in this study. Further, the heavy-duty drive cycle is introduced and the operating points used in this study are justified.

3. **Chapter 3** details the experimental work performed to study the aftertreatment warm-up potential of EEVO and iEGR at loaded idle operation, both at steady state and over the HD-FTP drive cycle. The warm up potential of a combination of EEVO and LIVC at off-idle operation below 7.6 bar BMEP over the HD-FTP drive cycle is also demonstrated.

4. **Chapter 4** presents the fuel efficiency and aftertreatment 'stay-warm' thermal management benefits shown by cylinder deactivation (CDA), both at steady state loaded idle operation, and over the HD-FTP drive cycle. Transient response of the engine when CDA is implemented at and near idle operation is characterized.

5. **Chapter 5** introduces dynamic cylinder activation (DCA) as a means to enable greater control over engine torsional vibration, and compares the torsional vibration characteristics and performance of DCA with CDA and six-cylinder operation. A recipe to enable engine operation away from driveline resonant

frequencies at all engine speeds, without compromising on fuel efficiency and thermal management performance, using DCA and CDA, is proposed.

6. **Chapter 6** introduces ventilated cylinder cutout (VCC) as a strategy to ameliorate potential oil accumulation concerns with CDA using a conventional piston ring pack. Three strategies to ventilate the non-firing cylinders to the intake/exhaust manifolds, during CDA-like operation, are explored. The effect of lower valve lifts in the non-firing cylinders, to enable easier production-viable implementation, is studied.

7. The work described in Chapters 1-6 is summarized and recommendations for future work are made in **Chapter 7**.

2. EXPERIMENTAL SETUP AND DATA ANALYSIS PROCEDURES

2.1 Experimental Setup

All experiments were performed on a six-cylinder Cummins diesel engine equipped with a camless variable valve actuation (VVA) system, as shown in Figure 2.1. The engine is coupled to an AC dynamometer that is capable of both steady state and transient engine testing.

The engine incorporates cooled high pressure exhaust gas recirculation (EGR), variable geometry turbine turbocharging (VGT), air-to-water charge air cooling (CAC), and high pressure common rail fuel injection. Figure 2.2 shows a schematic drawing of the air handling system of the engine. The engine-outlet location is immediately downstream of the turbocharger turbine. The phrases "engine-outlet temperature" and "turbine outlet temperature (TOT)" are used interchangeably through the remainder of the document.

Kistler 6067C and AVL QC34C pressure transducers are mounted on each of the six cylinders to log in-cylinder pressure through an AVL 621 Indicom module, and crank angle-referenced using an AVL 365C crankshaft position encoder. A hall-effect sensor is installed at the 173-tooth flywheel of the engine to measure the instantaneous velocity of the flywheel, measured by the AVL high-speed data acquisition system at a resolution of 0.1 crank angle degree, or 48 kHz at 800 RPM.

Fresh air flow is measured using a laminar flow element. Fuel flow rate is measured gravimetrically using a Cybermetrix Cyrius Fuel Subsystem (CFS) unit. CO_2 concentration is measured in the intake manifold as well as the exhaust pipe using Cambustion NDIR500 fast CO/CO_2 analyzers. NOx is measured in the exhaust pipe downstream of the turbocharger using a Cambustion fNOx400 analyzer. CO_2, NOx and UHC concentrations are also measured using California Analytical Instruments

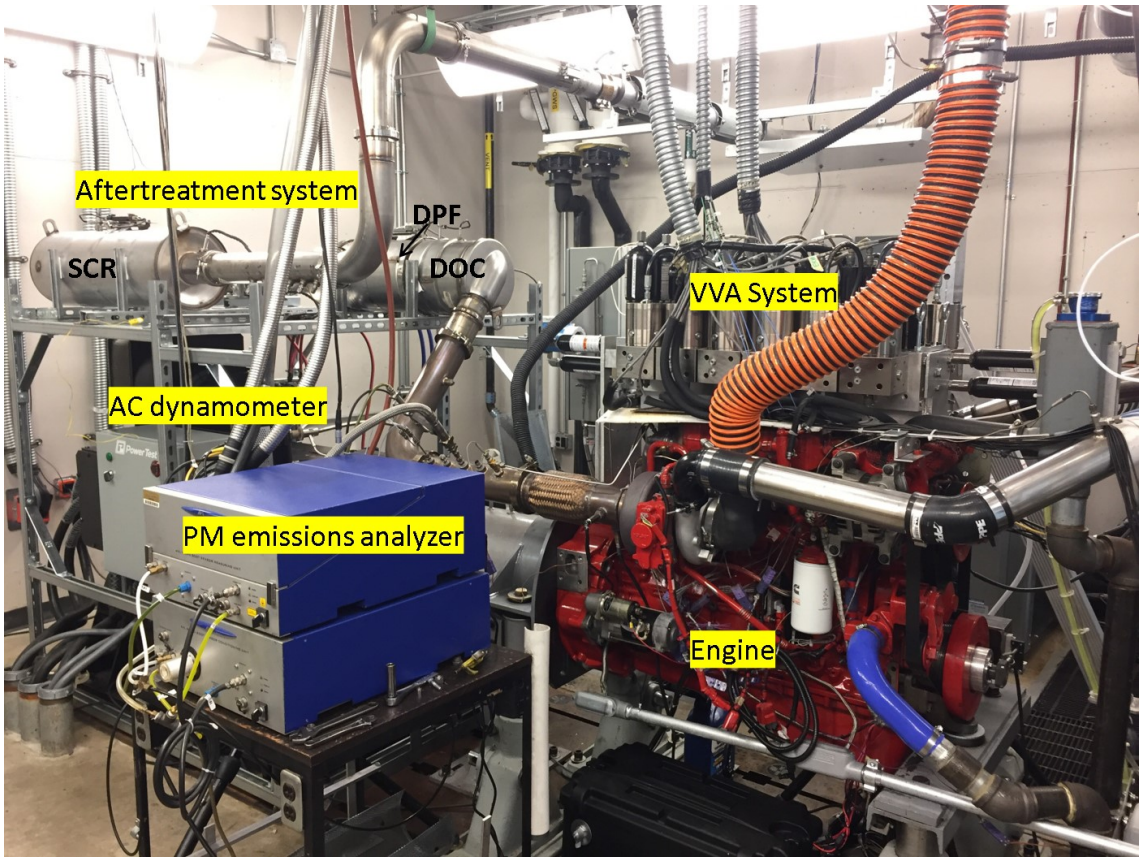

Figure 2.1. Experimental setup- Cummins mid-range diesel engine equipped with VVA and aftertreatment systems.

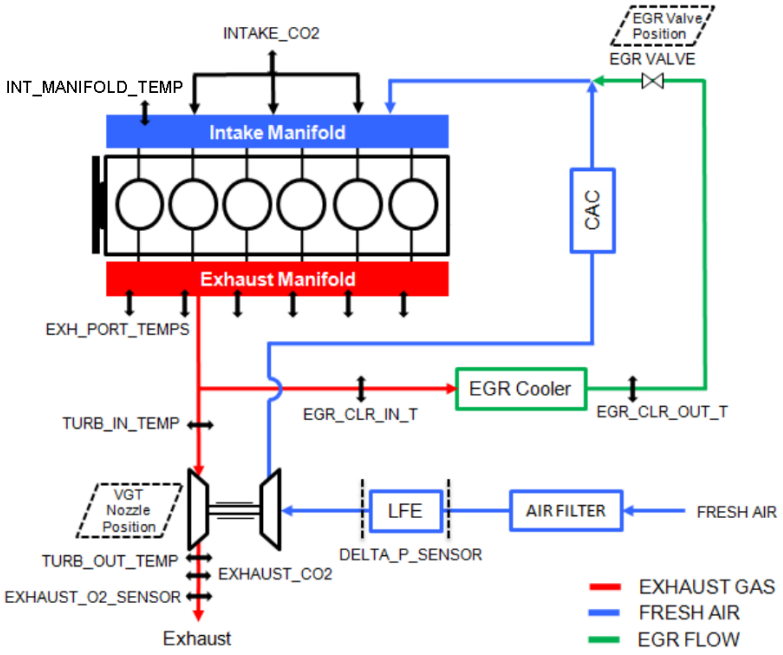

Figure 2.2. Schematic of air handling system of the engine.

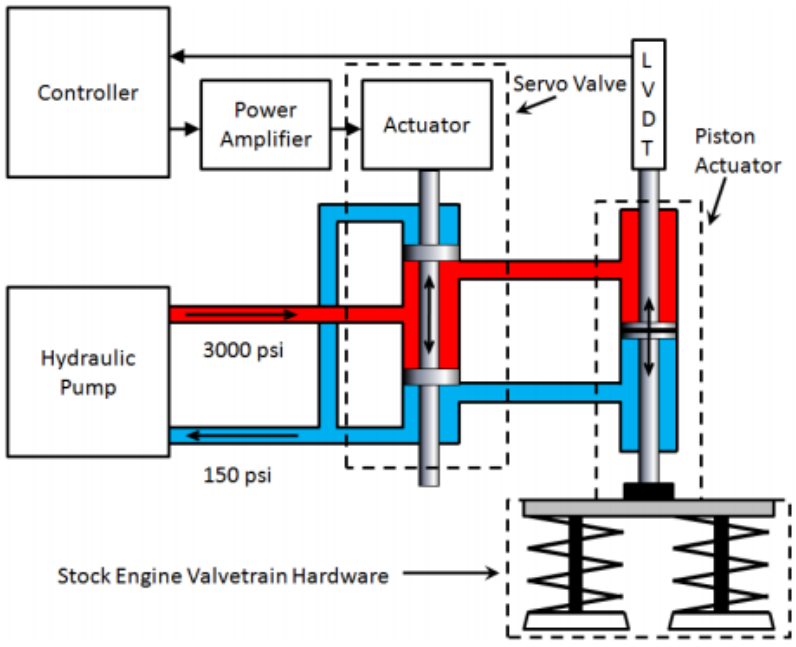

Figure 2.3. Schematic of the variable valve actuation setup.

(CAI) 600-series NDIR, HCLD and HFID analyzers, respectively. PM in the exhaust stream is measured using an AVL483 photo-acoustic transient analyzer. The coolant, oil and gas temperatures at various locations are measured using thermocouples. All data is monitored and logged through a dSPACE interface. The engine control module (ECM) is connected to the dSPACE system through a generic serial interface (GSI) link that allows for cycle-to-cycle monitoring and control of fueling and various other engine operating parameters.

Boundary conditions to the engine are maintained using a combustion air controller system and a CAC temperature controller system. The combustion air control system maintains the air at the inlet of the compressor at a temperature of 25°C, humidity at 50% and pressure at 1 bar. The CAC temperature controller maintains the coolant of the CAC at 25°C to ensure consistent heat rejection and avoid condensation at the CAC.

2.1.1 Variable Valve Actuation System

The VVA system allows for fully flexible, cylinder independent, cycle-to-cycle control of the valve events of the engine. The system includes twelve electro-hydraulic linear actuators, one for each intake and exhaust valve pair on a cylinder. The system is powered by a hydraulic pump, which maintains oil supply pressure at 3000 psi. Position feedback for each valve is measured using a Linear Variable Differential Transformer (LVDT). A real-time controller is run via dSPACE to control the linear actuators. A schematic of the actuators used in the VVA system is shown in Figure 2.3.

2.1.2 Aftertreatment System

A Cummins aftertreatment system, equipped with a DOC, DPF and SCR, is connected to the outlet of the engine, as shown in Figure 2.1. The aftertreatment is used in passive mode, i.e., the exhaust gas is passed through the system without active

urea injection, for measurement of catalyst bed temperatures. Thermocouples and thermistors are installed at the inlet and outlet of DOC, DPF and SCR to measure the temperature of gas entering and exiting each aftertreatment component. A differential pressure sensor is installed in the DPF to identify if the DPF is excessively clogged, so that an active regeneration may be performed.

2.2 Methodology

All experiments are subject to strict mechanical and thermal constraints, as shown in Table 2.1, so as not to cause any hardware damage to the engine and to make sure that the findings are relevant to real-use scenarios.

2.2.1 Cycle Efficiency Analysis

The net indicated mean effective pressure (NIMEP), which represents the indicated work normalized with displaced volume, is the sum of gross indicated mean effective pressure (GIMEP) and pumping mean effective pressure (PMEP). GIMEP represents the indicated work done in the "closed cycle" during compression and expansion strokes, while PMEP is indicative of the work done in the "open cycle", to pump the gas from the intake to the exhaust manifold during the exhaust and intake strokes. Figure 2.4 shows the open and closed cycles in a typical logarithmic in-cylinder pressure-volume curve.

$$BTE = OCE \times CCE \times ME \tag{2.1}$$

Table 2.1. Mechanical and thermal constraints.

Mechanical Parameter	units	limit
Turbine Inlet Temperature	°C	760
Compressor Outlet Temperature	°C	230
Turbo Speed	kRPM	126
Peak Cylinder Pressure	bar	172
Exhaust Manifold Pressure	kPa	500
Pressure Rise Rate	bar/ms	100
Firing frequency	Hz	> 10

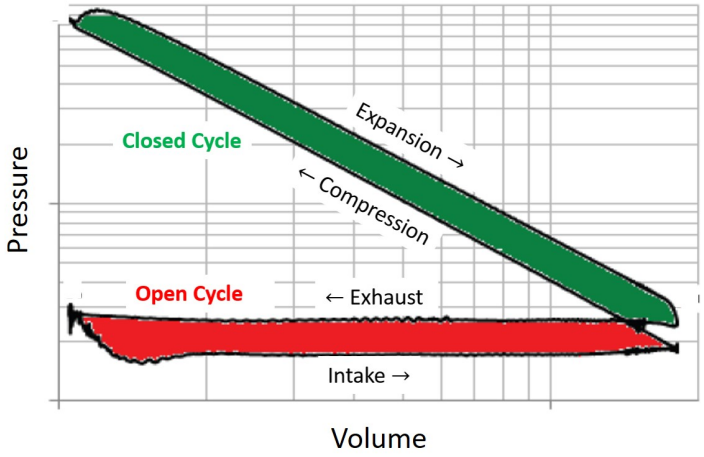

Figure 2.4. Open and closed cycles within an engine cycle.

$$OCE = \frac{NIMEP}{GIMEP} = 1 - \frac{PMEP}{GIMEP} \tag{2.2}$$

$$CCE = \frac{GIMEP \times V_d}{\dot{m}_{fuel} \times LHV_{fuel}} \tag{2.3}$$

$$ME = \frac{BTE}{OCE \times CCE} \tag{2.4}$$

Fuel consumption using various strategies are analyzed using an engine-cycle efficiency analysis. Brake thermal efficiency (BTE) is a product of open cycle efficiency (OCE), closed cycle efficiency (CCE) and mechanical efficiency (ME), as shown in Equation (2.1) [7]. OCE quantifies the effectiveness of the cylinder gas exchange process, and is lower when greater work is required by the engine to pump gas through the cylinders. OCE is inversely related to the difference between the intake and exhaust manifold pressures, or the size of the pumping loop in the logarithmic in-cylinder pressure-volume curve. The CCE captures the impact of the in-cylinder combustion energy release and heat transfer on the engine efficiency. Delay in heat release and increase in heat loss from the cylinder results in lower CCE. Mechanical efficiency quantifies all other losses in the engine, including heat loss to the oil, coolant

and surroundings and various friction and accessory loads. The cycle efficiencies are mathematically represented by Equations (2.1)-(2.4).

2.2.2 First Law Analysis

A first law-based energy analysis is implemented to evaluate the thermal management performance of various strategies by considering the entire engine system as a control volume. Figure 2.5 describes the various ways in which the fuel power entering the engine is spent. Energy enters the engine in the form of fuel injected into the cylinders and is then distributed as useful work done on the piston, energy of the exhaust gas, heat loss from the cylinder, pumping losses, heat loss through the EGR cooler, and various other mechanical and thermal losses including manifold losses, turbocharger losses, friction, CAC heat rejection and auxiliary losses. Brake power, exhaust heat rate, and various other losses can be mathematically represented by Equations (2.5)-(2.12). The variables used in the equations are described in Table 2.2.

$$\dot{W}_{brake} = Torque \times 4\pi \times \frac{N}{120} \tag{2.5}$$

$$\dot{Q}_{exh} = \dot{m}_{exh} C_{p,exh} (TOT - T_{ref}) - \dot{m}_{air} C_{p,air} (T_{amb} - T_{ref}) \tag{2.6}$$

$$\dot{W}_{indicated} = NIMEP \times V_d \times \frac{N}{120} \tag{2.7}$$

$$\dot{W}_{pumping} = PMEP \times V_d \times \frac{N}{120} \tag{2.8}$$

$$\dot{Q}_{chg} = \dot{m}_{chg,out} C_{p,chg,out} (T_{EM} - T_{ref}) - \dot{m}_{chg,in} C_{p,chg,in} (T_{IM} - T_{ref}) \tag{2.9}$$

$$\dot{Q}_{cyl} = \dot{E}_{fuel} - \dot{W}_{gross} - \dot{Q}_{chg} \tag{2.10}$$

Table 2.2. Definition and description of variables used in Equations (2.5)-(2.12).

Symbol	**Description**
$C_{p,air}$	Specific heat constant of fresh air
$C_{p,charge,in}$	Specific heat constant of charge entering the cylinders
$C_{p,charge,out}$	Specific heat constant of charge exiting the cylinders
$C_{p,exh}$	Specific heat constant of exhaust gas
LHV_{fuel}	Lower heating value of the fuel (diesel)
$\dot{m}_{air}$	Mass flow rate of fresh air entering the engine
$\dot{m}_{charge,in}$	Mass flow rate of charge entering the cylinders
$\dot{m}_{charge,out}$	Mass flow rate of charge exiting the cylinders
$\dot{m}_{EGR}$	Mass flow rate of exhaust gas recirculation
$\dot{m}_{exh}$	Mass flow rate of exhaust gas leaving from the engine
$\dot{m}_{fuel}$	Mass flow rate of fuel entering the engine
N	Engine speed (RPM)
$NIMEP$	Net indicated mean effective pressure
$PMEP$	Pumping mean effective pressure
$\dot{Q}_{charge}$	Rate of heat transfer to the in-cylinder charge
$\dot{Q}_{cyl}$	Rate of heat loss from the cylinders
$\dot{Q}_{EGR}$	Rate of heat rejection through the EGR cooler
$\dot{Q}_{exh}$	Rate of heat transfer to the exhaust stream
$\dot{Q}_{other}$	Rate of other mechanical/thermal energy loss
T_{amb}	Ambient air temperature
T_{brake}	Brake torque produced by the engine
T_{EM}	Exhaust manifold temperature
T_{IM}	Intake manifold temperature
T_{ref}	Reference temperature, taken as 25°C
$\Delta T_{EGRcooler}$	Temperature drop of the gas across the EGR cooler
TOT	Turbine outlet temperature
V_d	Displaced volume
$\dot{W}_{brake}$	Brake power developed by the engine
$\dot{W}_{indicated}$	Indicated power developed by the cylinders

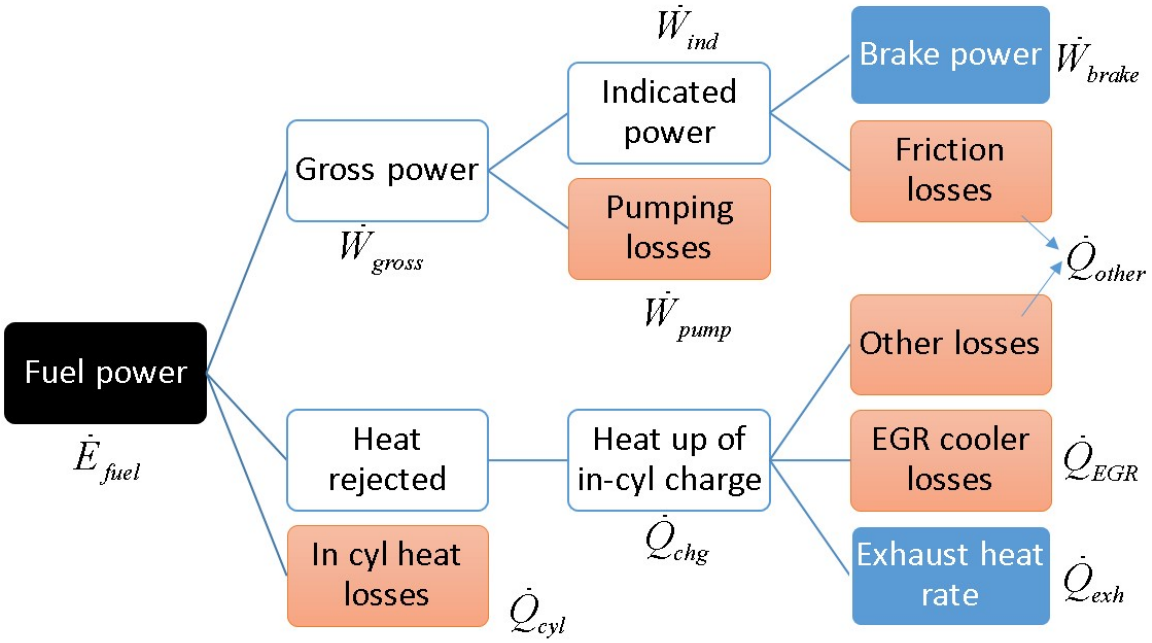

Figure 2.5. Fuel power entering the engine is spent as brake power, exhaust heat rate and losses such as pumping losses, in-cylinder heat losses, EGR cooler heat losses and other losses.

$$\dot{Q}_{EGR} = \dot{m}_{EGR} C_{p,EGR} \Delta T_{EGRcooler} \tag{2.11}$$

$$\dot{Q}_{other} = \dot{Q}_{chg} - \dot{Q}_{exh} + \dot{W}_{indicated} - \dot{W}_{brake} \tag{2.12}$$

2.2.3 Normalized Heat Transfer Analysis

The normalized heat transfer analysis models heat transfer from the exhaust gas to the aftertreatment system, and is an effective tool to understand the aftertreatment 'warm-up' and 'stay-warm' merits for various operating strategies. The DOC, DPF and SCR are treated as a single lumped catalyst bed at a temperature T_{cat}. The heat transfer from the exhaust gas to the catalyst bed is approximated by

$$Q = C \times \dot{m}_{exh}^{\frac{4}{5}} \times (TOT - T_{cat}) \tag{2.13}$$

This model yields an approximate heat transfer rate from the exhaust gas to the aftertreatment system, for a given lumped catalyst temperature, as a function of the experimentally measured exhaust flow rate and TOT. A positive heat transfer rate corresponds to catalyst warm-up, as heat is transferred from the exhaust gas to the catalyst when TOT is higher than the catalyst bed temperature T_{cat}. A negative heat transfer rate corresponds to catalyst cool-down, as the heat is transferred from the catalyst to the exhaust gas when T_{cat} is above TOT. The "zero crossing occurs when $T_{cat} = TOT$.

Per Equation (2.13), the slope of the normalized heat transfer lines in Figure 2.13 is proportional to $\dot{m}_{exh}^{\frac{4}{5}}$. The line slopes are therefore steeper for higher exhaust flow rates. Therefore, higher exhaust flow rates result in a higher rate of warm-up when TOT is higher than T_{cat}. However, higher exhaust flow rates also correspond to a faster catalyst cool-down when TOT is lower than T_{cat}.

Figure 2.6 illustrates the normalized heat transfer from the exhaust gas to the aftertreatment system for three hypothetical strategies shown in Table 2.3. The heat transfer rates are normalized with the heat transfer of strategy-1 at a catalyst bed temperature of 0°C. Strategy-1 has the same TOT as strategy-2 but a higher exhaust flow rate, as a result of which its normalized heat transfer rate is higher for lower catalyst temperatures, with a steeper slope. Strategy-2 has a less steep slope, with lower heat transfer rates at lower catalyst bed temperatures, but also a slower 'cool-down' rate when catalyst temperatures are higher. Therefore, between strategies 1 and 2, the strategy-1 is preferred for aftertreatment 'warm-up', while strategy-2 is preferred for aftertreatment 'stay-warm'. Strategy-3 has the same exhaust flow rate as strategy-2 but a higher TOT, thereby explaining its higher heat transfer at a similar slope.

Table 2.3. TOT and exhaust flow rates for hypothetical strategies.

Strategy	TOT	Exhaust flow rate
1	250°C	2 kg/min
2	250°C	1 kg/min
3	400°C	1 kg/min

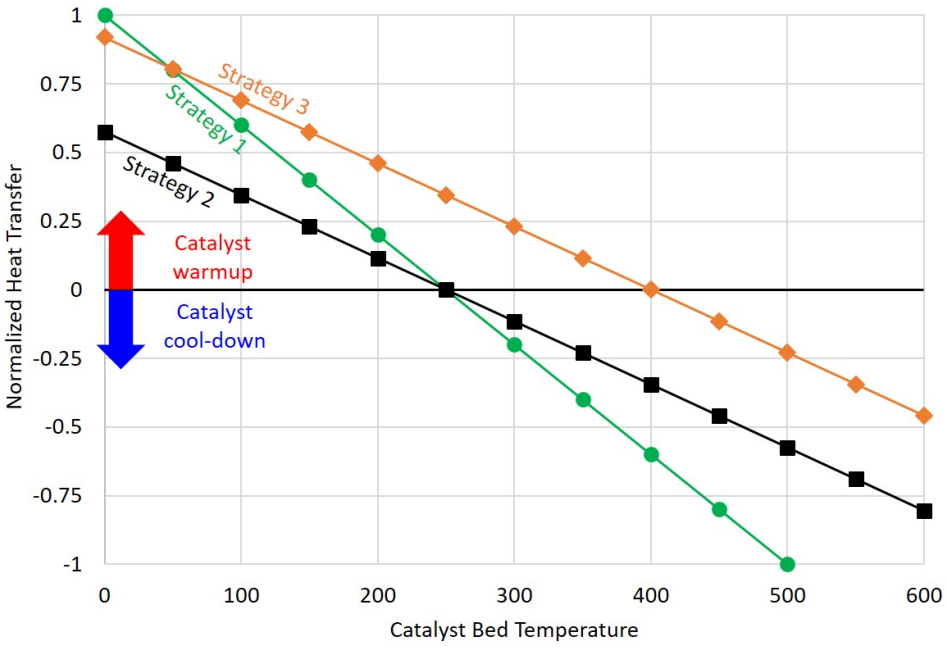

Figure 2.6. Normalized heat transfer plots, shown here for hypothetical strategies, can be used to identify aftertreatment 'warm-up' and 'stay-warm' strategies.

2.3 Heavy Duty Federal Test Procedure

The heavy duty federal test procedure (HD-FTP) is a transient cycle for emissions certification of on-road heavy-duty engines. The test procedure consists of a cold start drive cycle, followed by an identical hot start drive cycle with a soak period of twenty minutes between the cycles. The speed and torque profile for the HD-FTP drive cycle is shown in Figure 2.7.

2.3.1 Experimental and Data Analysis Procedure

In order to maintain repeatable starting conditions, a HD-FTP cycle was run after an overnight engine 'cold soak'. All the aftertreatment components were brought to the same initial conditions prior to starting the cold cycle, by flowing fresh air at 25°C from an external source through the aftertreatment system. The drive cycle was started after the inlet and outlet gas temperatures of all the catalysts stabilized at 25°C.

The composite fuel consumption and emissions from the drive cycles are calculated by dividing the weighted emissions and fuel consumption over the cold and hot cycles by the weighted brake work . The weighting factors for the cold- and hot-start drive cycles are $\frac{1}{7}$ and $\frac{6}{7}$, respectively, as mandated by the EPA [53]. It is the author's understanding that the weighting factors are used to represent real-life engine operation of a heavy duty vehicle, which typically operates with cold aftertreatment components for approximately 14% of its total operating time.

$$FC_{net} = \frac{1}{7}FC_{cold} + \frac{6}{7}FC_{hot} \tag{2.14}$$

$$NOx_{net} = \frac{1}{7}NOx_{cold} + \frac{6}{7}NOx_{hot} \tag{2.15}$$

$$PM_{net} = \frac{1}{7}PM_{cold} + \frac{6}{7}PM_{hot} \tag{2.16}$$

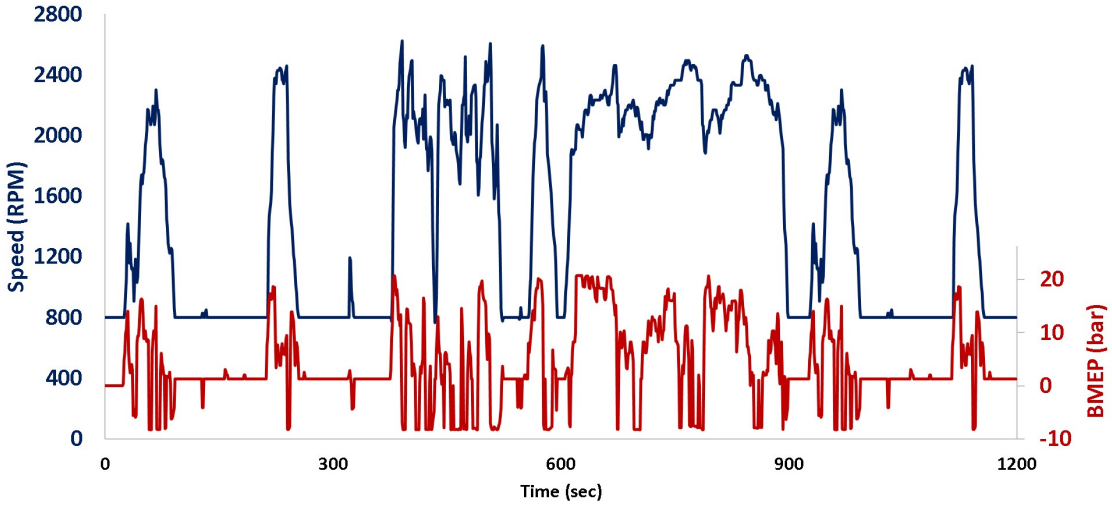

Figure 2.7. Speed and torque profiles for one HD-FTP drive cycle.

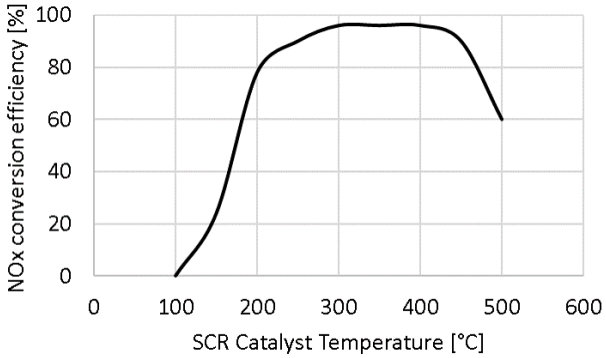

Figure 2.8. SCR NOx conversion efficiency curve, used to predict tailpipe-out NOx emissions over the drive cycle.

The turbine-outlet temperature and engine-out NOx and PM emissions are measured, as described in Section 2.1. The tailpipe-out emissions (at the outlet of the aftertreatment system) are estimated by passing the measured engine-out NOx emissions through an SCR conversion efficiency curve, which is a function of the SCR catalyst bed temperature, as shown in Figure 2.8. As illustrated, NOx conversion is assumed to start after the SCR exceeds 100°C, and reaches a maximum of 96% efficiency between 300°C and 450°C.

Table 2.4. Upper and lower bounds for regression analysis parameters for HD-FTP drive cycle.

Parameter	**Speed**	**Load**	**Power**
Slope (m)	$0.95 \leq m \leq 1.03$	$0.83 \leq m \leq 1.03$	$0.83 \leq m \leq 1.03$
Intercept (c)	$c \leq 75.0$	$c \leq 15.5313$	$c \leq 33.174$
SEE	$SEE \leq 117.955$	$SEE \leq 77.656$	$SEE \leq 33.174$
r^2	$r^2 \geq 0.97$	$r^2 \geq 0.85$	$r^2 \geq 0.91$

2.3.2 Relevance of Idle and Low Loads

The operating points of the HD-FTP can be categorized into eight operating modes, which are fixed fractions of maximum speed and torque. The operating points have weights assigned to them, either based on fuel consumed or time spent at each operating mode. Figure 2.9(a) shows the eight-mode distribution based on fuel consumption, where it is shown that idle regions consume approximately 5.8% of the total fuel consumed over a HD-FTP, while loads below 4 bar BMEP consume nearly 17% of the total fuel. Figure 2.9(b), which shows the time-based eight-mode distribution, suggests that approximately 43% of the time is spent at idle, and 67% of the time at low loads ($<$ 4 bar BMEP) displaying significant potential for improvement in aftertreatment thermal management at low loads.

Idle operation, therefore, is the major focus of this study. Chapter 2 describes the implementation of a combination of EEVO and iEGR via NVO at idle operation for faster aftertreatment component warm-up, with a fuel penalty, while Chapter 3 describes the use of cylinder deactivation at idle and low loads operation for improving both fuel efficiency and aftertreatment 'stay-warm' thermal management. Strategies described in chapters 5 and 6, namely, dynamic cylinder activation and ventilated cylinder cutout, respectively, are demonstrated, and compared with CDA, at idle operation.

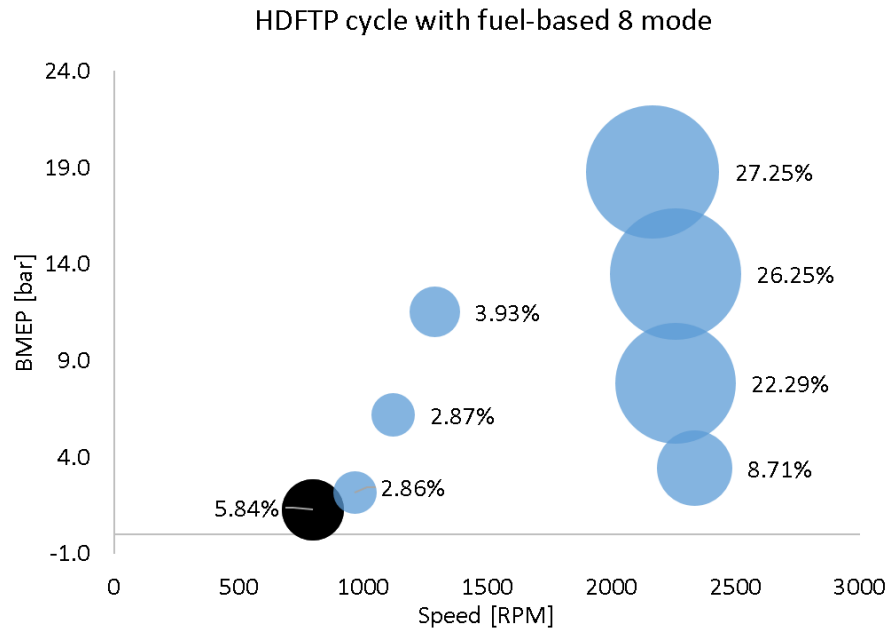

(a)

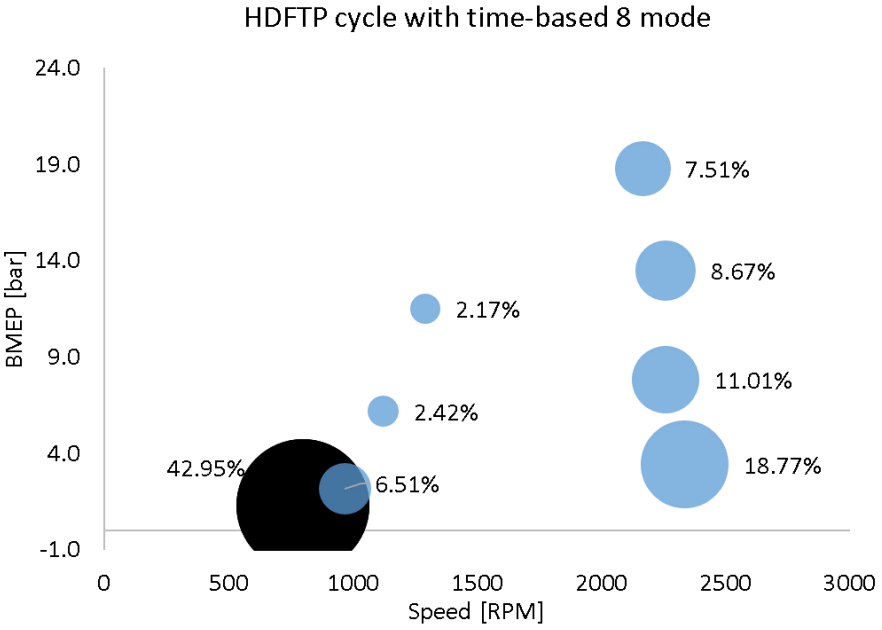

(b)

Figure 2.9. Idle and low-load operation over a HD-FTP (a) consumes approximately 6% of the total fuel and (b) spans for approximately 43% of the total time.

2.3.3 Regression Analysis for Drive Cycle Validation

The validity of a HD-FTP test is checked by performing a regression analysis between the commanded and feedback values of the drive cycle speed, torque and power [53]. The upper and lower bounds for various statistical parameters are shown in Table 2.4.

3. AFTERTREATMENT THERMAL MANAGEMENT VIA ACCELERATED CATALYST WARM UP

3.1 Introduction

It was noted earlier in Section 1.2 that aftertreatment warm-up is an important phase in aftertreatment thermal management as the catalysts are ineffective at low temperatures. Approximately 80% of the total allowable NOx emissions occur during the warm-up of the SCR system, as shown in Figure 1.7, as the engine-out NOx is not reduced before being released from the tailpipe [19]. This chapter focuses on implementation of internal EGR (iEGR) and early exhaust valve opening (EEVO) at idle operation to expedite the warm-up of the aftertreatment system following a cold start of the engine. Based on the normalized heat transfer analysis described in Section 2.2.3, high turbine-outlet temperatures and exhaust flow rates are desirable for the aftertreatment warm-up strategies.

This chapter is organized as follows:

1. Section 3.2 describes various VVA-enabled aftertreatment 'warm-up' thermal management strategies, and discusses their performance at steady state curb idle operation.

2. Section 3.3 demonstrates the improved aftertreatment thermal management upon implementation of the 'best' strategy from Section 3.2 over the HD-FTP drive cycle.

3.2 Early Exhaust Valve Opening and Internal EGR at Steady State Idle Operation

Steady state tests were performed at idle (800 RPM, 1.3 bar BMEP) to evaluate the benefits of EEVO and iEGR over conventional engine operation. The primary focus was on obtaining higher TOT and exhaust gas energy in order to accelerate aftertreatment component warm up. All experiments were subject to strict mechanical and thermal constraints, as shown in Table 2.1, so as not to cause any hardware damage to the engine and to make sure that the findings are relevant to real-use scenarios.

3.2.1 Description of Strategies

Four strategies, three for thermal management, one for fuel efficiency, at idle (800 RPM, 1.3 bar BMEP) are compared. This section describes the methodology for achieving each of the strategies, and the subsequent "Steady State Results" section quantitatively compares them. Figure 3.1 illustrates the representative intake and exhaust valve profiles, injection timings and heat release rates of the four strategies. Table 3.1 summarizes the valve timings, injection strategy, VGT settings and NOx mitigation philosophy for the strategies described in this section.

1. **Fuel Efficiency Baseline**: Conventional engine operation at idle incorporates two injection pulses near top dead center (TDC) to achieve high fuel efficiency, and elevated EGR fraction to reduce engine-out NOx. Figure 3.1(a) shows the location of the injections with respect to TDC, and the corresponding heat release rate. The nominal valve profiles used by the engine are also shown. This operation is hereafter referred to as fuel efficiency baseline (FE baseline).

2. **Thermal Management Baseline:** The conventional thermal management mode, hereafter referred to as the thermal management baseline (TM baseline) uses a fuel-path thermal management strategy incorporating four late injections

(per Figure 3.1(b)), and a mostly closed VGT nozzle. Nominal intake and exhaust valve profiles are used. The late injections result in delayed heat release, as shown in Figure 3.1(b). The mostly closed VGT nozzle increases the exhaust manifold pressure, elevating the pumping work. The delayed injections and elevated pumping work result in inefficient engine operation, requiring more fuel to maintain torque at idle, thereby increasing the turbine outlet temperature (TOT). In addition, the delayed injection strategy (a NOx reducer) eliminates the need for elevated EGR fractions to constrain NOx, such that both air and exhaust flow rates are higher. Elevated TOT and higher exhaust flow rate make TM baseline favorable for aftertreatment thermal management, as will be described in the "Steady State Results" section.

3. **Early Exhaust Valve Opening:** The implementation of early exhaust valve opening (EEVO), together with the same injection and VGT settings as the TM baseline strategy, further reduces engine efficiency, thereby increasing the required fueling, through a reduction in the effective expansion ratio. The result is an additional increase in engine-outlet temperature. As shown in Figure 3.1(c), the exhaust valve opening (EVO) was advanced while the exhaust valve closing (EVC) remained unchanged, increasing exhaust valve duration. The nominal intake valve profile was retained. Engine-out NOx emissions were controlled through modulation of the EGR fraction. Results from two EEVO settings with different AFRs are presented in the "Steady State Results" section in order to illustrate the trade-off between AFR, PM, NOx, exhaust flow rate, and fuel efficiency.

4. **Combination of Early Exhaust Valve Opening with Internal EGR via Negative Valve Overlap:** Per Figure 3.1(d), EEVO and negative valve overlap (NVO) were combined to decrease fuel efficiency, while implementing internal EGR (iEGR) for NOx control without needing external EGR. The aim with this strategy is to further increase engine-outlet temperatures via elimination

of heat loss from the external EGR path. The valve profiles, injection timings, and heat release of the implemented strategy are shown in Figure 3.1(d). The EVO was kept the same as that of the previously described EEVO strategy, and combined with early EVC (EEVC). The intake valve profile was phase-delayed, such that the duration of the intake valve profile remained unchanged, to avoid blowdown of the re-compressed exhaust gas into the intake manifold. External EGR was eliminated by shutting the EGR valve. The use of uncooled iEGR requires more dilution to control NOx, resulting in a low AFR, elevated engine outlet temperatures, and reduced exhaust flow rates. The VGT nozzle was opened further to avoid AFRs that are too low. The fuel injection strategy remained unchanged from TM baseline and EEVO strategies, as shown in Figure 3.1(d). Two EEVO+iEGR(NVO) settings with different AFR are presented in the "Steady State Results" section. Different AFRs were achieved through modulation of the amount of iEGR in order to illustrate the trade-off between AFR, PM, NOx, exhaust flow rate, and fuel efficiency.

3.2.2 Results and Discussion

Figure 3.2 compares the pressure-volume diagrams of the four strategies described. The FE baseline strategy has the smallest power and pumping loops due to the combination of early injections, open VGT and open EGR valve. The TM baseline strategy has a larger pumping loop as a result of the mostly closed VGT position which increases the exhaust manifold pressure. Late injections result in higher in-cylinder pressures at the end of the power stroke, which drive higher exhaust gas temperatures. The pumping loop for the EEVO strategies is slightly bigger than TM baseline due to blowdown of high pressure exhaust gas into the exhaust manifold. The EEVO+iEGR(NVO) strategies result in an increase in in-cylinder pressure during the exhaust stroke, due to re-compression of the trapped residual gas. The combination of EEVC with LIVO results in a 'gas spring' effect during the initial portion of

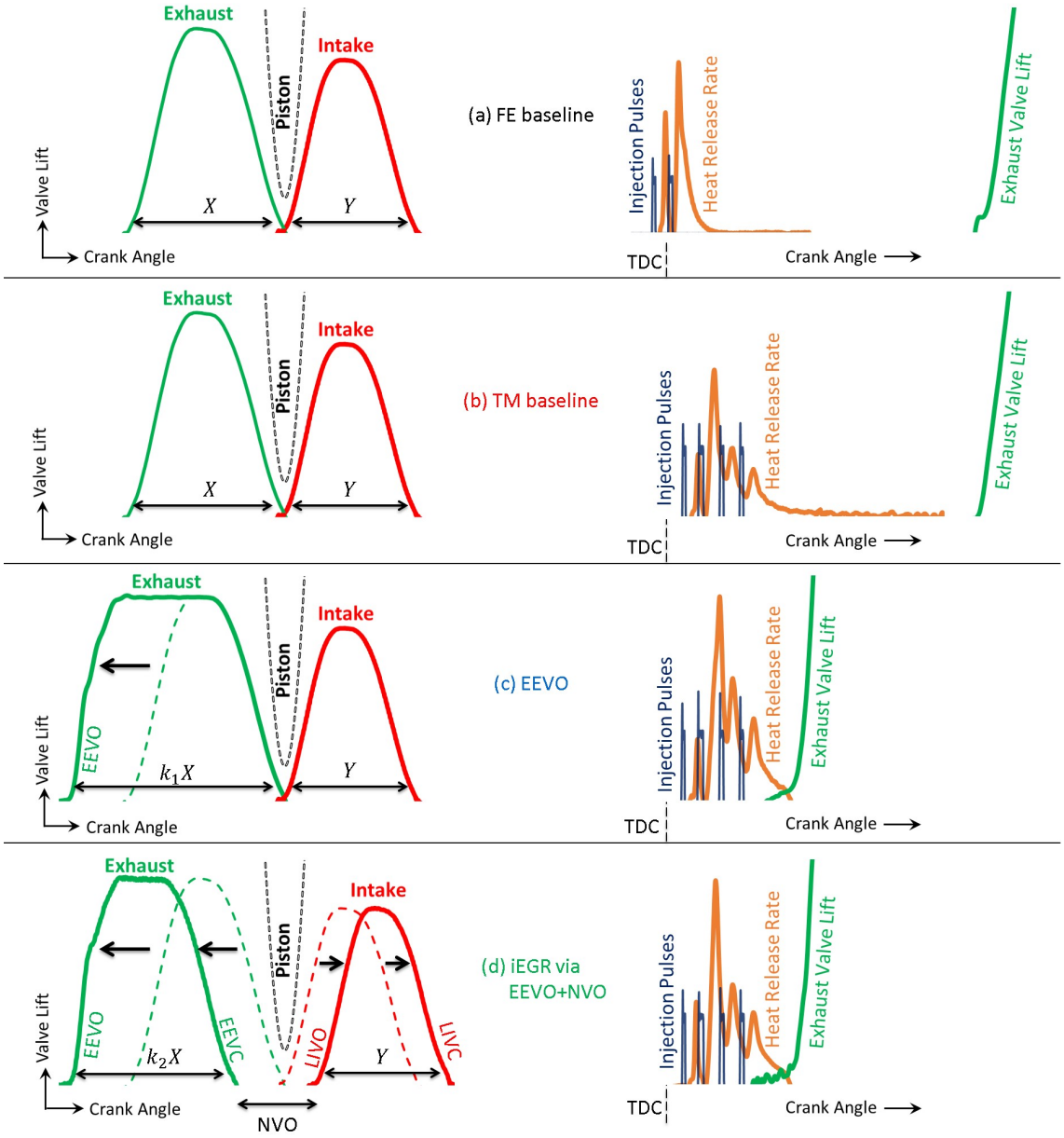

Figure 3.1. Valve profiles, injection timings and heat release rates for the aftertreatment warm-up strategies at idle, described in this section.

Table 3.1. Summary of the four strategies described in this work at idle.

Strategy	**Intake Valve**	**Exhaust Valve**	**Injection Strategy**	**VGT Position**	**NOx Mitigation**
FE Baseline	Nominal	Nominal	Two injections near TDC	Mostly closed	High EGR fraction
TM Baseline	Nominal	Nominal	Four late injections	Maximally closed	Low EGR fraction (due to late injections)
EEVO	Nominal	Early EVO, Nominal EVC	Four late injections	Maximally closed	EGR (higher than TM baseline)
EEVO + iEGR(NVO)	Phase-delayed	Early EVO, Early EVC	Four late injections	Open	High internal EGR (No external EGR)

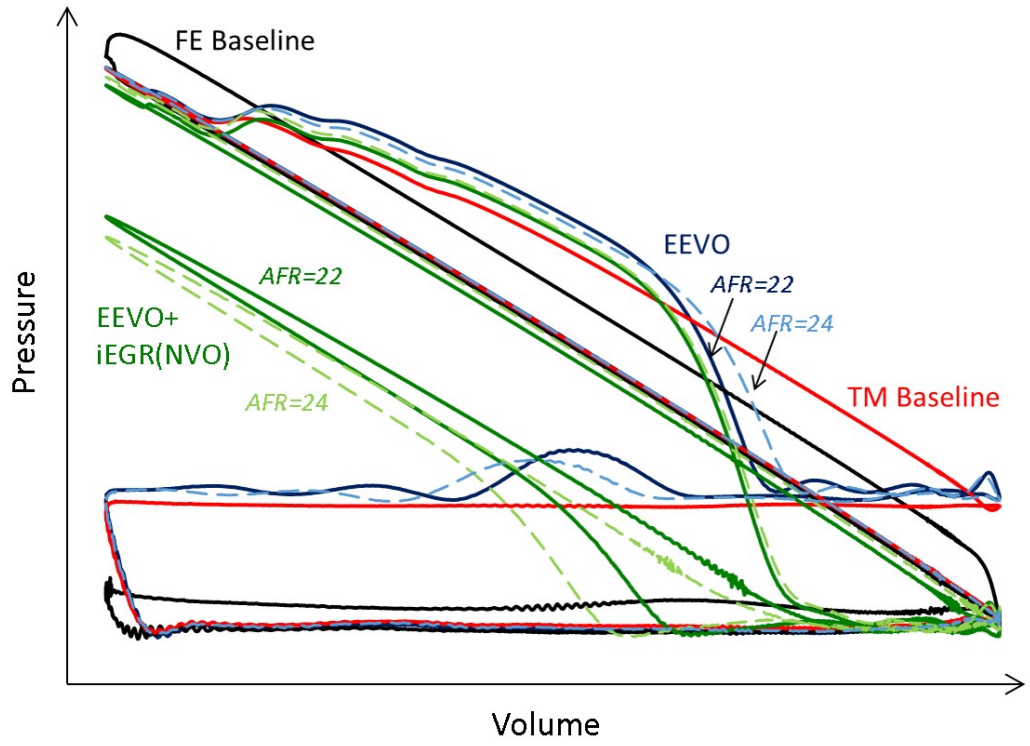

Figure 3.2. Logarithmic pressure-volume plots for the four aftertreatment warm-up strategies at idle.

the intake stroke, thereby reducing the pumping loop for the EEVO+iEGR(NVO) strategy. LIVC results in reduction of effective compression ratio, which results in lower in-cylinder pressure during the compression stroke for the EEVO+iEGR(NVO) strategy.

Figure 3.3 illustrates that the FE baseline exhibits a TOT of 140°C, which is notably lower than the desired aftertreatment component temperatures (>250°C), and consumes 37% less fuel than TM baseline. The TM baseline achieves a TOT of 255°C, which is close to the desired aftertreatment temperatures. The EEVO and iEGR strategies were implemented with AFRs of 22 and 24 to illustrate the trade-off between AFR, TOT, CCE, BTE, PM, and NOx. The EEVO strategies reach TOTs of 317°C and 346°C, and consume 42% and 56% more fuel than TM baseline, respectively. The EEVO+iEGR(NVO) strategies enable TOTs in excess of 380°C, at the

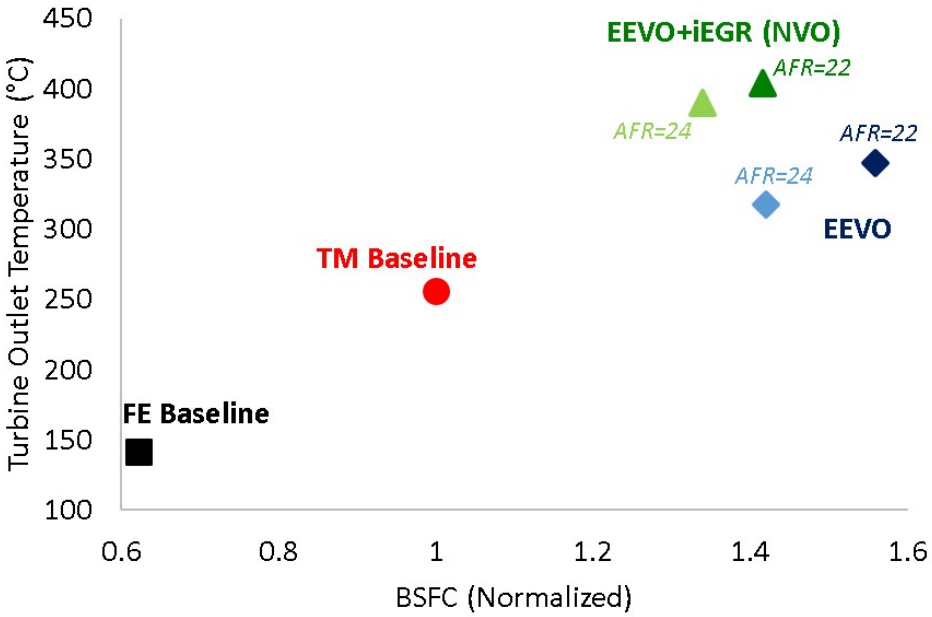

Figure 3.3. Turbine-outlet temperature vs fuel consumption (normalized) for aftertreatment warm-up strategies at steady state idle.

cost of 34% and 42% higher fuel consumption than TM baseline. The EEVO and EEVO+iEGR(NVO) strategies, owing to their higher steady state TOTs and comparable exhaust flow rates, therefore demonstrate potential for faster aftertreatment component warm up compared to the conventional TM baseline strategy.

The higher TOT of the EEVO and EEVO+iEGR(NVO) strategies can be explained by low air-to-fuel ratios (AFRs), as shown in Figure 3.4. The AFRs of FE baseline and TM baseline are 40 and 36, respectively. The two points for EEVO and EEVO+iEGR(NVO) strategies have AFRs of 24 and 22, each, with the lower AFR strategy in each case exhibiting higher TOT. Low AFRs with EEVO and EEVO+iEGR(NVO) strategies can be explained by higher fuel consumption and higher exhaust gas dilution required to control NOx. An increased amount of dilution is required with the EEVO+iEGR(NVO) strategies due to un-cooled iEGR,

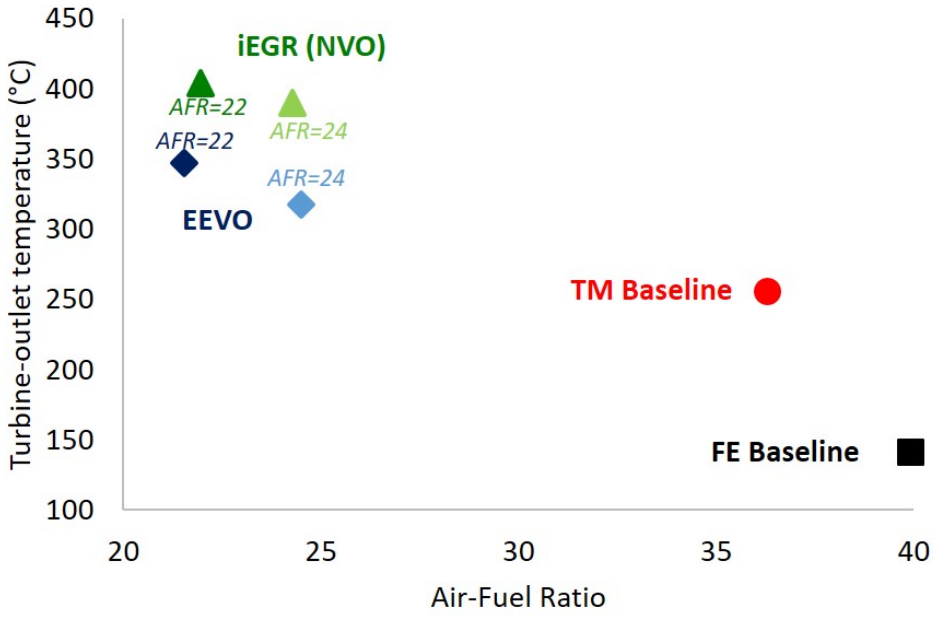

Figure 3.4. Turbine-outlet temperature vs air-fuel ratio for aftertreatment warm-up strategies at steady state idle.

which is not as effective as cooled EGR in controlling engine-out NOx (described below).

Figure 3.5 compares the brake thermal efficiency, and open and closed cycle efficiencies of the four strategies. The FE baseline has 60% higher BTE than TM baseline, as a result of 52% higher OCE and 5.4% higher CCE. Lower OCE of TM baseline can be explained by the increased pumping work (consistent with larger pumping loop in Figure 3.2) as a result of a mostly closed VGT position, and lower CCE is a result of the late injection strategy. The EEVO strategy with lower AFR (AFR=22) has 36% lower BTE than TM baseline, as a result of a 6% lower OCE due to a bigger pumping loop, and 30% lower CCE due to early blowdown. EEVO with higher AFR (AFR=24) has 30% lower BTE than TM baseline as a result of 5% lower OCE and 25% lower CCE.

The EEVO+iEGR(NVO) strategy with lower AFR (AFR=22) has 29% lower BTE than TM baseline. The OCE is 42% higher, given the open VGT position and the 'gas

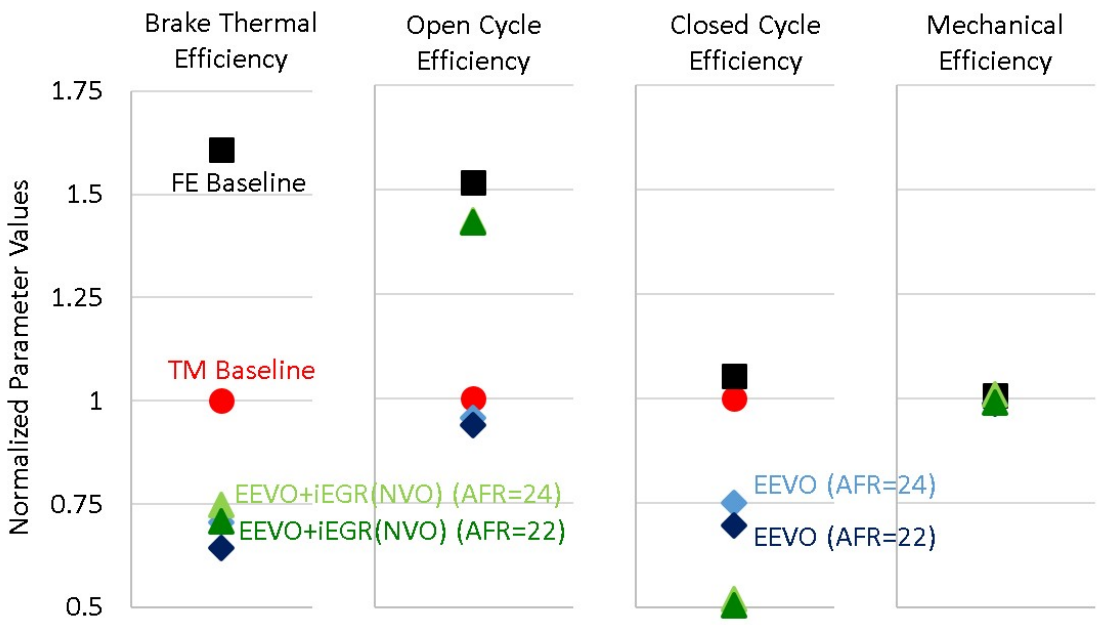

Figure 3.5. Brake thermal efficiency, and open cycle, closed cycle and mechanical efficiencies for aftertreatment warm-up strategies at steady state idle.

spring' effect caused by the re-compressed exhaust gas during the intake stroke, both of which result in a smaller pumping loop. The CCE is 50% lower, due to a greater quantity of internal EGR and consequently higher heat loss from the cylinder. EEVO, which is used as a part of the EEVO+iEGR(NVO) approach, also contributes to the lower CCE. Similarly, the EEVO+iEGR(NVO) strategy with higher AFR (AFR=24) has 25% lower BTE than TM baseline, as a result of 43% higher OCE and 48% lower CCE. In contrast to the TM baseline and EEVO strategies, which rely on reduction in OCE to drive elevated TOT, the EEVO+iEGR(NVO) strategies have low CCE and high OCE. Mechanical efficiency is fairly consistent among these strategies, as shown.

Per Figure 3.6, similar engine-out NOx for all strategies was targeted through modulation of the EGR or iEGR fractions. The FE baseline requires an elevated EGR fraction due to early fuel injections which promotes elevated NOx. The TM baseline

strategy is able to achieve similar NOx levels with a 17% lower EGR fraction than FE baseline, due to its late injection strategy. The EGR fraction reduction results in higher fresh air flows, and consequently, higher exhaust flow rate (per Figure 3.7). The EEVO strategies require higher EGR fractions to achieve the same NOx due to higher injected fuel mass, as a result of which the exhaust flow rates are slightly lower. iEGR is not quite as effective in reducing engine-out NOx as cooled EGR, as the iEGR gas is "hot". The EEVO+iEGR(NVO) strategy with higher AFR, which has lower trapped residual exhaust gas, has higher NOx due to lower dilution of in-cylinder charge, while the EEVO+iEGR(NVO) strategy with lower AFR has NOx level close to that of TM baseline. Higher residual exhaust gas for the EEVO+iEGR(NVO) strategies, in addition to late IVO, also reduces the volumetric efficiency, resulting in lower fresh air and exhaust flow rates.

PM emissions of the thermal management strategies are higher than the FE baseline strategy, with the TM baseline showing ∼8 times higher PM, as illustrated in Figure 3.6. The EEVO and EEVO+iEGR(NVO) strategies with AFR=24 have ∼6 and ∼8 times higher PM than TM baseline, respectively, while those with AFR=22 emit ∼12 and ∼18 times higher PM. The large amount of hot residual exhaust gas in the EEVO+iEGR(NVO) strategy contributes to the high PM production at steady state. It is shown later in this chapter that the amount of PM generated during idle is relatively low compared to higher speed and load conditions; therefore, the increase in cumulative PM generated over the EEVO+iEGR(NVO) drive cycle is not as pronounced.

Figure 3.8 describes an alternate approach to understanding the fuel consumption, TOT and exhaust flow rate trends, using the first law energy analysis illustrated by Figure 2.5 and Equations (2.5)-(2.12). The total fuel consumption of each strategy is shown, and categorized into energy expended into brake work, exhaust heat, pumping loss, heat loss through the cylinders, heat rejection to the EGR cooler, and other thermal and mechanical losses. The brake power of all strategies is the same, corresponding to the same operating condition (curb idle). The exhaust gas energy in FE

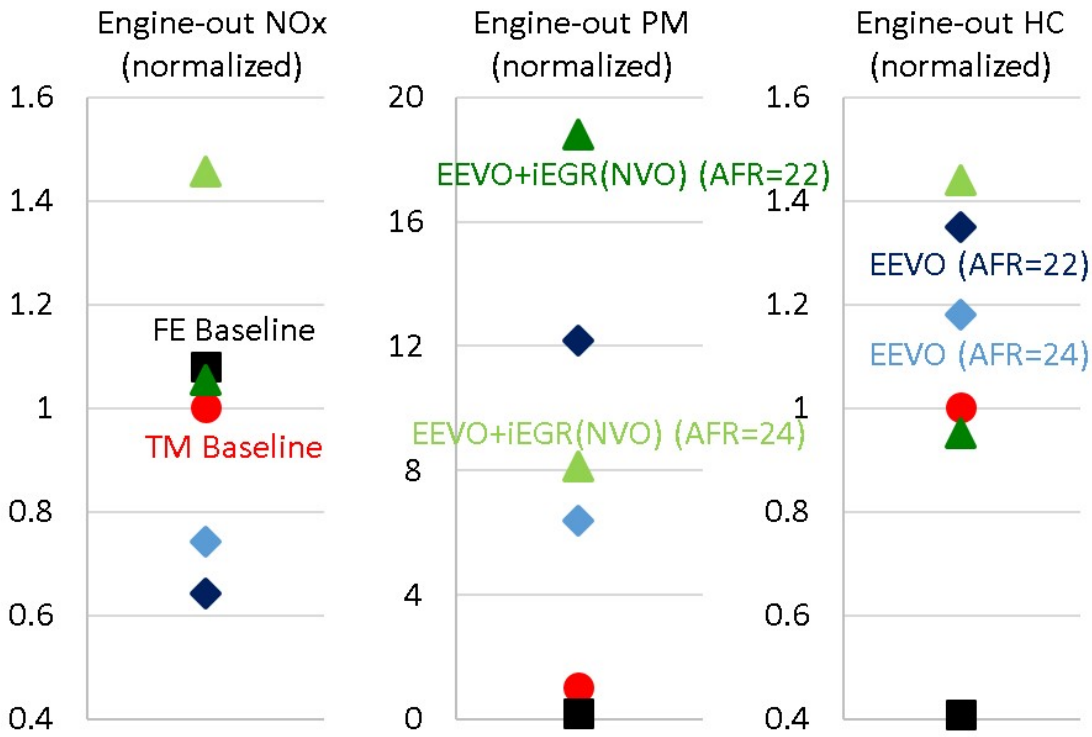

Figure 3.6. Engine-out NOx, PM and HC emissions, and EGR fraction, for aftertreatment warm-up strategies at steady state idle.

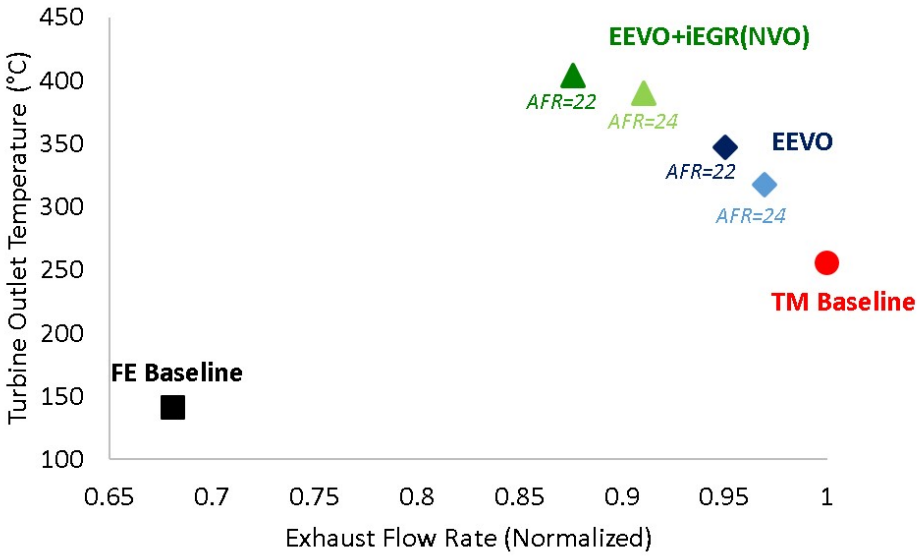

Figure 3.7. Turbine-outlet temperature vs exhaust flow rate for aftertreatment warm-up strategies at steady state idle.

baseline is 68% lower than TM baseline, due to the lower TOT and exhaust flow rate. The EEVO strategies with high and low AFRs produce 25% and 36% higher exhaust heat than TM baseline, respectively, as a result of elevated TOT, while both the EEVO+iEGR(NVO) strategies produce 49% higher exhaust heat than TM baseline, and 24% and 13% higher than the EEVO strategies, despite having lower exhaust flow rate. The exhaust flow rates for both the EEVO+iEGR(NVO) strategies compensate for the differences in TOT to yield the same exhaust heat. As described earlier, the pumping losses are lower for the EEVO+iEGR(NVO) strategies as compared to the EEVO and TM baseline strategies due to the more open VGT position. The in-cylinder heat losses are higher for the EEVO+iEGR(NVO) strategies than the EEVO strategies due to the un-cooled trapped gases rejecting more heat through the cylinder walls, with the lower AFR EEVO+iEGR(NVO) strategy showing higher heat loss due to a greater quantity of trapped residual gas. Higher in-cylinder heat losses for the EEVO+iEGR(NVO) strategies are more than compensated for by the absence of heat rejection to the EGR cooler (due to the absence of external EGR), and lower pumping losses, which make the EEVO+iEGR(NVO) strategies more fuel efficient than EEVO while maintaining higher exhaust heat rates.

Figure 3.9 shows an alternate representation of the first law analysis, where the energy transferred to the exhaust gas is plotted against injected fuel energy. The dotted contours represent the percentage of the injected fuel energy that leaves the engine via the exhaust gas flow. A higher percentage, along with higher fuel energy, yields a higher exhaust gas energy, which is generally preferable for exhaust thermal management. The EEVO+iEGR(NVO) strategies show the highest conversion of fuel energy to exhaust heat ($\sim$22% and 24%), followed by TM baseline ($\sim$20%). The conversion efficiency of the EEVO strategies is lower than TM baseline due to higher losses ($\sim$18%), although the exhaust energy is higher on account of higher fuel consumption for the EEVO approach. FE baseline, which is most fuel efficient, results in approximately 10% of the injected fuel energy in the exhaust stream heat.

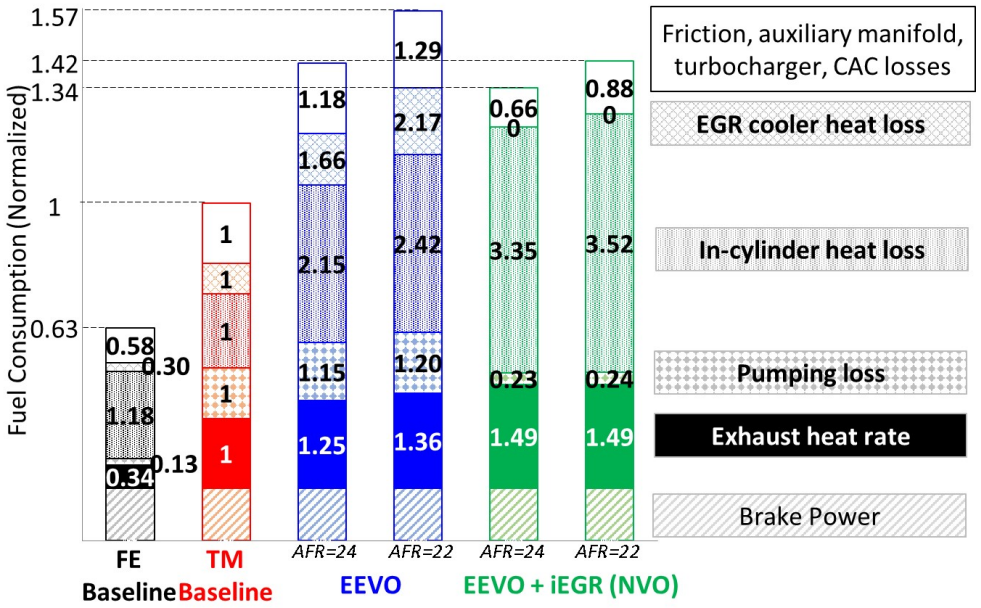

Figure 3.8. First law analysis for aftertreatment warm-up strategies at steady state idle.

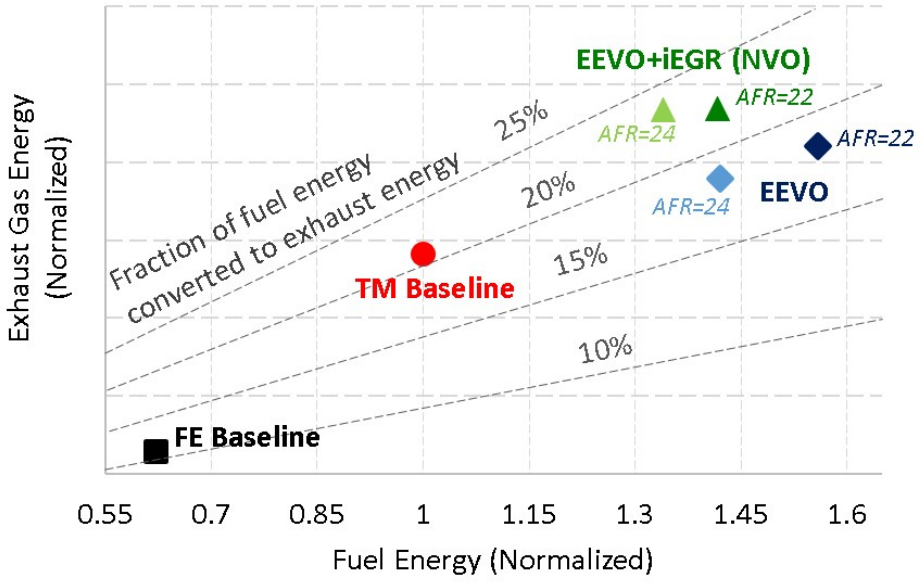

Figure 3.9. Fraction of fuel energy being converted to exhaust energy, for aftertreatment warm-up strategies at steady state idle.

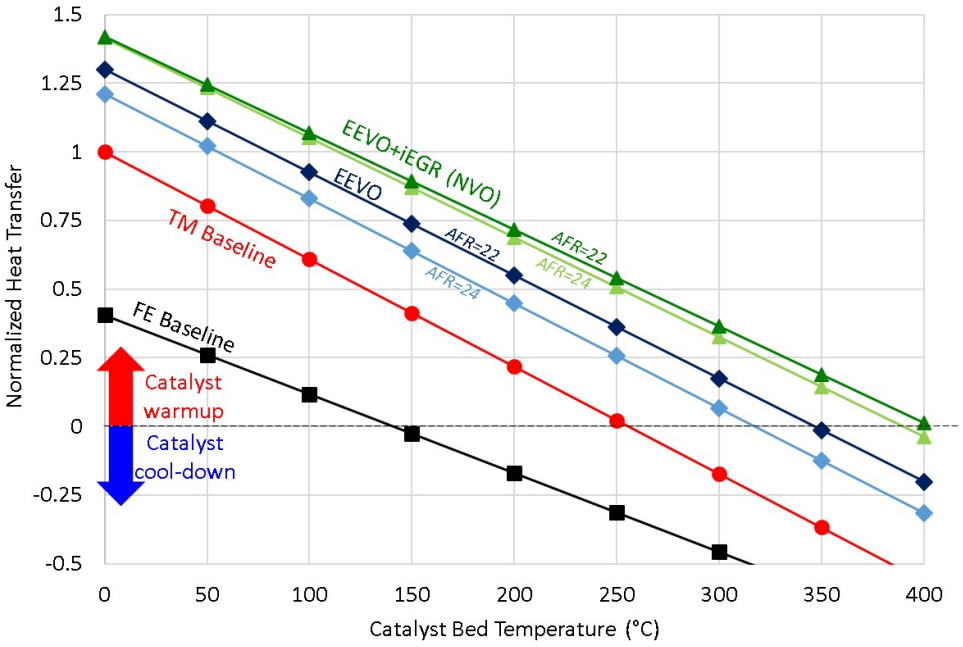

Figure 3.10. Normalized heat transfer rates for the aftertreatment warm-up strategies at different lumped catalyst bed temperatures.

Aftertreatment thermal management depends both on turbine outlet temperature and exhaust flow rate. The exhaust gas energy represented in Figures 3.8 and 3.9 does not take into account the dynamic temperature variation of the aftertreatment system. The impact of exhaust flow rate and TOT on warm up of the aftertreatment system can be understood using a 'normalized heat transfer' analysis.

Figure 3.10 compares the normalized heat transfer rates (described in section 2.2.3) for the six strategies. The EEVO+iEGR(NVO) strategies show the highest heat transfer, followed by the EEVO and TM baseline strategies. Both the high and low AFR EEVO+iEGR(NVO) strategies display similar heat transfer rates at lower catalyst temperatures which are more representative of the 'warm up' phase, while they diverge at higher catalyst temperatures where the effect of TOT becomes more dominant. The EEVO strategy with lower AFR shows higher heat transfer than EEVO with higher AFR as a result of its elevated TOT and similar exhaust flow rates.

It may therefore be concluded that EEVO+iEGR(NVO) shows the best potential for accelerating the warm up of the SCR catalyst owing to its high TOT and comparable exhaust flow rate, with lower fuel consumption than EEVO, at idle operation. The following section demonstrates the implementation of EEVO+iEGR(NVO) at idle over the HD-FTP drive cycle.

Table 3.2. Settings/calibrations used over the HD-FTP for various drive cycles.

Drive cycle	**Idle operation**	**Other operating conditions**
FE baseline cycle	FE baseline	FE baseline calibration
TM baseline cycle	TM baseline	TM baseline calibration
iEGR cycle	EEVO + iEGR(NVO)	TM baseline calibration

3.3 Implementation of Early Exhaust Valve Opening and Internal EGR at Idle over the HD-FTP Drive Cycle

3.3.1 Methodology

EEVO+iEGR(NVO) was implemented at all curb idle regions of the cold-start HD-FTP cycle, and during the first 600 seconds of the hot-start cycle, as represented by the shaded regions in Figure 3.11, to maximize the SCR outlet gas temperature during both the drive cycles. While both the iEGR strategies described earlier are expected to display similar SCR warm up characteristics, as shown in Figure 3.10, the low-AFR EEVO+iEGR(NVO) strategy was implemented over the drive cycle as a result of the lower steady state NOx emissions. The engine was operated in the stock thermal management calibration over all other operating conditions for the iEGR and TM baseline drive cycles. The FE baseline drive cycle was run with the best fuel consumption settings both at idle and other operating conditions. Table 3.2 summarizes the operating calibrations used by the three drive cycles at idle and non-idle operating conditions.

3.3.2 Results and Discussion

Turbine-outlet temperatures achieved during the three drive cycles are shown in Figure 3.12. The EEVO+iEGR(NVO) strategy results in the highest TOT when implemented at curb idle, followed by the TM baseline and FE baseline strategies,

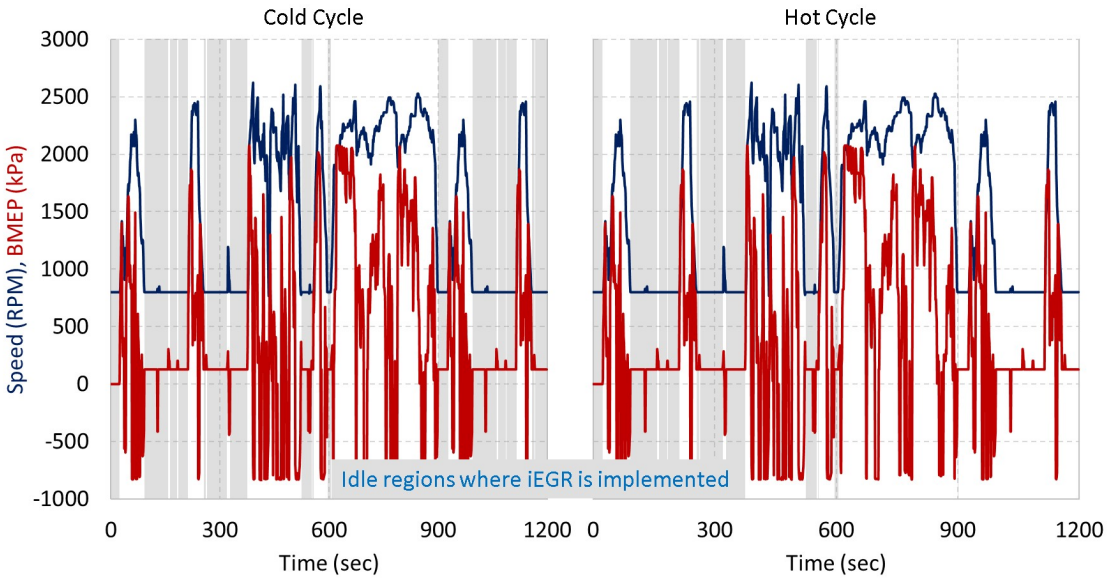

Figure 3.11. HD-FTP speed and torque profile, with shaded regions indicating where EEVO+iEGR(NVO) was implemented.

consistent with the steady state results shown in Figure 3.3. EEVO+iEGR(NVO) also shows higher TOT at other operating conditions as a result of heating up the engine block, exhaust manifold, and turbo-charger more quickly. It can be observed that the TOT for the TM baseline strategy reduces during curb idle regions of the drive cycle, thereby cooling the engine, while the TOT for the EEVO+iEGR(NVO) drive cycle increases towards its steady state TOT, and continues to heat up the engine block. As a result, higher TOTs are maintained at subsequent non-idle conditions even though the EEVO+iEGR(NVO) strategy is not being implemented at all operating conditions. Although the steady state TOT is not reached during any of the curb idle regions, it may be observed that the TOT increases faster for strategies having higher steady state TOT.

Figure 3.13 demonstrates that the EEVO+iEGR(NVO) and TM baseline thermal management strategies outperform the FE baseline with regard to the SCR outlet gas temperature. The EEVO+iEGR(NVO) drive cycle shows higher SCR outlet gas temperature between ∼450 and ∼750 seconds of the cold cycle, and between ∼100 and ∼800 seconds of the hot cycle, although the increase in the SCR outlet gas temperature is not as pronounced as the increase in TOT. The SCR outlet temperature at the beginning of the hot cycle increases faster for the EEVO+iEGR(NVO) cycle as compared to the TM baseline cycle as a result of a greater quantity of heat trapped in the SCR catalyst at the end of the cold cycle.

Figure 3.14 shows the estimated SCR conversion efficiency corresponding to the predicted SCR temperature. Peak SCR efficiency is achieved when the SCR temperature reaches 300°C, which occurs around 670 seconds into both the cold and hot drive cycles. The EEVO+iEGR(NVO) strategy shows higher SCR conversion efficiency during the regions mentioned above when the SCR outlet gas temperature is higher.

The measured cumulative engine-out NOx and predicted cumulative tailpipe-out NOx over both the cold and hot drive cycles are shown in Figure 3.15. The predicted tailpipe-out NOx is the same as engine-out NOx until approximately 450 seconds

in the cold cycle since the SCR has not yet reached sufficient temperatures to operate efficiently, per Figures 3.13 and 3.14, after which the cumulative tailpipe-out NOx becomes almost constant due to higher SCR conversion efficiencies. Although the EEVO+iEGR(NVO) strategy has slightly higher engine-out NOx than the TM baseline drive cycle, better SCR warm up with EEVO+iEGR(NVO) results in higher conversion efficiency, as a result of which the predicted tailpipe-out NOx is the lowest. It may therefore be concluded that using EEVO+iEGR(NVO) at idle operation allows reduction of tailpipe-out NOx to levels not achievable via conventional engine operation, through faster warm up of the aftertreatment system. The FE baseline drive cycle has higher engine-out NOx than the TM baseline cycle due to the earlier injection timings at all operating conditions, which trades off an increase in engine-out NOx for a reduction in fuel consumption.

The EEVO+iEGR(NVO) strategy with AFR of 22 has been shown to emit $\sim$18 times higher PM than the TM baseline strategy at steady state curb idle operation, as illustrated in Figure 3.6. However, Figure 3.16 demonstrates that the cumulative increase in PM over the cold and hot cycles is only $\sim$ 6.8%. This is a result of low exhaust flow rates during idle operation, which reduces the impact of elevated idle PM over the drive cycle. Increased engine-outlet PM is undesirable, however, it is straightforward to perform an active, or passive regeneration, albeit with a fuel penalty. The DPF can trap PM without reaching elevated temperatures; therefore, engine-out PM will not reach the tailpipe when the aftertreatment system is cold, unlike the SCR system which requires warm up for efficient NOx conversion.

Figure 3.17 shows the additional fuel consumption required to achieve the predicted reduction in tailpipe-out NOx, with respect to the TM baseline operation. The EEVO+iEGR(NVO) drive cycle consumes most fuel, followed by TM baseline and FE baseline cycles. The difference between TM baseline and FE baseline drive cycles occurs throughout the cycle as the FE baseline cycle uses a more fuel efficient calibration both at idle as well other operating conditions. The difference in fuel consumption between the TM baseline and EEVO+iEGR(NVO) cycles occurs only

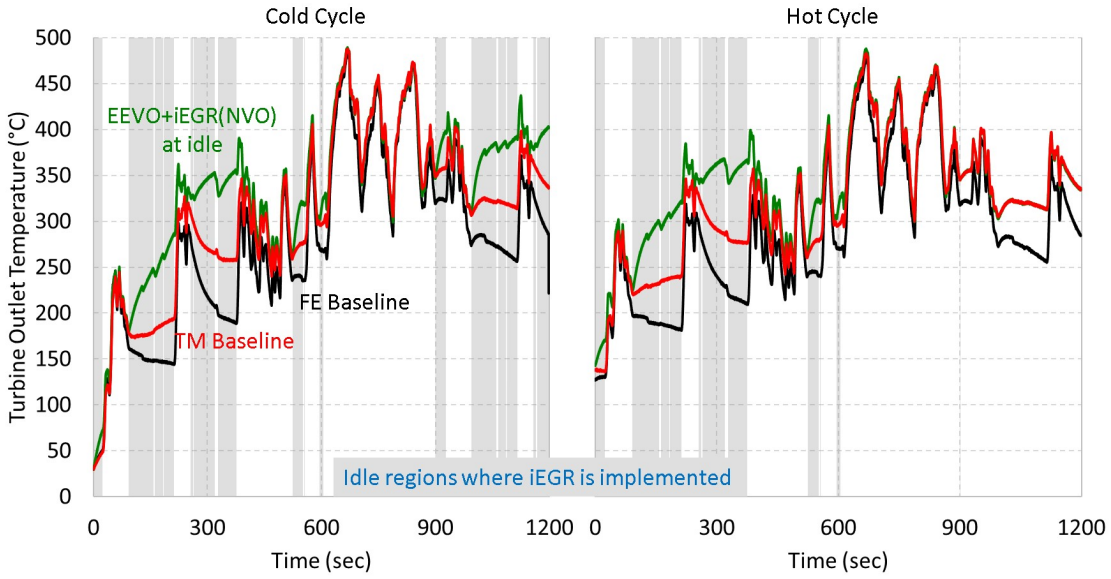

Figure 3.12. Turbine-outlet temperature over the HD-FTP for the aftertreatment warm-up strategies.

during idle regions where EEVO+iEGR(NVO) is implemented, consistent with the steady state curb idle results from Figure 3.3, since the same TM baseline strategy is implemented at all non-idle operating conditions. The net weighted fuel consumption increase is 2.1% for the EEVO+iEGR(NVO) drive cycle.

The trade-off curves among cumulative predicted tailpipe-out NOx, fuel consumption and engine-out PM produced at the end of both drive cycles are shown in Figures 3.18(a) and 3.18(b). Figure 3.18(a) demonstrates that the EEVO+iEGR(NVO) drive cycle enables tailpipe-out NOx levels lower than that possible via conventional means, lying on the same trade-off curve between the two baseline drive cycles. Specifically, the TM baseline strategy of delayed injections and mostly closed VGT reduces predicted tailpipe-out NOx by 36% from the fuel efficient FE baseline operation, by consuming 6% higher fuel, which is inevitable with conventional 6-cylinder operation to meet the current emission regulations. Implementation of EEVO+iEGR(NVO) at idle operation during the 'warm up' phase further reduces tailpipe-out NOx by 7.9%, with consumption of 2.1% more fuel over the drive cycle. Figure 3.18(b) shows the

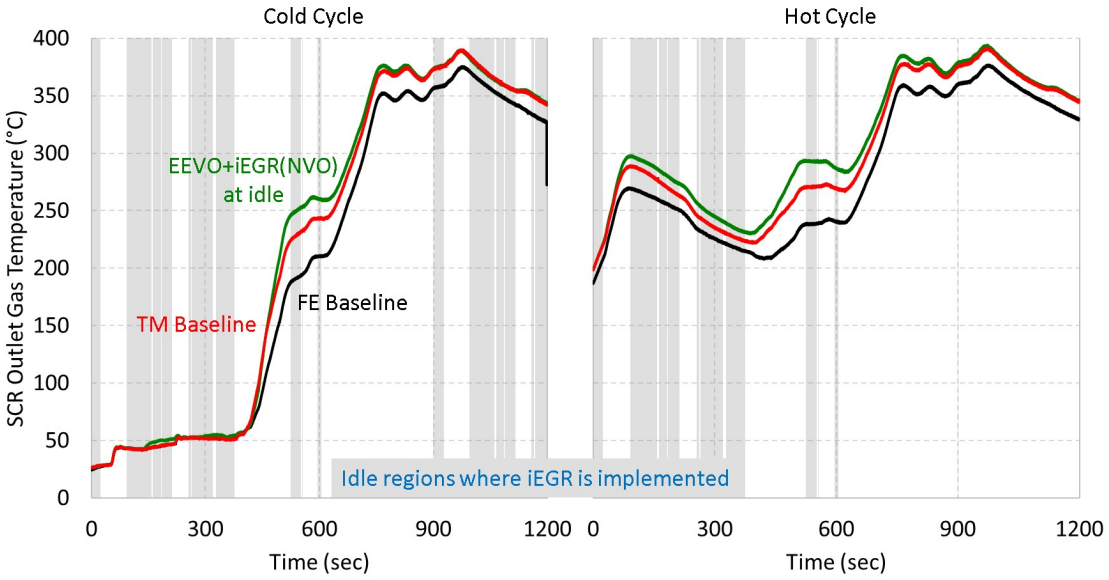

Figure 3.13. SCR outlet gas temperature over the HD-FTP for the aftertreatment warm-up strategies.

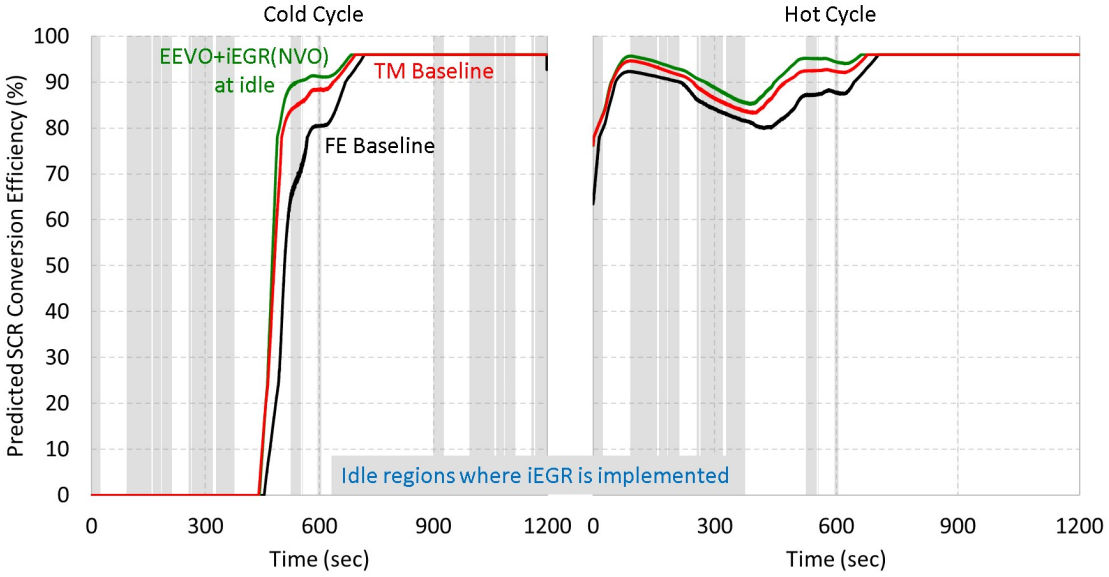

Figure 3.14. Predicted SCR conversion efficiency over the HD-FTP for the aftertreatment warm-up strategies.

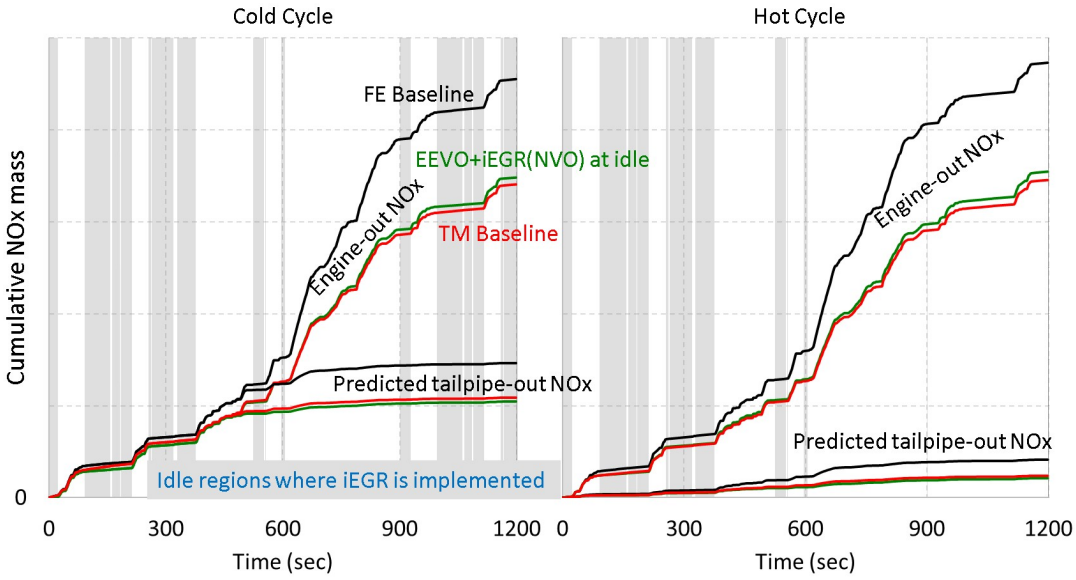

Figure 3.15. Engine-out and tailpipe-out NOx emissions over the HD-FTP for the aftertreatment warm-up strategies.

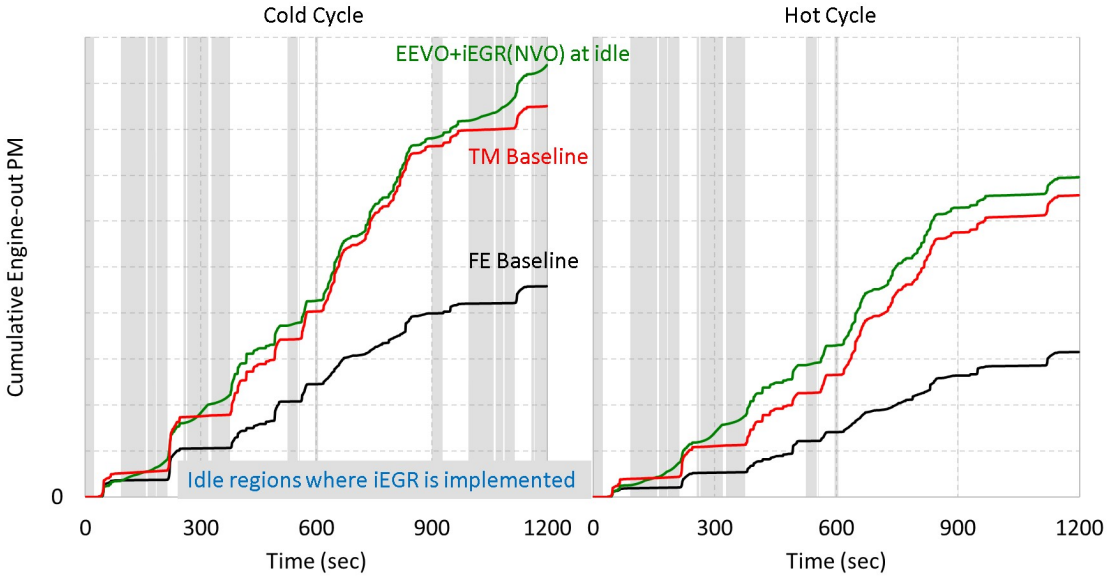

Figure 3.16. Engine-out PM emissions over the HD-FTP for the aftertreatment warm-up strategies.

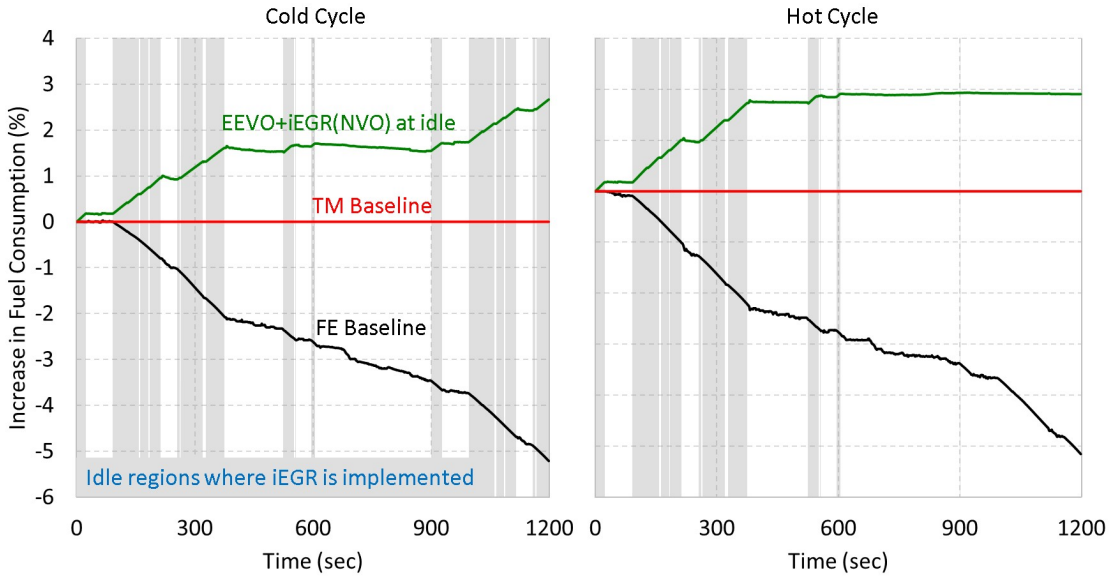

Figure 3.17. Increase in fuel consumption with respect to TM baseline cycle, over the HD-FTP for the aftertreatment warm-up strategies.

trade-off between predicted tailpipe-out NOx and engine-out PM, demonstrating that the EEVO+iEGR(NVO) drive cycle increases engine-out PM emissions by 6.7% over both the cycles for a 7.9% reduction in tailpipe-out NOx.

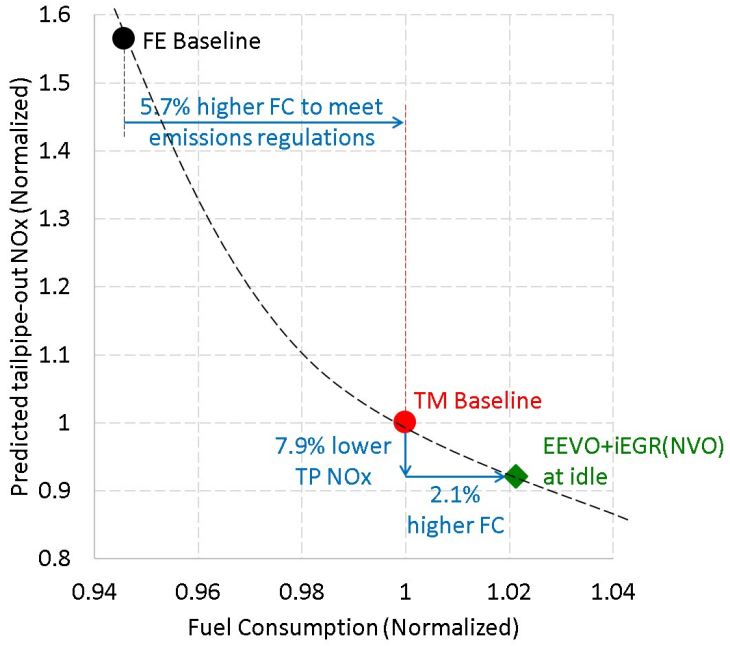

(a)

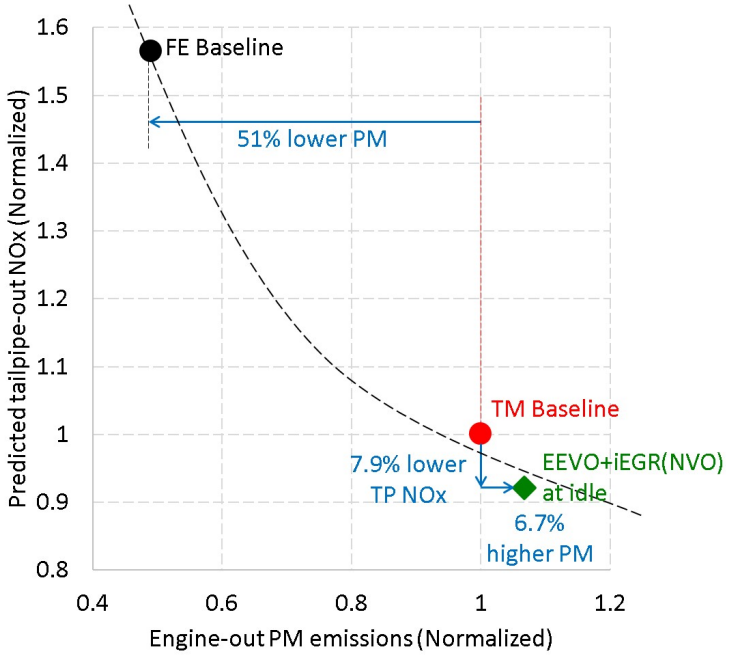

(b)

Figure 3.18. Trade-off between fuel consumption, tailpipe-out NOx and engine-out PM emissions over the combined HD-FTP drive cycle for the aftertreatment warm-up strategies.

3.4 Aftertreatment warm-up Strategies at Off-Idle Operating Conditions

3.4.1 Introduction and Methodology

This section presents the aftertreatment warm-up thermal management performance achievable via implementation of advanced gas exchange strategies at off-idle operating conditions. Specifically, a combination of early exhaust valve opening (EEVO) and late intake valve closure (LIVC) was implemented at all loads below 7.6 bar BMEP throughout the cold start drive cycle and up to 600 seconds in the hot start drive cycle. The combination of EEVO and LIVC was expected to demonstrate favorable warm-up characteristics because:

- EEVO is expected to result in higher TOTs, consistent with the results observed at idle operation.
- LIVC at high speed engine operation is expected to increase volumetric efficiency due to dynamic charging, as demonstrated by Vos et al. [54, 55]. Higher airflow resulting from higher volumetric efficiencies increases exhaust flow rate, which is an important factor for aftertreatment warm-up.

The valve profiles for this strategy are shown in Figure 3.19. The warm-up strategy described in sections 3.2 and 3.3, namely EEVO + iEGR(NVO), was implemented during the corresponding idle sections to implement the most aggressive warm-up strategy at both idle and off-idle conditions. Figure 3.20 describes the regions over the HD-FTP where the idle and off-idle warm-up strategies are implemented. The yellow shaded regions correspond to the implementation of EEVO+LIVC at off-idle conditions, and the grey shaded regions correspond to implementation of EEVO+iEGR(NVO) at idle operation. These strategies will be referred to as "idle warm-up strategy" and "off-idle warm-up strategy" for the reminder of this section.

Figures 3.21- 3.27 compare the performance of three drive cycle strategies- (i) TM baseline drive cycle, (ii) drive cycle implementing only the idle warm-up strategy, and

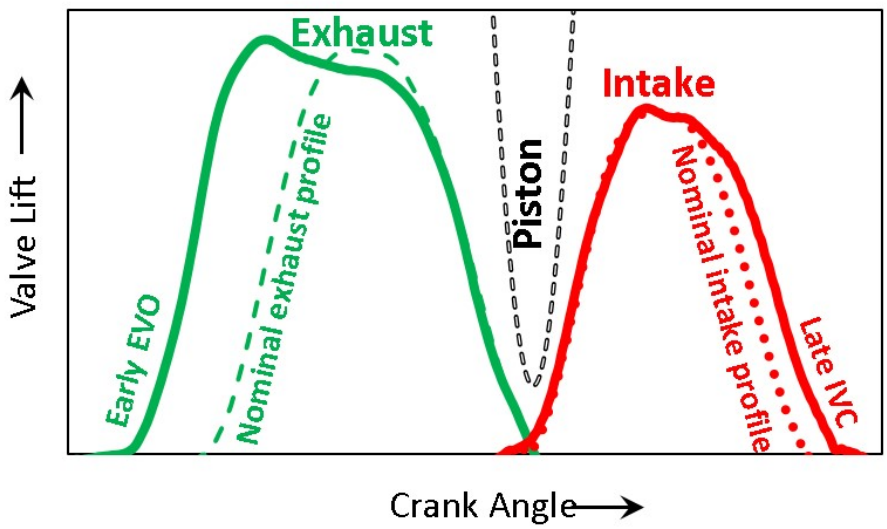

Figure 3.19. Valve profiles for the 'EEVO+LIVC' strategy implemented at off-idle drive cycle operation.

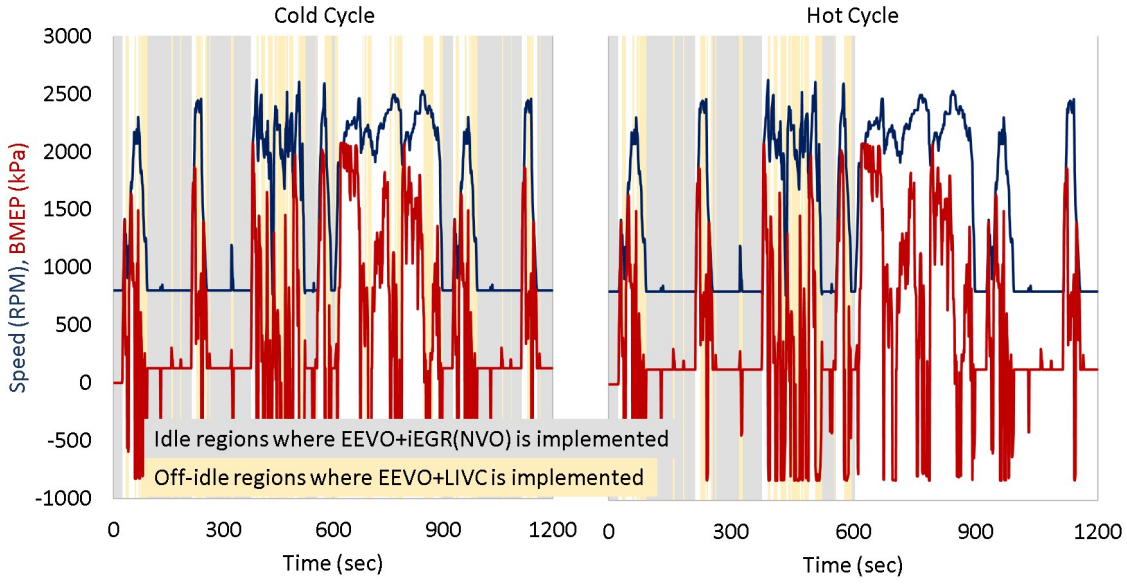

Figure 3.20. EEVO+LIVC is implemented at off-idle operation below 7.6 bar BMEP, represented by the yellow regions.

(iii) drive cycle implementing a combination of idle and off-idle warm-up strategies. A comparison between drive cycles (ii) and (iii) above presents the additional thermal management benefits shown by implementation of the EEVO+LIVC off-idle warm-up strategy.

3.4.2 Results and Discussion

Figure 3.21 compares the turbine outlet temperatures of the three drive cycle strategies. The drive cycle implementing both the idle and off-idle warm-up strategies shows higher TOT, not only during the off-idle regions below 7.6 bar BMEP (represented by yellow shaded portions), but also during the idle regions. Higher TOT during idle operation can be attributed to the engine block having been heated to higher temperatures during off-idle conditions, thereby resulting in lower heat loss.

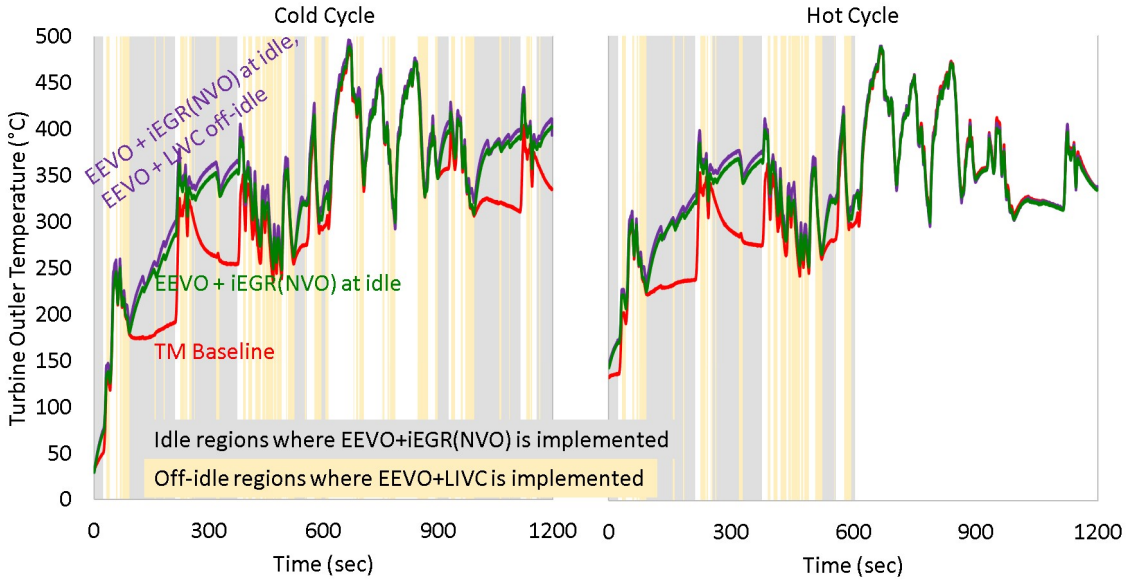

Figure 3.21. Turbine outlet temperatures over the cold start and hot start HD-FTP duty cycle upon implementation of idle and off-idle warm-up strategies.

Figure 3.22 compares the temperature of the exhaust gas at the inlet and outlet of the SCR for the three drive cycles. The drive cycle with both idle and off-idle warm-up strategies shows higher temperatures both at the inlet and the outlet of the SCR, indicating higher mean SCR catalyst temperature. Higher catalyst temperatures are a result of higher TOT via implementation of EEVO+LIVC, as shown in Figure 3.21, and higher exhaust flow rates. Figure 3.23 shows the predicted SCR efficiency based on the measured SCR outlet gas temperature (Figure 3.22) and the SCR efficiency curve shown in Figure 2.8. Higher SCR efficiency is predicted for the drive cycle whereboth idle and off-idle warm-up strategies are implemented.

Figure 3.24 shows the cumulative engine-out NOx and predicted tailpipe-out NOx over the cold start and hot start drive cycles. Slightly higher engine-out NOx is observed during the cold cycle when both idle and off-idle warm-up strategies are implemented, as the EGR fractions at the corresponding off-idle operating conditions remain unchanged from their baseline targets, which is not optimal for the warm-up strategy. However, the predicted tailpipe-out NOx is similar due to more efficient

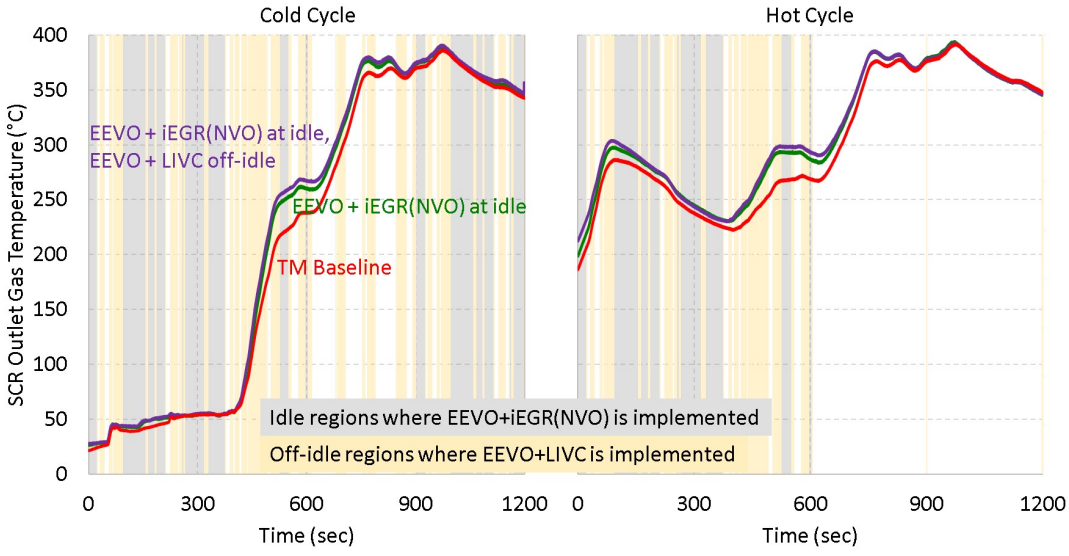

Figure 3.22. Temperature of the exhaust gas at the outlet of the SCR over the cold start and hot start HD-FTP duty cycle.

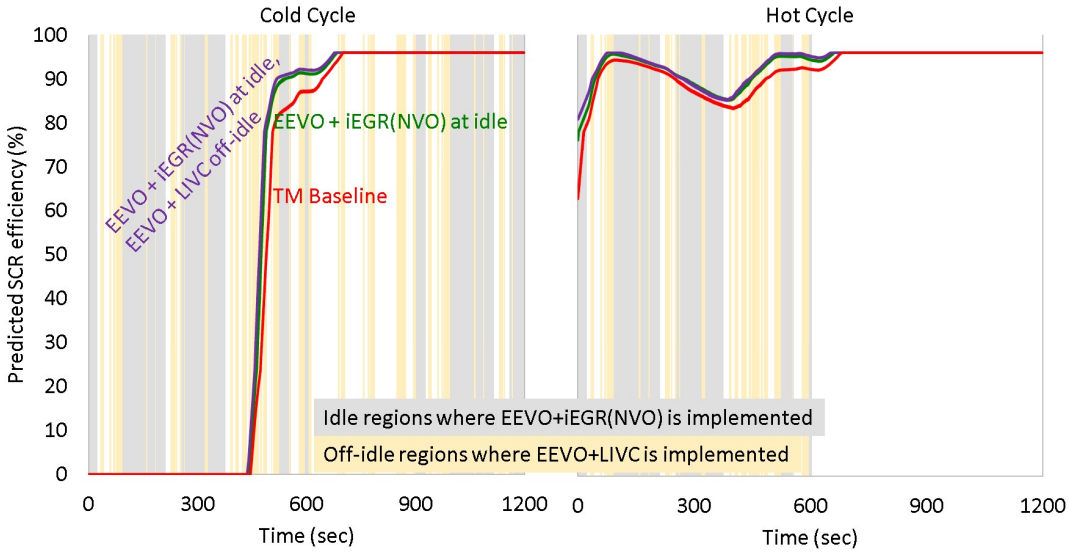

Figure 3.23. Predicted SCR conversion efficiency over the drive cycle based on SCR outlet gas temperature over the cold start and hot start HD-FTP duty cycle.

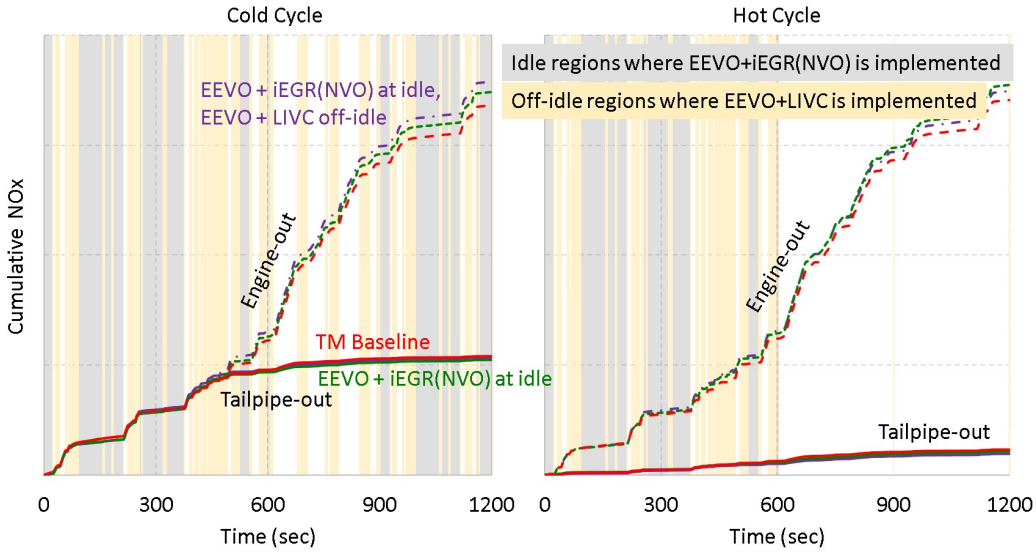

Figure 3.24. Cumulative engine-out NOx and predicted tailpipe-out NOx emissions over the cold start and hot start HD-FTP duty cycle.

predicted SCR conversion efficiencies for the cold start drive cycle. Lower tailpipe-out NOx is predicted during the hot start cycle for the drive cycle implementing both idle and off-idle warm-up strategies, as a result of more efficient predicted SCR operation.

Figure 3.25 shows the cumulative engine-out PM emissions for the three drive cycle strategies. The drive cycle implementing the off-idle warm-up strategy shows significantly higher PM flow rates than both the idle warm-up, and baseline, strategies, over both the cold start and hot start drive cycles. The cumulative PM emissions curve is steeper during implementation of EEVO+LIVC at off-idle operation (yellow-shaded regions), justifying that the implementation of the off-idle warm-up strategy leads to higher PM emissions over the drive cycle. The cumulative drive cycle PM emissions, when both idle and off-idle strategies are implemented, are 38% higher than the TM baseline drive cycle, with 32% of the additional PM emissions a result of the off-idle warm-up strategy.

Figure 3.26 shows the relative increase in fuel consumption as a result of the idle and off-idle warm-up strategies, with respect to the TM baseline drive cycle. An

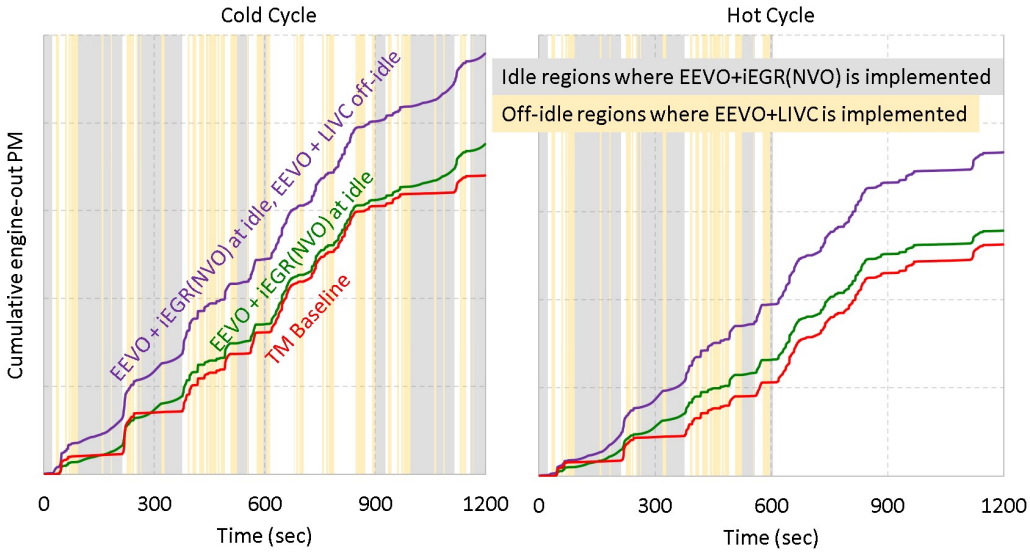

Figure 3.25. Cumulative engine-out PM emissions over the cold start and hot start HD-FTP duty cycle.

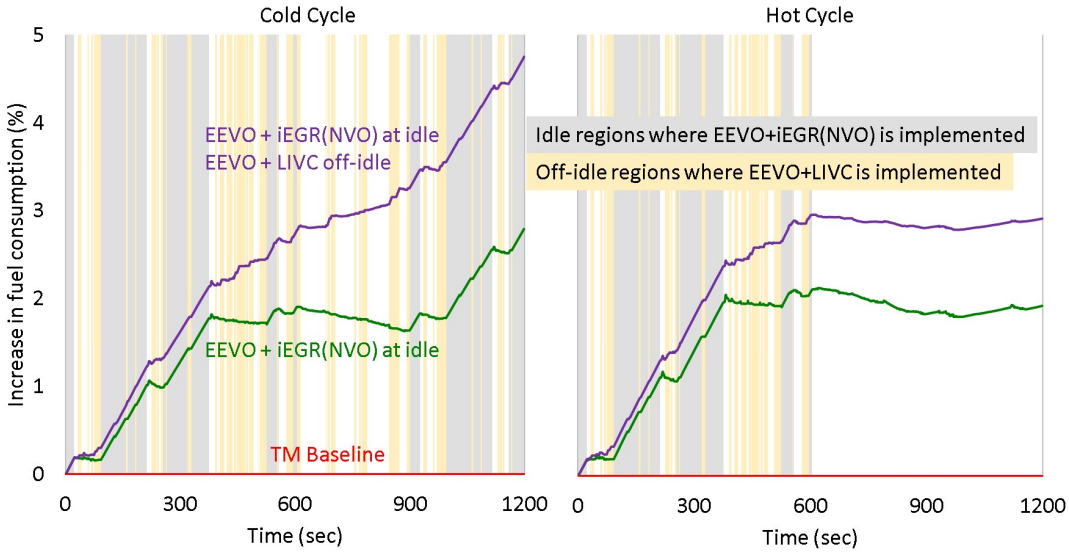

Figure 3.26. Difference in fuel consumption over the cold and hot start HD-FTP duty cycle.

increase in fuel consumption is observed both during implementation of idle, and off-idle warm-up strategies, as expected. The drive cycle implementing only the idle warm-up strategy results in a 2.1% fuel penalty with respect to the TM baseline cycle, while implementation of the off-idle warm-up strategy (EEVO+LIVC below 7.6 bar BMEP) results in a further 1% fuel penalty.

The trade-off curves among cumulative predicted tailpipe-out NOx, fuel consumption and engine-outlet PM produced at the end of both the drive cycles are shown in Figures 3.27(a) and 3.27(b). Figure 3.27(a) demonstrates that implementation of EEVO and LIVC at off-idle conditions below 7.6 bar BMEP results in a further reduction in predicted tailpipe-out NOx than that demonstrated in section 3.3. Specifically, implementation of the off-idle warm-up strategy results in a 10.1% reduction in predicted tailpipe-out NOx, at a fuel penalty of 3.1% with respect to the TM baseline drive cycle. Figure 3.27(b) shows that the off-idle warm-up drive cycle increases the engine-out PM emissions by 38% while predicting a 10.1% reduction in tailpipe-out NOx.

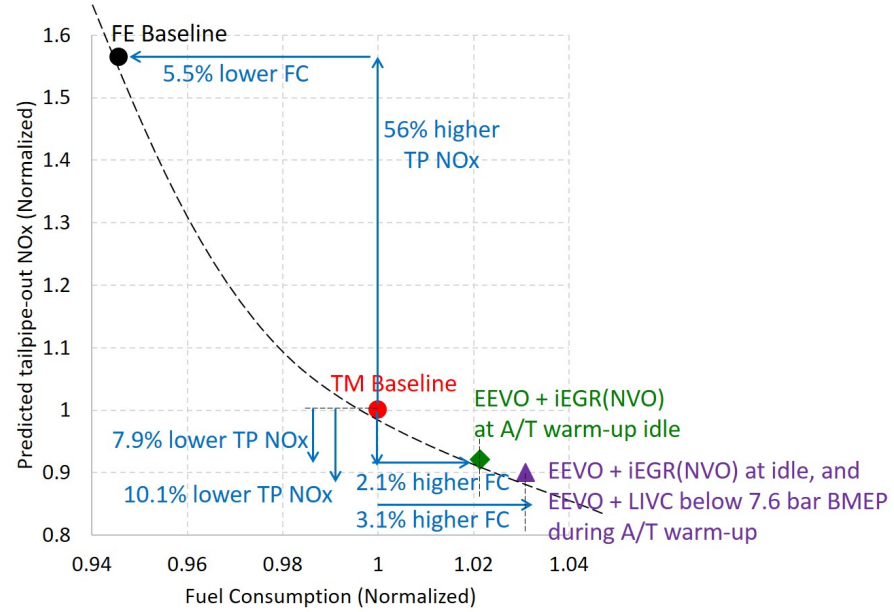

(a)

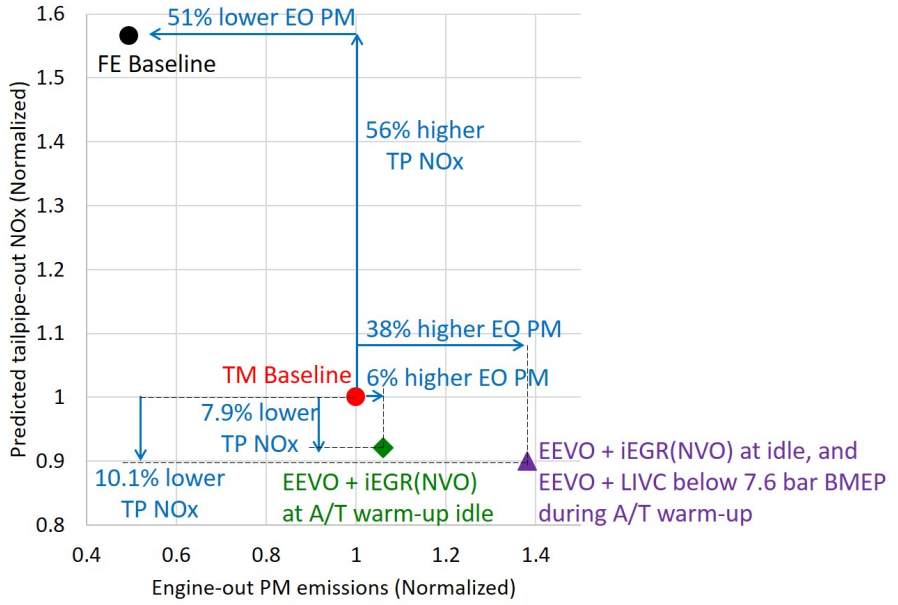

(b)

Figure 3.27. Trade-off between fuel consumption, tailpipe-out NOx and engine-out PM emissions over the combined HD-FTP drive cycle for the A/T warm-up strategies implemented at off-idle operating conditions.

3.5 Summary

EEVO+iEGR(NVO) has been demonstrated as an effective strategy at idle operation to achieve fast aftertreatment component warm-up, thus showing potential for reduction of tailpipe-out NOx, with a minor, but likely manageable, increase in fuel consumption and engine-out PM emissions. Absence of external EGR, in addition to a more open VGT position, make this strategy likely more amenable to a simpler turbocharger configuration like a fixed geometry turbine turbocharger.

A combination of EEVO and LIVC at off-idle operation below 7.6 bar BMEP shows a 10.1% reduction in predicted tailpipe-out NOx with a 3.1% further fuel penalty with respect to the baseline operation. However, this strategy results in 38% higher PM emissions over the drive cycle.

4. CYLINDER DEACTIVATION FOR FUEL-EFFICIENT AFTERTREATMENT THERMAL MANAGEMENT

4.1 Introduction

It was shown in the earlier chapters that both elevated engine-outlet temperatures and exhaust flow rates are desirable to accelerate the initial warm-up of the aftertreatment components. Once the aftertreatment components have reached desirable temperatures, elevated engine-outlet temperatures are required to maintain those temperatures, however elevated exhaust flow rates are no longer necessary. Lower exhaust flow rates are preferred in order to reduce cooling effects in the case engine-outlet temperatures drop below the temperature of a sufficiently warmed-up aftertreatment system.

Cylinder deactivation (CDA) has been studied as an effective means for maintaining elevated turbine-outlet temperatures with fuel economy benefits at low-load operating conditions. This chapter describes the fuel economy, aftertreatment thermal management, and transient performance of CDA at steady state operation and over the heavy-duty drive cycle.

This chapter is organized as follows. Section 4.2 describes the strategies used for implementing CDA and the resulting fuel economy and turbine-outlet temperature benefits observed at steady state curb idle operation. Section 4.3 studies the transient response of the engine dynamically operating in CDA and concludes that transient response is unaffected when CDA is implemented at and around idle operation, up to loads of 3 bar BMEP. Section 4.4 shows the fuel economy and thermal management benefits of implementing CDA over the HD-FTP transient cycle, which is representative of heavy-duty applications.

4.2 Cylinder Deactivation at Steady State Curb Idle Operation

4.2.1 Methodology and Description of Strategies

Steady state tests were performed at curb idle operation (800 RPM, 1.3 bar BMEP) to evaluate the benefits of 3-cylinder CDA over conventional 6-cylinder operation. 3-cylinder CDA, also known as half-engine CDA, was performed by cutting both fuel injection and airflow to the three inactive cylinders. Airflow was cut by deactivating both the intake and the exhaust valves, while the valve profiles of the three active cylinders were kept the same as conventional stock valve profiles, as shown in Figure 4.1. The three consecutive cylinders on either end, per Figure 4.2 are used as the combination of active cylinders. The firing order, which is 1-5-3-6-2-4 during baseline 6-cylinder operation, is 1-x-3-x-2-x when cylinders 4, 5 and 6 are deactivated, and x-5-x-6-x-4 when cylinders 1,2 and 3 are deactivated. This chapter shows results when cylinders 4, 5 and 6 are deactivated, while deactivation of the other bank has also been studied and found not to make a significant difference to the results. The EGR valve and VGT position, rail pressure, timings of pilot and main injection, and quantity of pilot injection were modulated to achieve a trade-off between fuel consumption and turbine outlet temperature.

The engine-out emissions of NOx, unburned hydrocarbons (UHC) and particulate matter (PM) during steady state CDA tests were kept below the levels observed during stock engine operation, as will be described in the following section. All experiments were also subject to the same mechanical and thermal constraints shown earlier in Table 2.1.

Results from three strategies each using 3-cylinder CDA are presented in the next section, and compared with similar 6-cylinder strategies. In addition to the "FE Baseline" and "TM Baseline" 6-cylinder strategies described in Chapter 3 which focus on best BSFC and aftertreatment warm-up respectively, another 6-cylinder strategy aimed at aftertreatment 'stay-warm' performance is presented in this section. The strategies are described below in greater detail and summarized in Table 4.1.

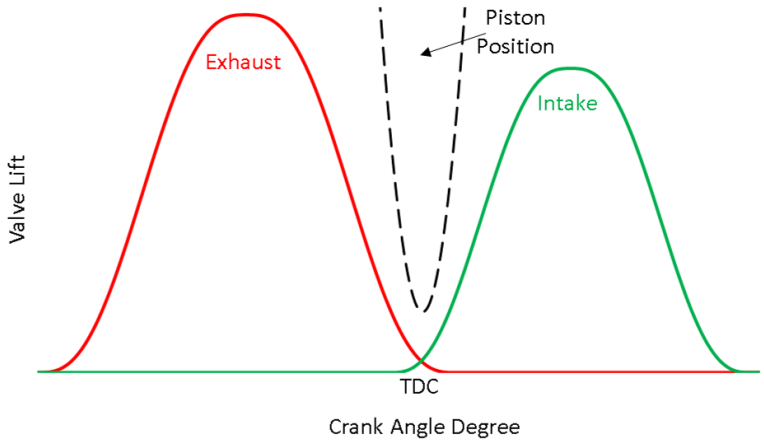

Figure 4.1. Nominal intake and exhaust valve profiles, which were used for CDA operation, with piston position from the cylinder head overlaid.

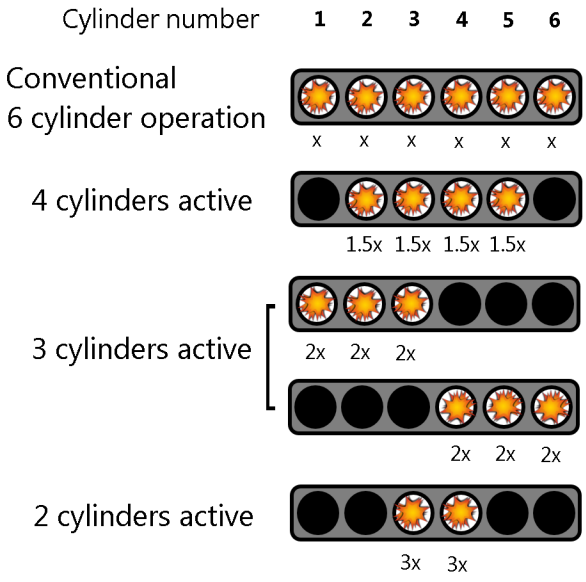

Figure 4.2. Schematic of an inline six-cylinder engine representing various CDA configurations with different sets of active cylinders, including approximate relative fuel quantity injected in the active cylinders.

1. **3-cylinder strategy for best BSFC** - This strategy represents engine operation targeting the best brake specific fuel consumption (BSFC) with three active cylinders. This is achieved using fuel-efficient injection timings such that the heat release begins near the top dead center, as shown in Figure 4.3(a). Adequate EGR was flowed for NOx mitigation by fully opening the EGR valve and modulating the VGT position so as to minimize the exhaust manifold pressure (EMP), and consequently the negative pumping work. This strategy has a TOT close to, but below, 200°C, and is therefore not the most ideal for stay-warm operation.

2. **3-cylinder strategy for aftertreatment 'stay-warm'** - This strategy represents 3-cylinder engine operation with focus on maintaining elevated aftertreatment component temperatures in the most fuel-efficient way possible. This is achieved by delaying the injection timings from the best BSFC strategy to the latest timing possible, as shown in Figure 4.3(b). In addition to elevating TOT by ~ 25°C at a small fuel penalty, delayed injections also result in lower engine-out NOx. Lower exhaust flow rates from only three active cylinders enhances the 'stay-warm' performance of this strategy as compared to corresponding six-cylinder strategies.

3. **3-cylinder strategy for high TOT** - This strategy is characterized by four delayed injections with the same timings as the 'TM Baseline' strategy, as shown in Figure 4.3(c), and maximally closed VGT position, in order to achieve the highest TOT possible with three active cylinders using conventional valve timings. This strategy has a higher fuel consumption than the 'stay-warm' strategy, and achieves a further ~ 25°C increase in TOT.

4. **6-cylinder strategy for aftertreatment 'stay-warm'** - This 6-cylinder strategy focuses on maintaining elevated aftertreatment component temperatures while being as fuel efficient as possible. It is characterized by four delayed injections with the same timings as the 'TM Baseline' strategy and mostly closed

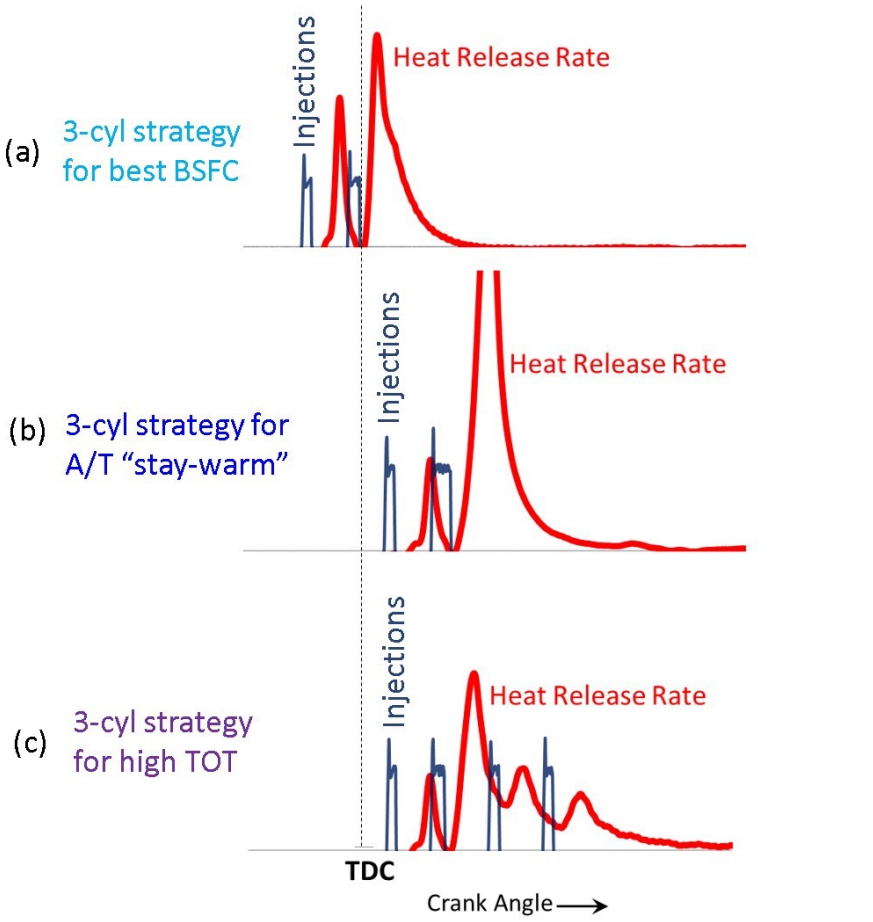

Figure 4.3. Injection timings and heat release rates for the three CDA strategies.

(partially open) VGT position. A more open VGT position relative to the 'TM Baseline' helps improve fuel efficiency via reduced pumping losses.

For the remainder of this chapter, 'FE Baseline' and 'TM Baseline' are referred to as '6-cylinder strategy for best BSFC' and '6-cylinder strategy for aftertreatment warm-up', to remain consistent with the nomenclature for 3-cylinder CDA operation.

The results presented do not consider the work done for actuation of the valves, as the valve motion is externally powered through a hydraulic pump. It is expected that the fuel savings for CDA will be higher in production systems, as actuation of fewer valves in CDA leads to lower parasitic losses than 6-cylinder operation.

Table 4.1. Summary of the CDA- and 6-cylinder-based strategies at curb idle.

Strategy	**Injections**	**VGT Position**
3-cyl strategy for best BSFC	2 injections near TDC	80% closed
3-cyl strategy for A/T 'stay-warm'	2 late injections	80% closed
3-cyl strategy for high TOT	4 late injections	100% closed
6-cyl strategy for best BSFC (FE Baseline)	2 injections near TDC	94% closed
6-cyl strategy for A/T 'stay-warm'	4 late injections	98% closed
6-cyl strategy for A/T warm-up (TM Baseline)	4 late injections	100% closed

4.2.2 Results and Discussion

Half-engine CDA shows a more favorable trade-off between TOT and BSFC, as shown in Figure 4.4. The best BSFC 3-cylinder CDA operation shows a 13% reduction in fuel consumption, along with a 45°C increase in TOT, as compared to the best BSFC 6-cylinder strategy. At the same TOT, the fuel benefit with CDA is between 25% and 40%, with higher fuel economy benefits at higher temperatures. In addition, CDA shows an approximately 75°C increase in TOT at fuel-neutral conditions. The 6-cylinder and CDA strategies for 'stay-warm operation lie in between the respective strategies for best BSFC and aftertreatment warm-up. It is intended that the TOT for stay warm strategies is above 200°C in as fuel-efficient way as possible. It is also worthwhile to note that the 3-cylinder strategy for aftertreatment stay-warm, despite not being the most fuel-efficient CDA strategy, is 7% more fuel-efficient than the best BSFC 6-cylinder strategy.

Figure 4.5 shows that the engine-out NOx, PM and HC emissions for 3-cylinder CDA strategies are similar, or less than the corresponding emissions for the 6-cylinder strategies. The low NOx for the 3-cylinder strategies for high TOT and aftertreatment 'stay-warm' can be attributed to the delayed injection timings, with similar EGR fraction as the best BSFC 3-cylinder CDA strategy. Therefore, in addition to showing fuel savings and higher TOT, CDA lies within the emission limits of 6-cylinder operation.

Reduced fuel consumption with the CDA-based strategies is primarily a result of the improved open cycle efficiency as compared to its 6-cylinder counterparts, as shown in Figure 4.6. The increase in open cycle efficiency is a result of lower air flow through the cylinders, which decreases the pumping work, as characterized by the smaller pumping loop in Figure 4.7. The 6-cylinder strategy for aftertreatment warm-up, and 3-cylinder strategy for high TOT have the lowest open cycle efficiencies among 6-cylinder and 3-cylinder strategies, respectively, because of the maximally closed VGT position, which results in higher pumping losses, illustrated by the bigger

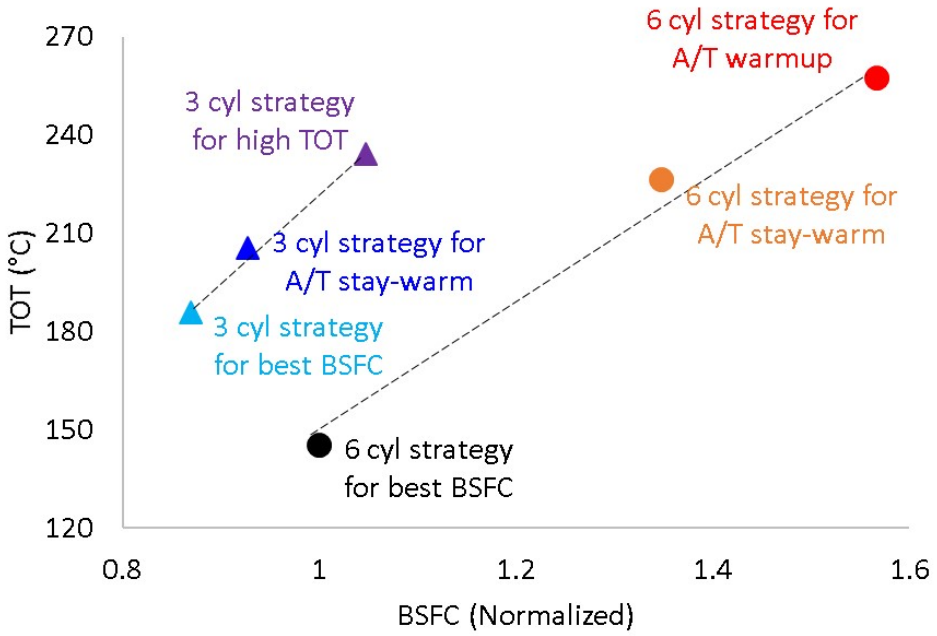

Figure 4.4. Turbine outlet temperature vs brake specific fuel consumption (normalized) at steady state curb idle for CDA-based strategies.

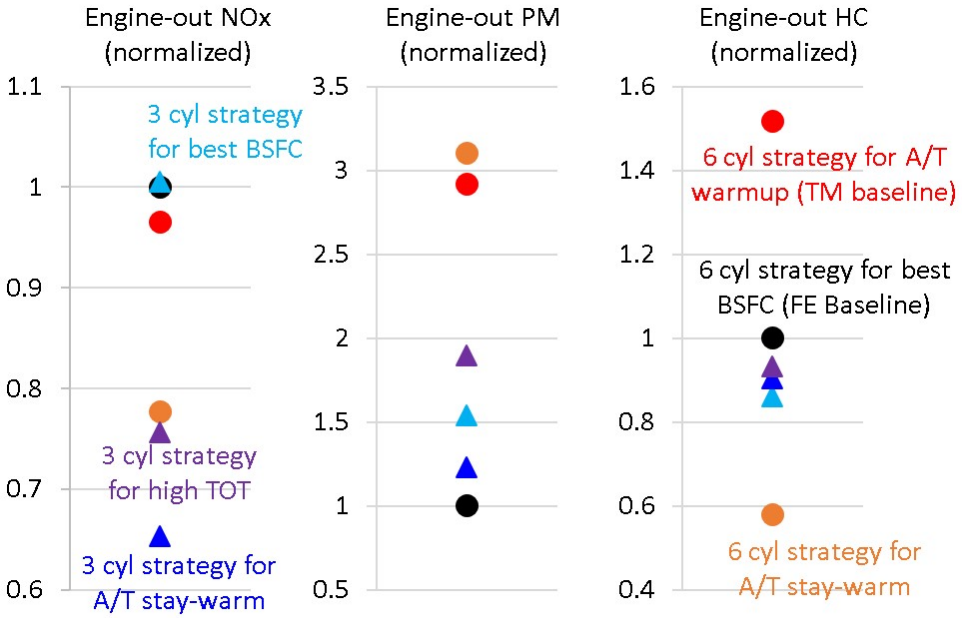

Figure 4.5. PM vs NOx emissions at steady state curb idle for CDA-based strategies.

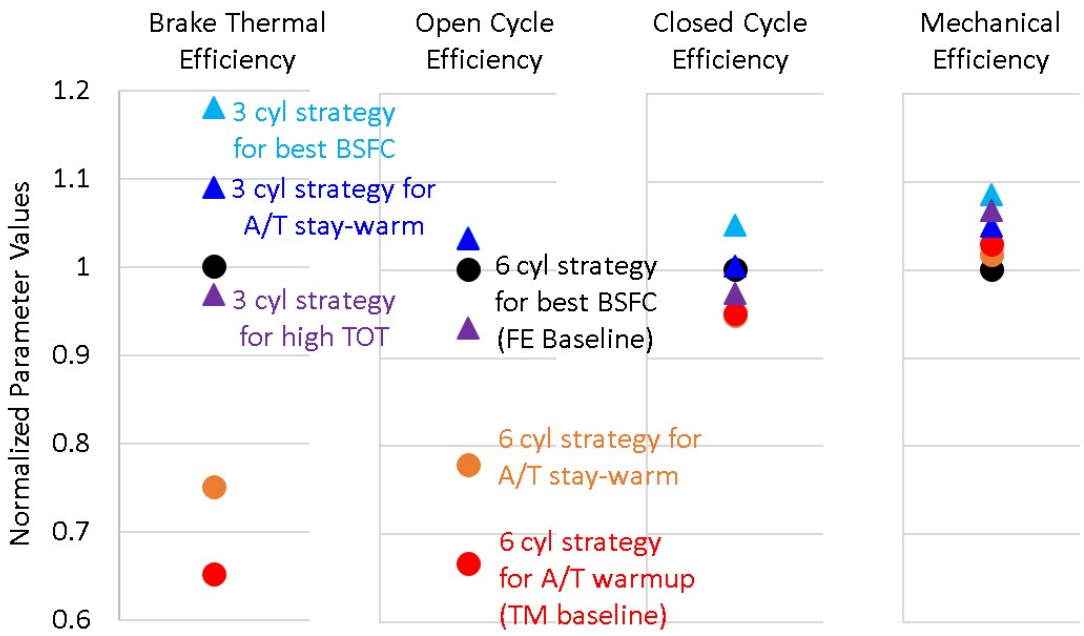

Figure 4.6. Comparison of cycle efficiencies at steady state curb idle for CDA-based strategies.

pumping loop in Figure 4.7. The 3-cylinder strategies for best BSFC and aftertreatment 'stay-warm' have the highest OCE due to fewer active cylinders and a relatively more open VGT position, both factors resulting in a smaller pumping loop. Further, lower heat loss from the engine due to combustion happening in fewer cylinders results in conversion of a greater proportion of fuel energy to work, thereby marginally increasing the closed cycle efficiency for CDA.

The increase in TOT with CDA results from a reduction in air-fuel ratio, as a greater quantity of fuel is combusted per unit airflow, i.e., the active cylinders are running at a higher load operating condition than in 6-cylinder operation [25, 35]. However, the maximum TOT with 6-cylinder operation is higher than that achieved with 3 cylinders active, as a result of 50% higher fuel being combusted due to greater engine inefficiency.

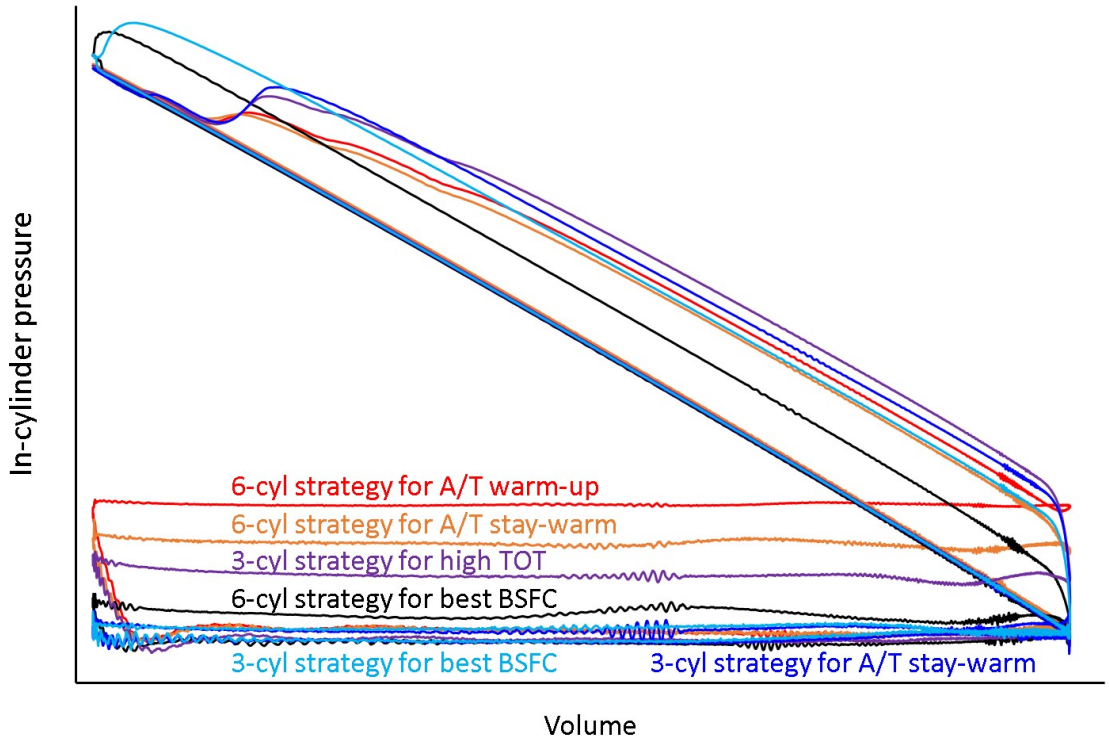

Figure 4.7. Log P- log V plot at steady state curb idle for CDA-based strategies.

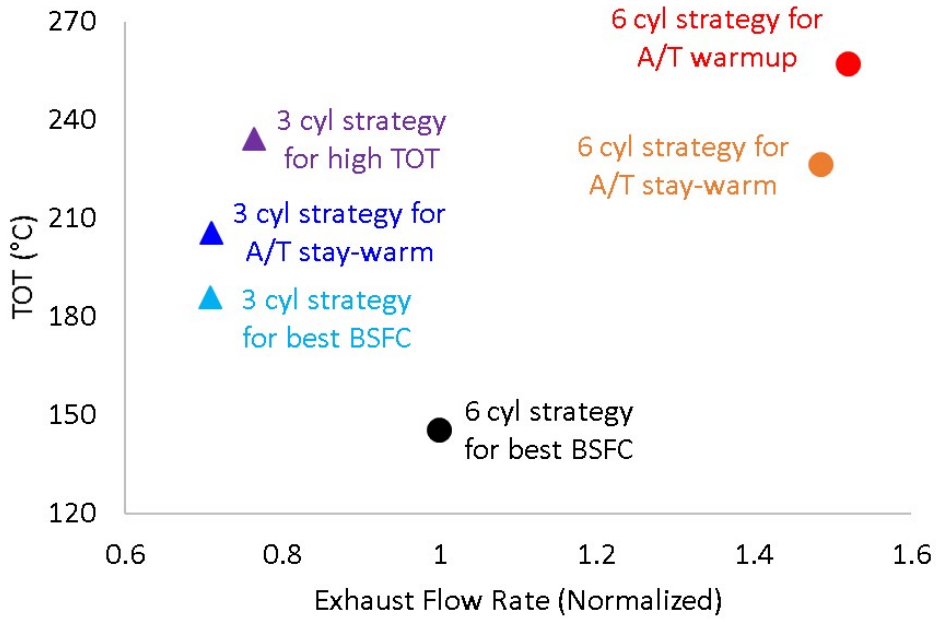

Figure 4.8. Turbine outlet temperature vs exhaust flow rate at steady state curb idle for CDA-based strategies.

In addition to high TOT, low exhaust flow rates are desired in 'stay-warm' operation, as it is intended to minimize the rate of cool-down of the aftertreatment components once they have reached an excess of 200°C. Figure 4.8 shows that the 3-cylinder CDA strategies have lower exhaust flow rates than the 6-cylinder strategies, due to airflow in fewer cylinders, thus making them more favorable to maintain elevated aftertreatment temperatures.

Figure 4.9 shows the normalized heat transfer curves for the strategies described in this section. The 6-cylinder strategy for aftertreatment warm-up is most preferred below catalyst bed temperatures of $200°C$ due to its superior heat transfer rate. At temperatures above $200°C$, the 3-cylinder CDA 'stay-warm' strategy is preferred due to its comparable cool-down rate at lower fuel consumption.

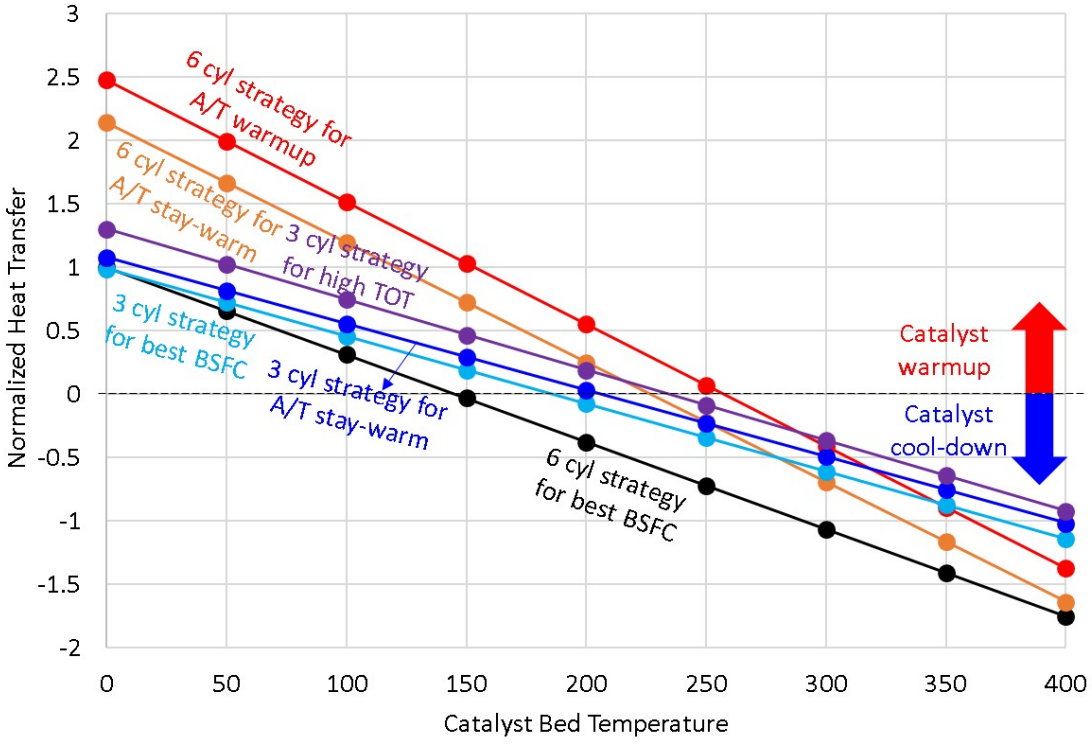

Figure 4.9. Normalized aftertreatment heat transfer at various catalyst bed temperatures for CDA-based strategies.

4.3 Transient Response of Cylinder Deactivation During Dynamic Diesel Engine Operation

It is noted from Section 4.2 that CDA improves fuel efficiency and after treatment thermal management at low-load operation. However, reduction in airflow during CDA poses a challenge to transient response as the rate of torque increase, which depends on the quantity of fuel injected, is limited by the available airflow through the engine. The reduced airflow during CDA needs to be managed properly to ensure acceptable transient torque/power response. This section demonstrates that it is possible to operate a diesel engine at low loads in CDA without compromising its transient torque/power capabilities, which is a key finding in enabling the practical implementation of CDA in diesel engines.

4.3.1 Methodology

Transient response starting from 2, 3 and 4 active cylinders at low loads is studied in this section. As described earlier, 3-cylinder CDA is implemented by deactivating cylinders 4, 5 and 6, such that the firing order is 1-x-3-x-2-x. Cylinders 1 and 6 are deactivated when 4 cylinders are active, and cylinders 1, 2, 5 and 6 are deactivated when 2 cylinders are active, to minimize external heat loss from the active cylinders. The resulting firing order is x-x-3-x-x-4 with 2 cylinders active, and x-5-3-x-2-4 with 4 cylinders active. The different modes of CDA are illustrated in Figure 4.2 with the approximate fuel quantity injected in each cylinder shown below the cylinder.

The transient response of the engine from CDA operation at idle and motoring conditions, upon transitioning directly to 6-cylinder operation upon acknowledging a 'hard' transient, is studied in this section. Different times of transition between CDA and 6-cylinder operation during the acceleration are studied. The set points to achieve best fuel economy during CDA at idle were used while control was reverted back to the ECM after transitioning to six cylinder operation during the acceleration.

Portions of the HD-FTP, as shown in Figure 4.10, are used to compare the transient response with and without CDA. The transient response of the engine using the stock calibration in 6-cylinder operation, which is used in production systems, is used as the baseline to compare the response when transitioning out of CDA. The quality of transients is defined by the closeness of the load response and emissions to that achieved using stock 6-cylinder operation.

Figure 4.11 shows the order of the valve and injection events for a deactivated cylinder during reactivation, when transitioning from CDA to six-cylinder operation. The deactivated cylinders experience a decay in in-cylinder pressures as a result of heat loss and blowby through the piston rings [47], and therefore, adequate oxygen is not present inside the deactivated cylinder for combustion. Injection of fuel before reactivation of valves leads to a spike in UHC and PM emissions. Therefore, in this study, the exhaust valves of the deactivated cylinders are opened first to purge any residual gas to the exhaust manifold, followed by opening of the intake valve to induct fresh charge from the intake manifold. Fuel injection takes place after the valve events to ensure that there is sufficient oxygen available for combustion to take place.

4.3.2 Results and Discussion

Cylinder deactivation is used predominantly at low-load operating conditions, where the desired torque can be provided by a fewer number of cylinders. The maximum fueling rate is limited by the air flow rate, which is lower when fewer cylinders are breathing. The number of cylinders that can be deactivated depends on load, with higher loads requiring a higher number of active cylinders.

Figure 4.12 shows the torque produced by the engine with different modes of CDA run throughout the first hill of the HD-FTP, with comparison to the torque response of 6-cylinder operation. As expected, CDA cannot meet high load requirements with the peak load produced varying monotonically with, and approximately proportional to, the number of cylinders that are active.

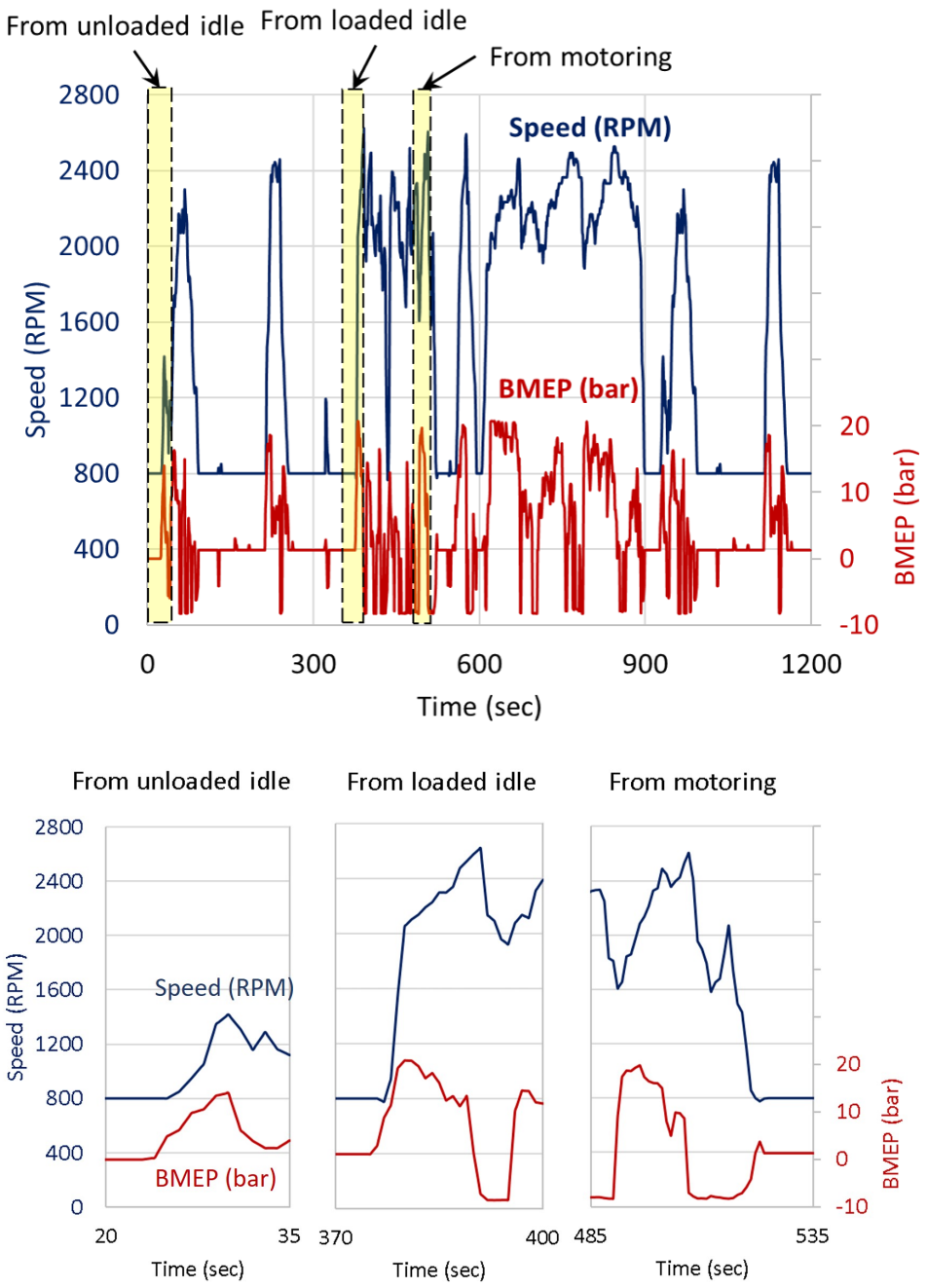

Figure 4.10. Regions of HD-FTP over which transients starting from CDA are studied.

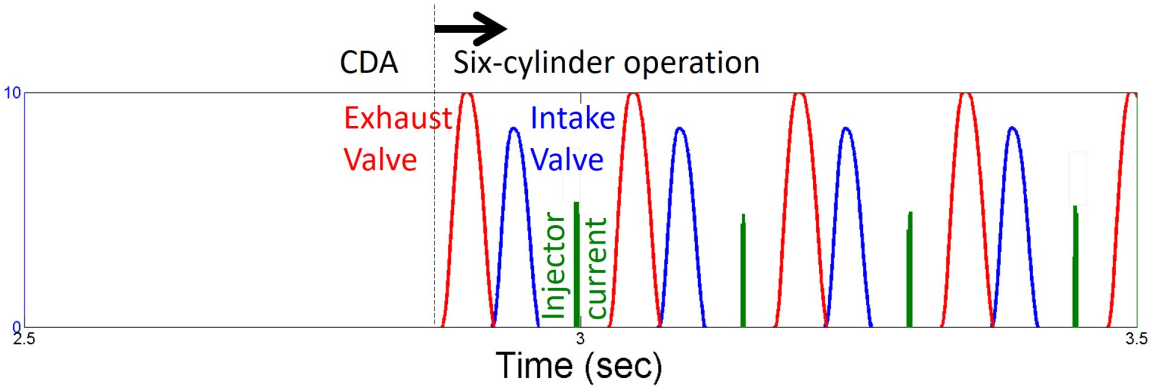

Figure 4.11. Order of valve timings and injections during reactivation of deactivated cylinders.

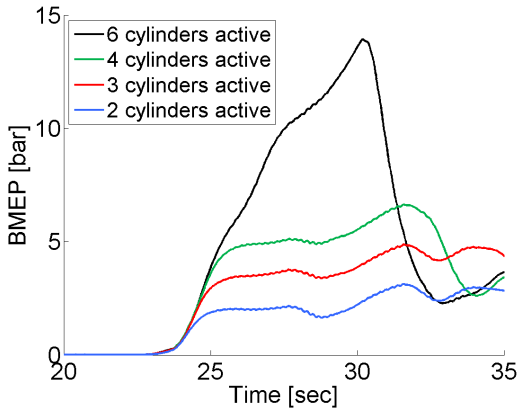

Figure 4.12. Load response when the entire first acceleration was run in CDA, compared to conventional 6-cylinder load response.

High-load operating conditions require all cylinders to be active. It is therefore necessary to dynamically transition between CDA and 6-cylinder operation during transient operation in order to achieve fuel economy and thermal management benefits of CDA at low loads while still meeting the requirements for higher load,

4.3.3 Part I: CDA at Unloaded Idle

The engine produces zero load at unloaded idle with just enough fueling to overcome mechanical losses. Fuel savings at unloaded idle are expected to be higher than that at curb idle as the efficiency of CDA increases with lower loads. The same recipe used to obtain 11% fuel savings with 3-cylinder CDA at curb idle is used for all modes of CDA at unloaded idle.

Transition at the Onset of an Acceleration:

Transient response from different modes of CDA upon reactivation of inactive cylinders at the onset of the acceleration is studied in this section. Figure 4.13(a) compares the load response of each of the cases for the first acceleration of the HDFTP where the engine, which is initially at unloaded idle (BMEP = 0 bar), accelerates up to a BMEP of 13.5 bar at 1400 RPM. As shown, transitioning from CDA to 6 cylinder operation at the beginning of the acceleration produces a similar torque response as that when running throughout with 6 cylinders active.

The air-fuel ratio during the transient is shown in Figure 4.13(b). As expected, during unloaded idle prior to the acceleration, the air-fuel ratio is lower for CDA than for 6-cylinder operation due to lower air flow, while during the acceleration, the AFR remains just above stoichiometric in all the cases.

Figure 4.13(c) shows that despite there being lower initial air flow rates with CDA, the particulate matter emissions during the acceleration are very similar to that of 6-cylinder operation, indicating that there is sufficient air flow through the cylinders following the transition. Figure 4.13(d) shows that the NOx emissions are very similar as well.

Figure 4.13 demonstrates that the engine is able to meet the most aggressive HDFTP load transient starting from 2, 3, or 4 cylinders active at unloaded idle, when the CDA-to-6 cylinder transition happens at the beginning of the acceleration.

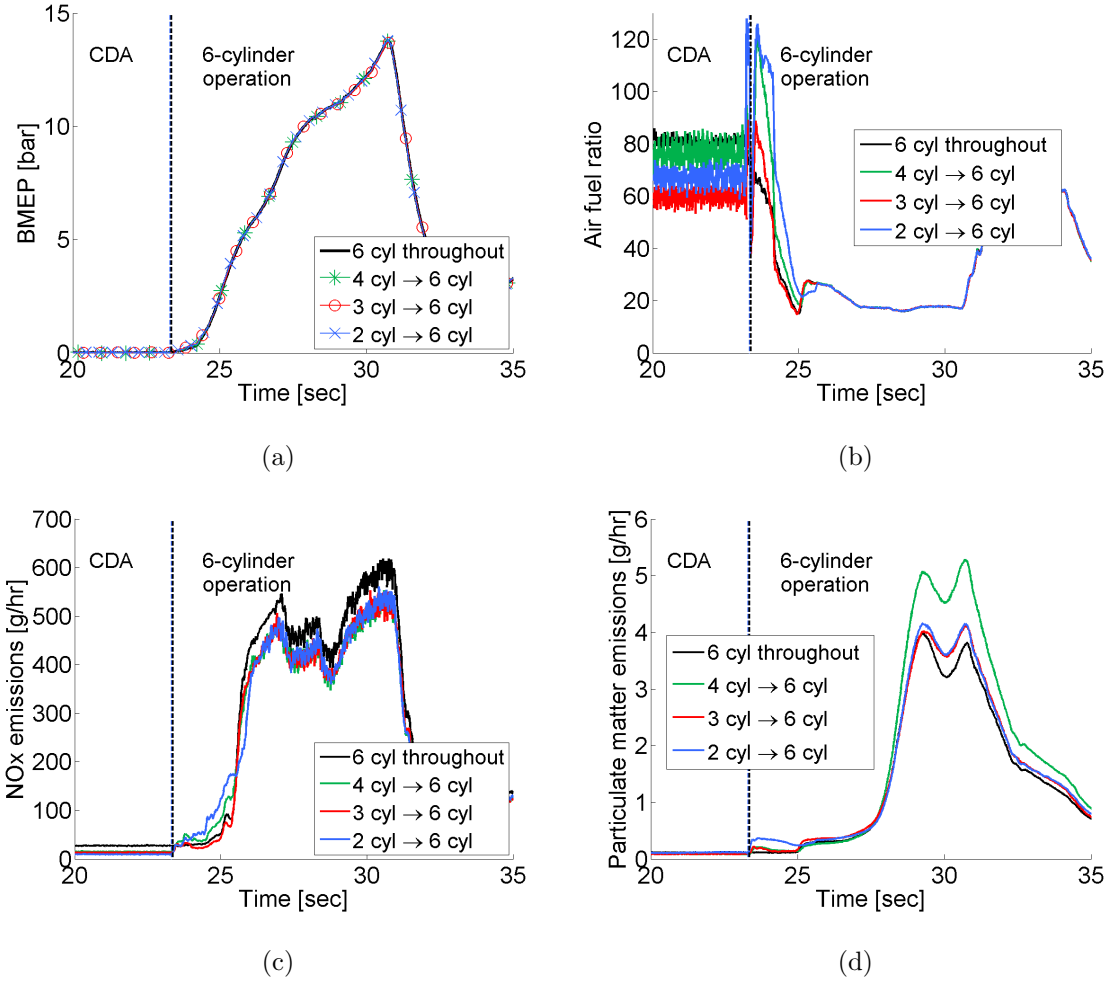

Figure 4.13. Transitioning from CDA at unloaded idle to 6-cylinder mode at the onset of the acceleration (a) gives as good a load response as does running throughout with 6 cylinders, (b) shows lower AFR with CDA at unloaded idle, while AFR remains close to stoichiometric during the acceleration, (c),(d) shows similar particulate matter and NOx emissions as that of 6-cylinder operation throughout.

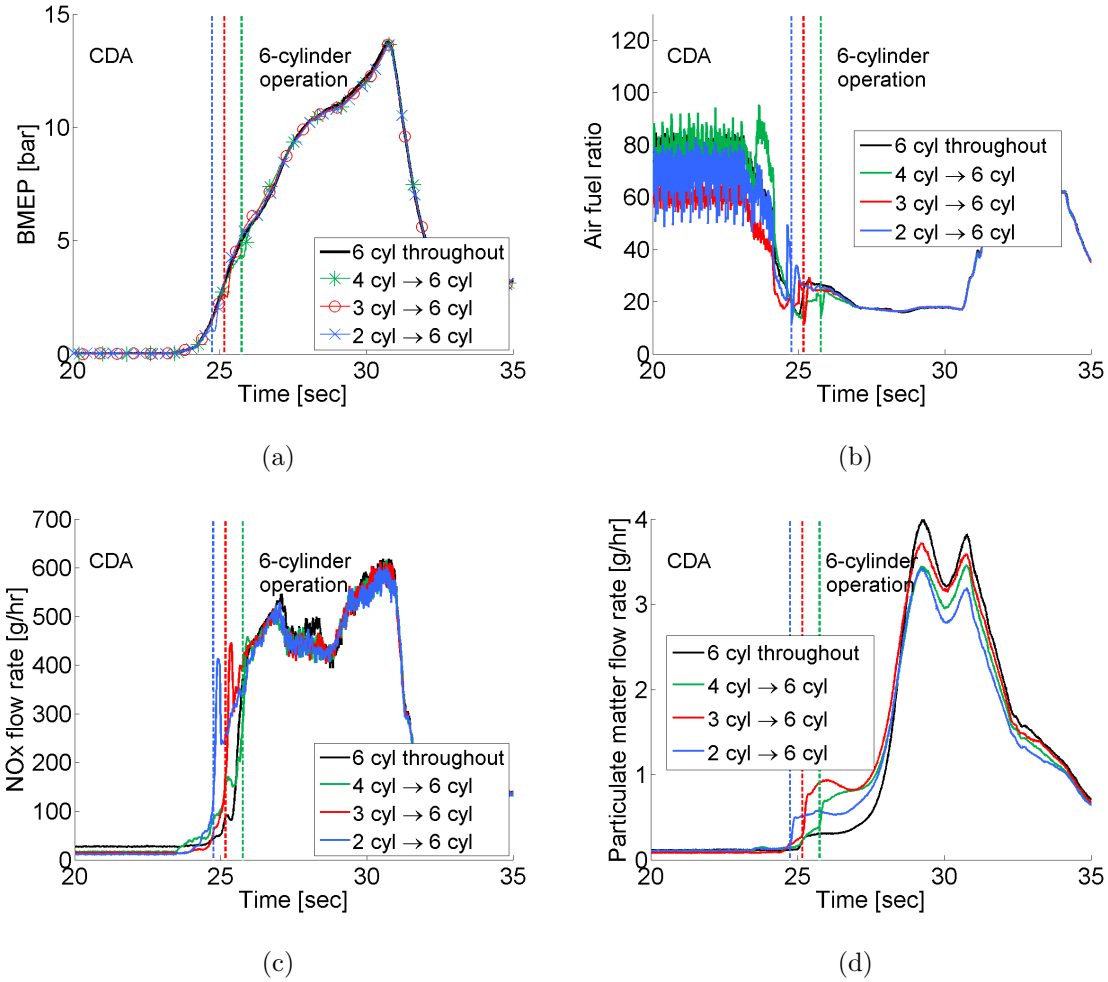

Figure 4.14. Transitioning from CDA at unloaded idle to 6-cylinder mode at the AFR limit during the acceleration, (a) gives a good torque response with modest discontinuities at the point of transition, (b) shows AFR reaching stoichiometric in each case before transitioning to 6-cylinder operation, (c),(d) shows higher particulate matter and NOx emissions than 6-cylinder operation during the initial portion of the acceleration.

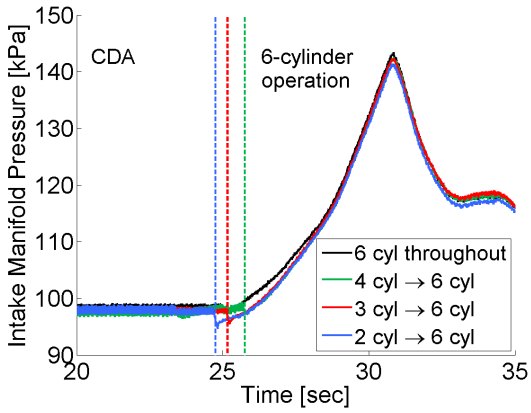

Figure 4.15. When starting from CDA at unloaded idle, and transitioning to 6-cylinder mode at AFR limit, intake manifold pressure decreases upon reactivation of inactive cylinders at the point of transition.

Transition at AFR Limit During the Acceleration:

Maintaining CDA during the load transition for as long as possible would be advantageous in increasing the benefits extracted from CDA. Figure 4.12 suggests that this should be possible during the initial portion of the acceleration. This section studies transients when the engine transitions from CDA to 6-cylinder operation at the AFR limit during the acceleration. In other words, the engine runs in CDA during a portion of the acceleration until the reduced air flow cannot meet the transient load demand, at which point it transitions to 6-cylinder operation. The best BSFC settings for CDA are used at unloaded idle while the ECM controls the engine during the acceleration.

The load response upon transition from CDA to 6-cylinder operation at AFR limit is shown in Figure 4.14(a). Although there are modest discontinuities in the load response at the point of transition, the peak load is achieved similar to the 6-cylinder case. The discontinuity in load occurs due to a sudden increase in pumping work, and drop in intake manifold pressure, per Figure 4.15, upon reactivation of cylinders.

Figure 4.14(b) shows the AFR dynamics during the acceleration. As expected, just prior to, and during, the transition, the AFR is slightly lower for the CDA cases, resulting in slightly higher PM emissions during the acceleration, as shown in Figure 4.14(c). Figure 4.14(d) shows that the NOx emissions are higher during the initial portion of acceleration in CDA, but converge quickly to that of 6-cylinder operation upon reactivation of cylinders. The NOx and PM trends can both be explained by the EGR and VGT valve dynamics as represented by EGR fraction in Figure 4.16. The EGR valve closes to drive EGR fraction to 0 when running with 2 cylinders active during the acceleration in order to ensure enough air flow to the cylinders, as a result of which its NOx is higher and PM is lower than the other two CDA modes. The EGR fraction remains higher for longer with 3 cylinders active before decreasing to 0, explaining why particulate matter is higher than the other two CDA modes and NOx is lower than that of the 2 cylinders active case. It should also be noted that the stock engine control module (ECM) is tuned for 6-cylinder operation, and as such, its modulation of the VGT and EGR valve position during CDA-to-six cylinder transitions cannot be expected to be optimal.

In summary, via comparison of Figure 4.14 with Figure 4.13, and as expected, it is clear that delaying the transition from the beginning of the acceleration to the point at which AFR limit is first reached causes a deterioration, albeit likely an acceptable one, in both load and emissions response. Furthermore, an improved transient response during CDA-to-six cylinder mode transition is expected if/when the air handling controls are developed for the specific purpose. Cylinder deactivation in transient operation is practical, as evidenced by load demands met with transitions from CDA to 6 cylinder mode.

Effect of Transition Time on Transient Response:

As expected, Figure 4.17(a) shows that additional delay in the transition between 3 cylinder CDA and 6-cylinder operation causes the load and PM response to degrade further. As also shown in Figure 4.14, transition between CDA and 6-cylinder

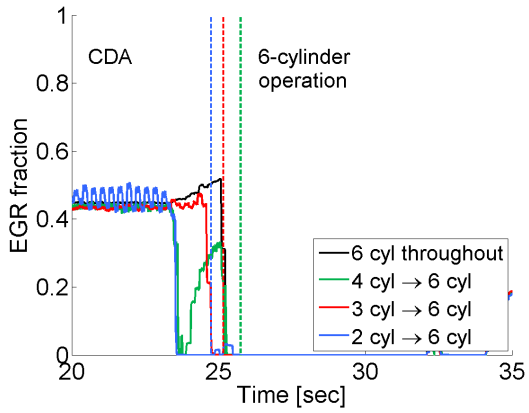

Figure 4.16. When starting from CDA at unloaded idle and transitioning to 6-cylinder mode at AFR limit, EGR fraction for 2 or 4 cylinders active is lower as compared to 3 or 6 cylinders active due to the dynamics of EGR and VGT valves during the transition.

operation at, or just before, the AFR limit point is generally acceptable depending on drivability and emissions constraints.

4.3.4 Part II: CDA at Curb Idle

Loaded idle refers to the operating condition where the engine produces a BMEP of 1.3 bar while running at 800 RPM. CDA with 3 cylinders active shows a fuel economy benefit of 11% over 6-cylinder operation at steady state curb idle, as demonstrated earlier. Fuel savings are expected with 2 and 4 cylinders active, although the results are not shown here. The same recipe as that identified for 3-cylinder CDA is used when 2 and 4 cylinders are active at curb idle.

The engine runs in curb idle for 35% of the time and consumes approximately 6% of the total fuel consumed in a HDFTP.

Transition at the Onset of an Acceleration and at AFR Limit:

Figures 4.18(a) and 4.19(a) show the load response of the engine during an aggressive HDFTP acceleration starting from CDA at curb idle with transitions to 6-cylinder operation at the beginning of the acceleration and at the AFR limit during

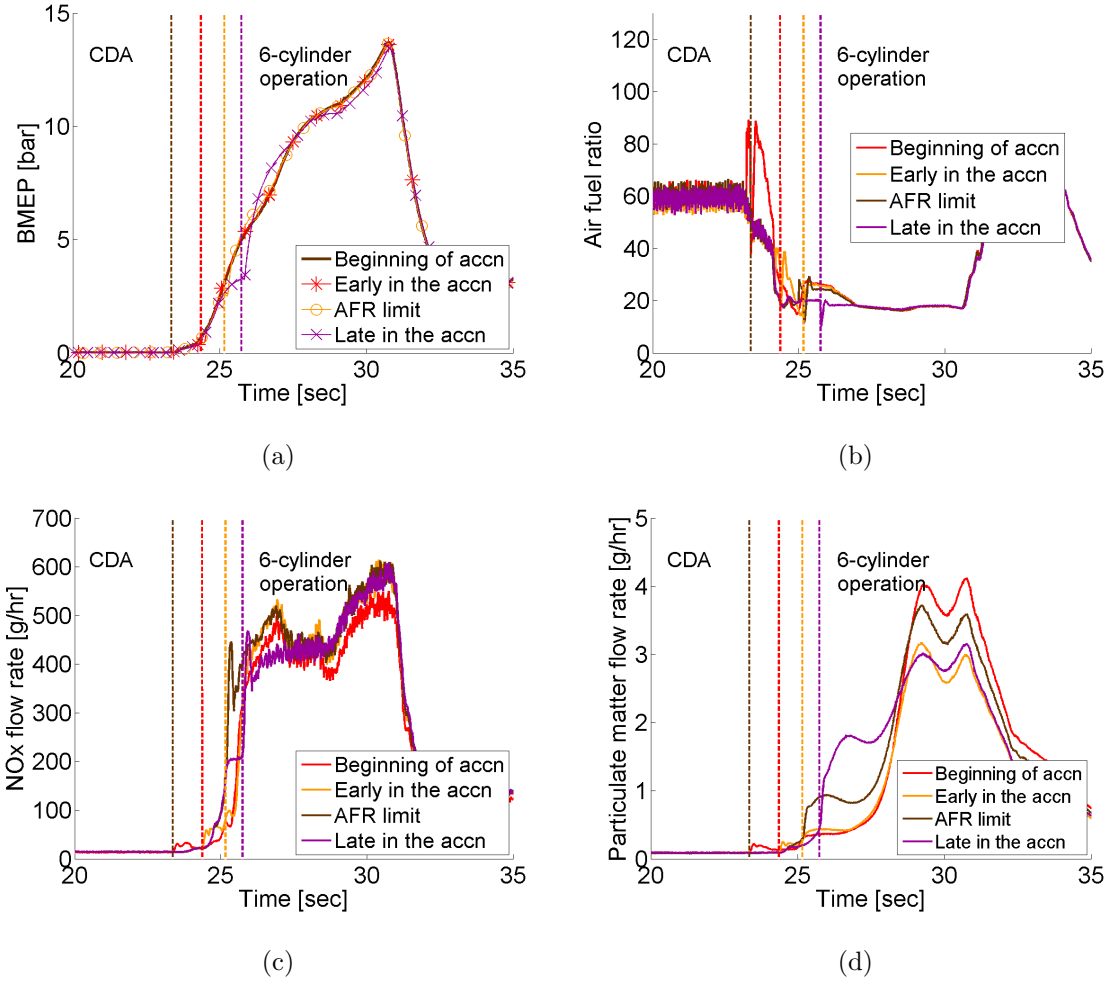

Figure 4.17. As the transition between 3 cyl CDA at unloaded idle and 6-cylinder operation is delayed, (a) the load response deteriorates and has bigger discontinuities, although peak load is achieved, (b) AFR is seen to stay close to its stoichiometric value between AFR limit and point of transition, indicating fuel limiting action, (c),(d) PM emissions are initially high when transition occurs after AFR limit, while NOx emissions are similar.

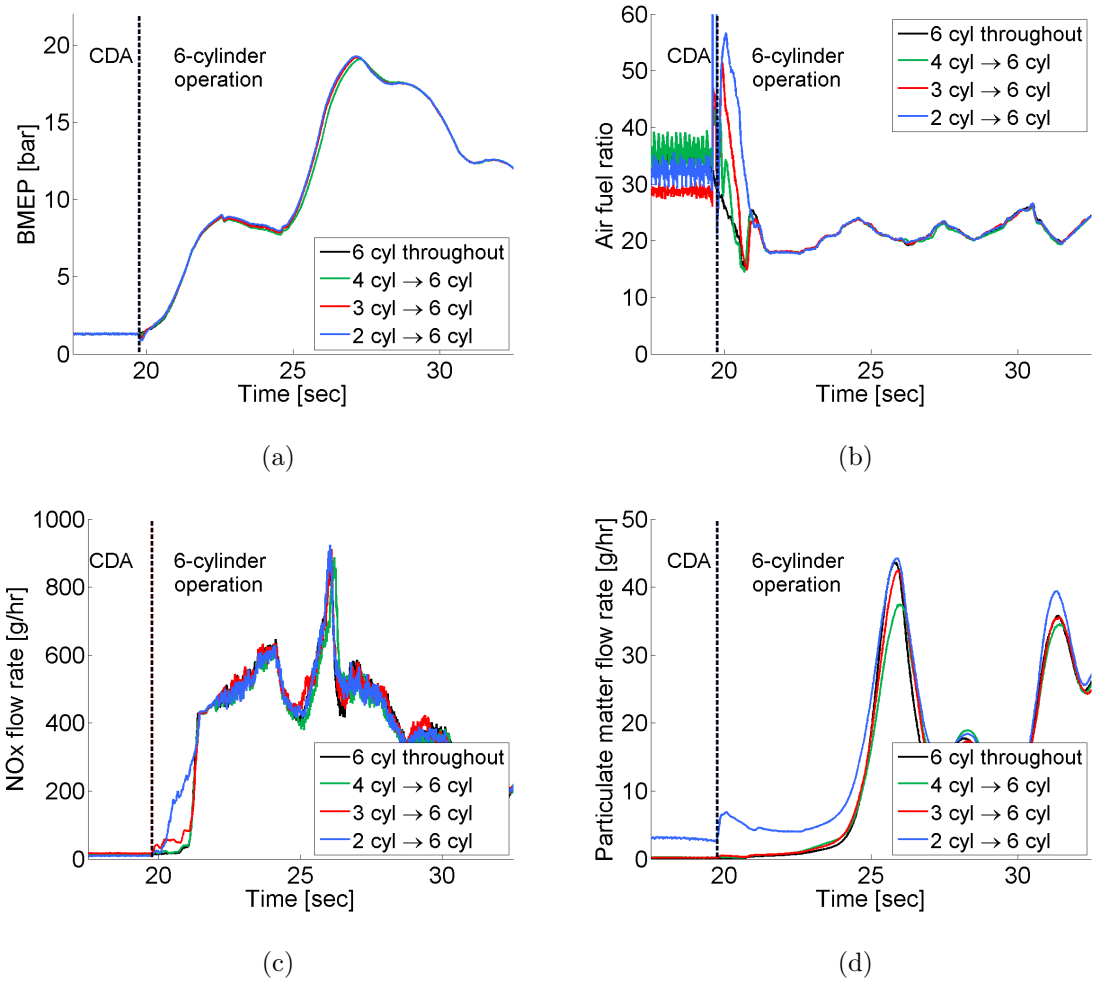

Figure 4.18. Transitioning from CDA at curb idle to 6-cylinder mode at the beginning of the acceleration shows (a) a good load response similar to that when run throughout with 6 cylinders, (b) lower AFR with CDA at curb idle, while AFR remains close to stoichiometric during the acceleration, (c),(d) shows that although PM and NOx are high when starting with 2 cylinders active, they are similar to that of 6-cylinder operation throughout when starting with 3 or 4 cylinders active.

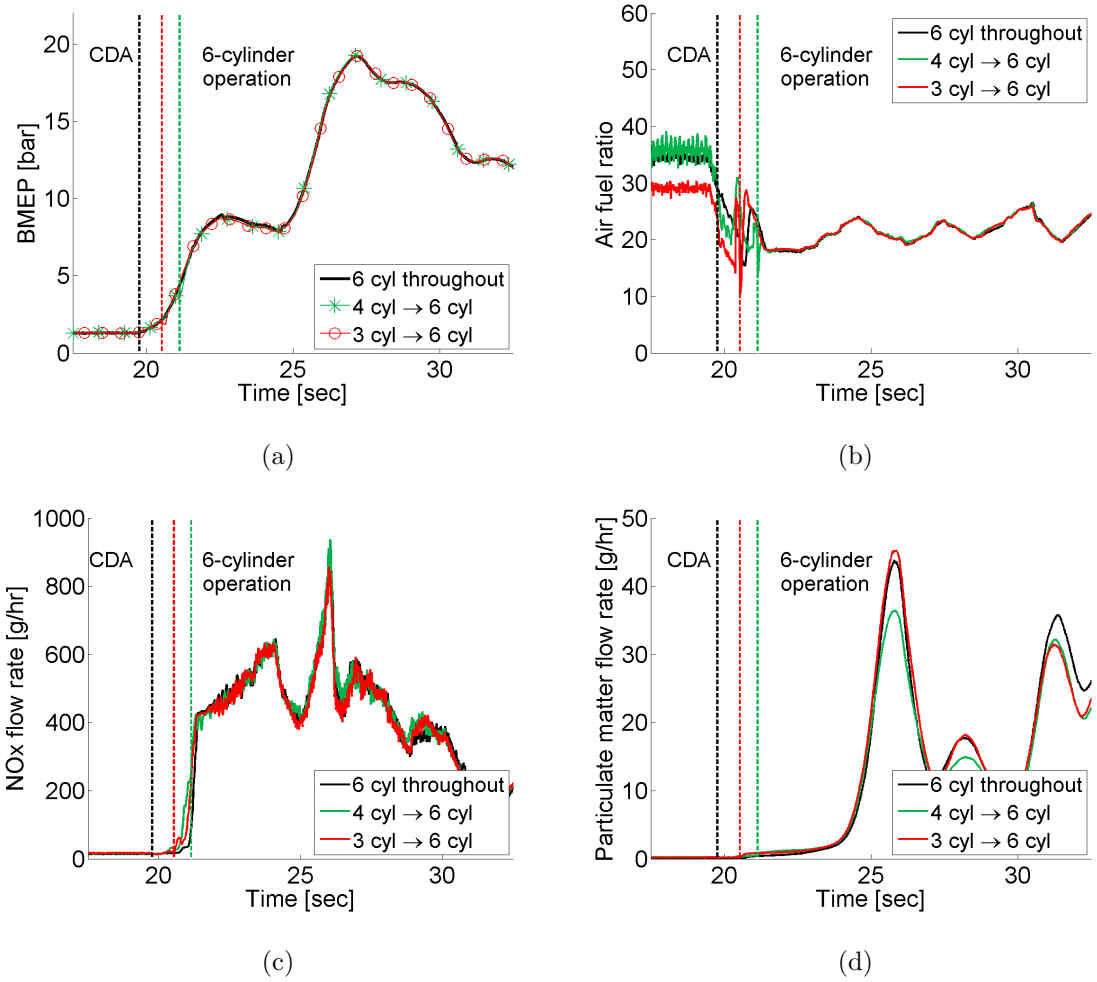

Figure 4.19. Transitioning from CDA at curb idle to 6-cylinder mode at the AFR limit during the acceleration shows (a) as good a load response as running throughout with 6 cylinders, but with small discontinuities at the point of transition, (b) lower AFR with CDA at unloaded idle, while AFR remains close to stoichiometric during the acceleration, (c),(d) similar PM and NOx emissions as that of 6-cylinder operation throughout when starting with 3 and 4 cylinders active.

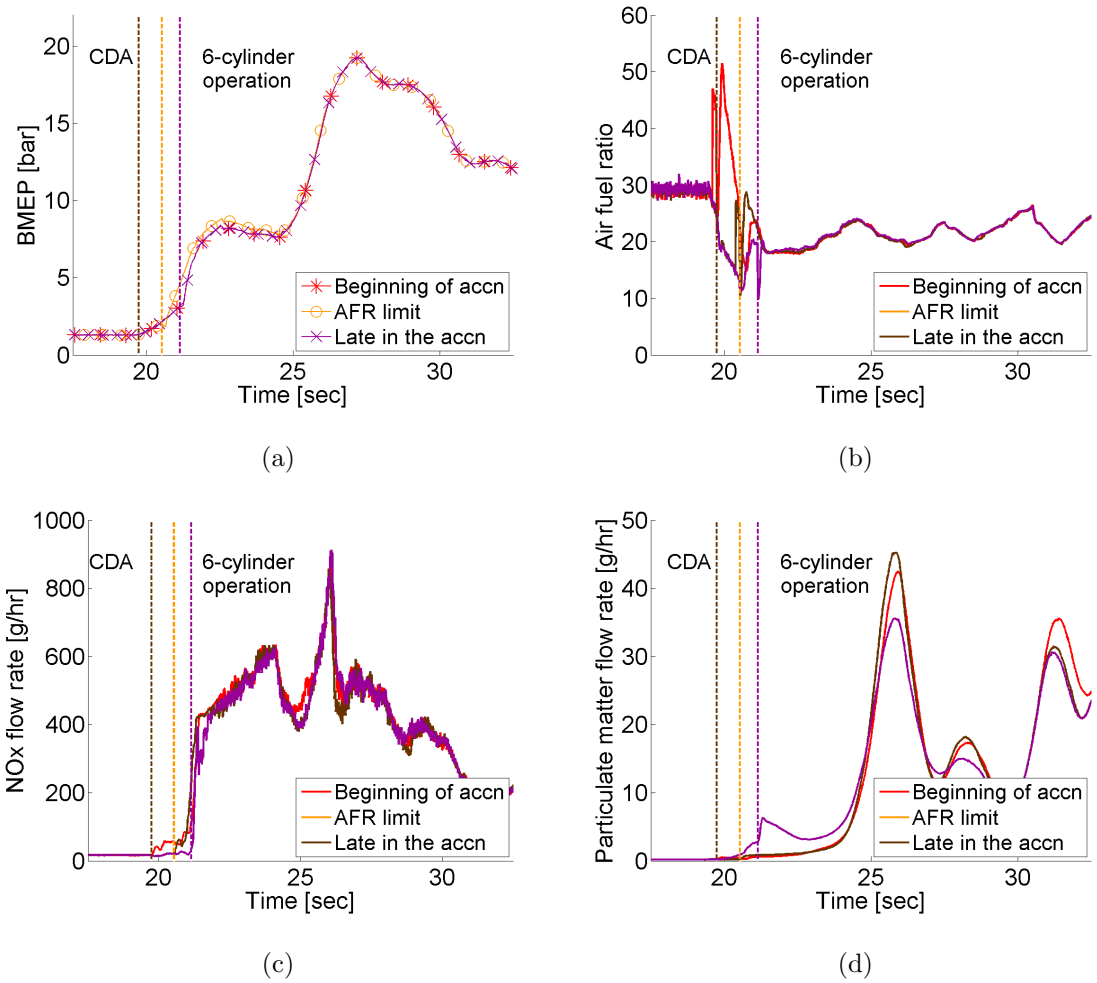

Figure 4.20. Starting from 3 cylinder CDA at curb idle and delaying the time at which transition to 6-cylinder operation is made, (a) transition from CDA to 6-cylinder operation later than the point of AFR limit leads to deterioration in load response, (b) later transitions keep the AFR closer to stoichiometric, as expected, (c),(d) PM emissions are high when transition occurs after the AFR limit, while NOx emissions for all cases are identical.

the acceleration. The response starting from CDA is as good as that when run in 6-cylinder operation throughout. Similar to Figure 4.14(a), all modes of CDA show a small dip in torque at the point of transition due to an instantaneous increase in pumping work upon reactivation of cylinders, which are likely to be too small to be perceived by a driver.

As shown in Figure 4.18(c), running with 2 cylinders active produces higher particulate matter than 6-cylinder operation and the other CDA modes, not only during curb idle but also upon acceleration. This is because there is not enough oxygen to sustain low-PM curb idle with only 2 active cylinders. Figure 4.19(b) shows that while the AFR during the initial portion of the acceleration is higher with 4 cylinders active, as expected, the AFR is identical for all cases during the acceleration. From Figures 4.18(c) and 4.19(c), PM emissions with 3 cylinders and 4 cylinders active are very similar to those of 6-cylinder operation both when the transition occurs at the beginning of the acceleration and at AFR limit. Figures 4.18(d) and 4.19(d) show that the transient NOx emissions are very similar for all cases.

Effect of Transition Time on Transient Response:

Figure 4.20 shows that additional delay in the transition between 3 cylinder CDA and 6-cylinder operation, starting from 3 cylinder CDA at curb idle, causes the load and PM response to degrade. Transition between CDA and 6-cylinder operation at, or just before, the AFR limit point would be acceptable for drivability and emissions constraints.

In summary, Figures 4.13, 4.14, 4.18 and 4.19 demonstrate that there are no issues transitioning from CDA mode at unloaded or curb idle to 6 cylinder mode at the onset of an acceleration, or as the AFR limit is reached during an acceleration. These results are profound as they demonstrate that transient engine load and emissions responses are not compromised when CDA is used at either loaded or unloaded idle.

4.3.5 Part III: CDA at Motoring

Motoring refers to the engine operation where the engine is driven by an external load, therefore, fuel is not injected in the cylinders. CDA during motoring provides aftertreatment "stay-hot" thermal management benefits as less air is pumped through the engine. In this study, the engine motors at 1600 RPM in CDA and switches to 6-cylinder operation before accelerating to a BMEP of 20 bar at 2500 RPM, as

shown in Figure 4.10. This maneuver corresponds, for instance, to a driver pressing the accelerator pedal abruptly after cruising downhill without pressing the pedal. Strategies during motoring and their corresponding transient performance are likely to be different for engines that use an engine brake.

The load response of the engine upon transitioning out of CDA at motoring is slower as compared to 6-cylinder operation during the entire maneuver, as illustrated in Figure 4.21(a). The reason for this lag is the lower availability of airflow during the acceleration from a CDA motoring condition, as shown in Figure 4.22(a). This is because the turbocharger speed is lower when fewer cylinders are active, as shown in Figure 4.22(c), as a result of which the boost pressure is lower. The turbocharger takes a longer time to increase its speed upon application of load, thus resulting in lower air flow to the engine.

Figure 4.21(b) shows that the AFR is close to stoichiometric throughout the acceleration. Figure 4.21(c) shows that PM emissions are higher when run throughout with 6 cylinders active and are lower with fewer active cylinders at motoring. This discrepancy is due to the fact that the load achieved is lower when starting from fewer active cylinders at motoring, meaning that lesser fuel is injected during the acceleration, as illustrated in Figure 4.22(b). Also, Figure 4.22(d) indicates that the EGR and VGT valve dynamics drive higher EGR when running throughout with 6-cylinders active, which also contributes to PM.

Figure 4.21(d) shows that starting from CDA results in a spike in NOx compared to starting from 6-cylinder operation. NOx is lower when starting from motoring with more active cylinders due to higher EGR fraction made available, as shown in Figure 4.22(d). The ECM allows flow of higher EGR when starting from more active cylinders at motoring due to availability of higher air flow during the acceleration, thus reducing NOx but increasing PM emissions.

Overall, from Figures 4.21 and 4.22, the transition from CDA at motoring to 6-cylinder operation shows poorer, although acceptable, transient response than running in 6-cylinder operation throughout.

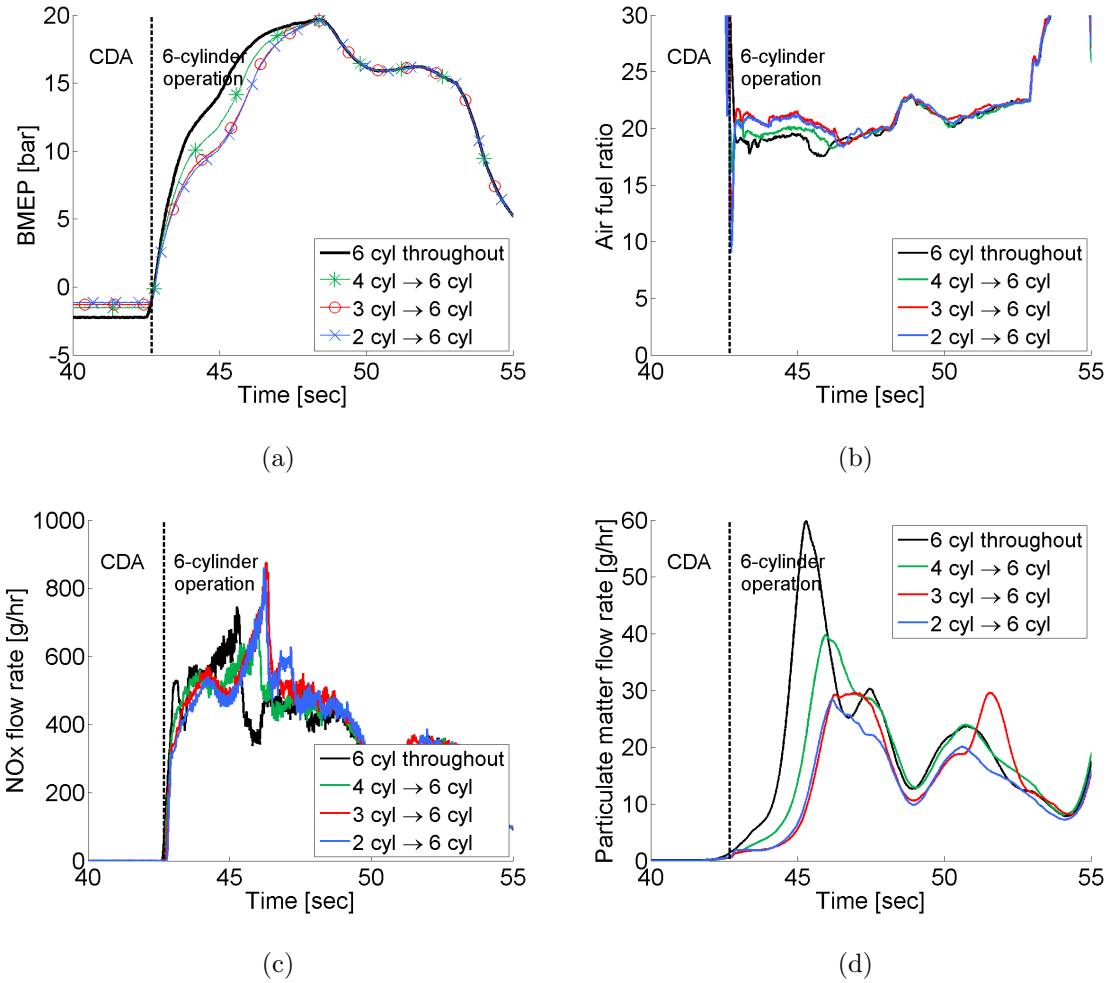

Figure 4.21. Employing CDA during motoring and transitioning to 6-cylinder operation at the onset of the acceleration (a) shows a torque response that lags that of 6-cylinder operation throughout, although the peak load is achieved, (b) achieves close to stoichiometric AFR throughout the acceleration (c),(d) emits lower PM and higher NOx than 6-cylinder operation.

It may therefore be concluded from this section that transient response of the engine remains unaffected when CDA is implemented at conditions with minimal/low boost pressure like idle, while transient response deteriorates when the use of CDA reduces turbocharger speed and boost pressure, typically at high engine speeds.

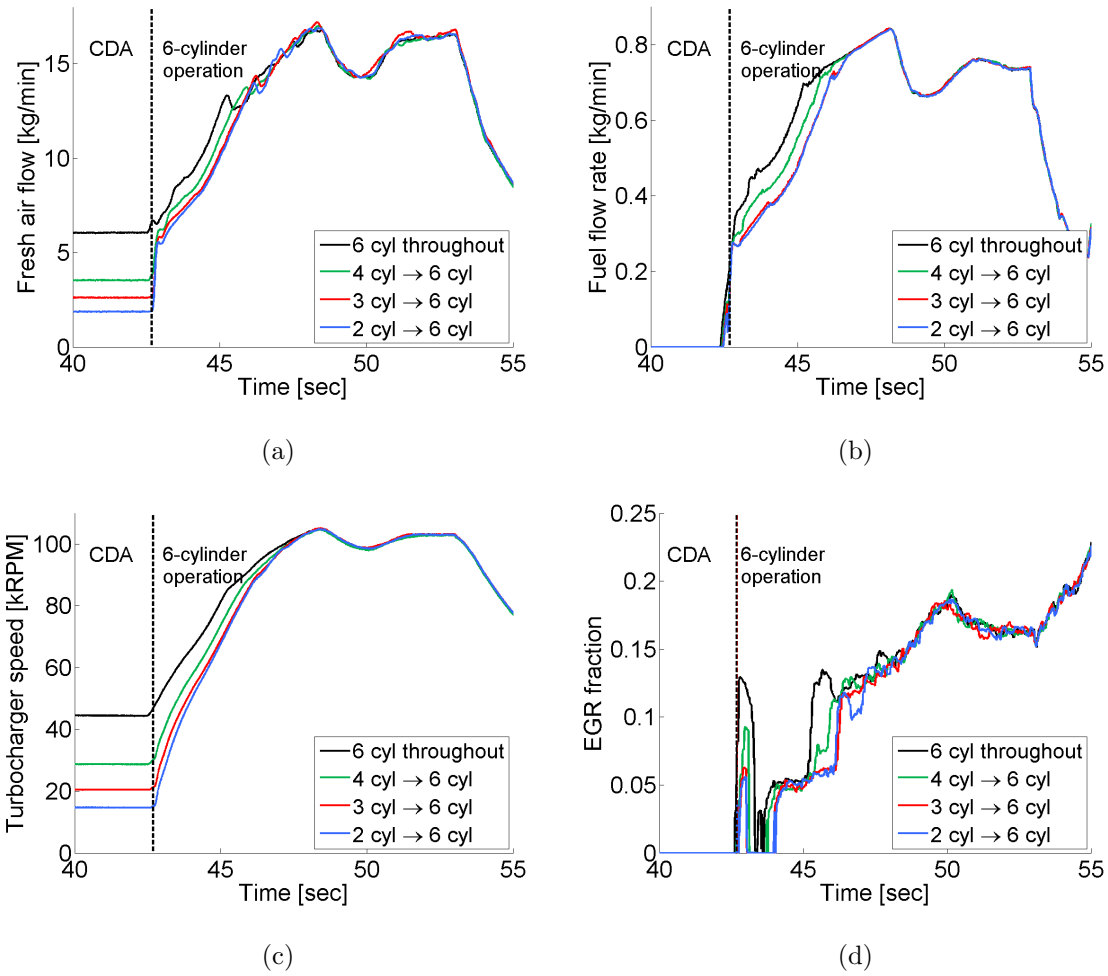

Figure 4.22. Employing CDA during motoring and transitioning to 6-cylinder operation at the onset of the acceleration shows (a) lower air flow rate during the acceleration despite an initial sharp rise upon transition, (b) lower fuel flow during the acceleration, (c) lower turbocharger speed throughout the test, and (d) lower EGR fraction than that seen for 6-cylinder operation throughout.

4.4 Cylinder Deactivation over the HD-FTP Transient Cycle

4.4.1 Introduction and Methodology

Section 4.2 describes the fuel economy and thermal management benefits of CDA, while it is seen from Section 4.3 that transient response of the engine is not compromised when CDA is implemented at and near idle operation. This section describes the fuel economy and thermal management benefits of implementing CDA over the HD-FTP drive cycle.

It was concluded from section 4.2 that the 6-cylinder strategy for aftertreatment warm-up is most preferred to increase the catalyst bed temperatures while the 3-cylinder strategy for aftertreatment 'stay-warm' is preferred for maintaining elevated aftertreatment temperatures. Therefore, the 6-cylinder strategy for aftertreatment warm-up (addressed as TM baseline in Chapter 3) was used during the initial aftertreatment warm-up period, while CDA was implemented after the SCR catalyst bed temperature exceeded 200°C. This corresponds to the 'warm-up' period being between 0 and 900 seconds over the cold cycle, while the 'stay-warm' period includes the remainder of the cold cycle and the entire hot cycle. Figure 4.23 shows the speed and torque profile of the HD-FTP, with the aftertreatment 'warm-up' period shaded in red and the 'stay-warm' period shaded in green.

In the various drive cycles compared in this section, the 6-cylinder strategy for aftertreatment 'warm-up' is implemented during the 'warm-up' period of the HD-FTP (i.e., 0-900 seconds of the cold cycle), and the corresponding engine calibration ('TM Baseline') is used at all off-idle operating conditions over both the cold and hot drive cycles. As shown earlier in chapter 2, the 'TM baseline' calibration is characterized by delayed fuel injections at all possible operating conditions (including non-idle conditions) in order to increase engine outlet temperatures and flow rates. In addition, the late injections also reduce engine-outlet NOx, which together with faster aftertreatment component warm-up, reduce tailpipe NOx to acceptable levels.

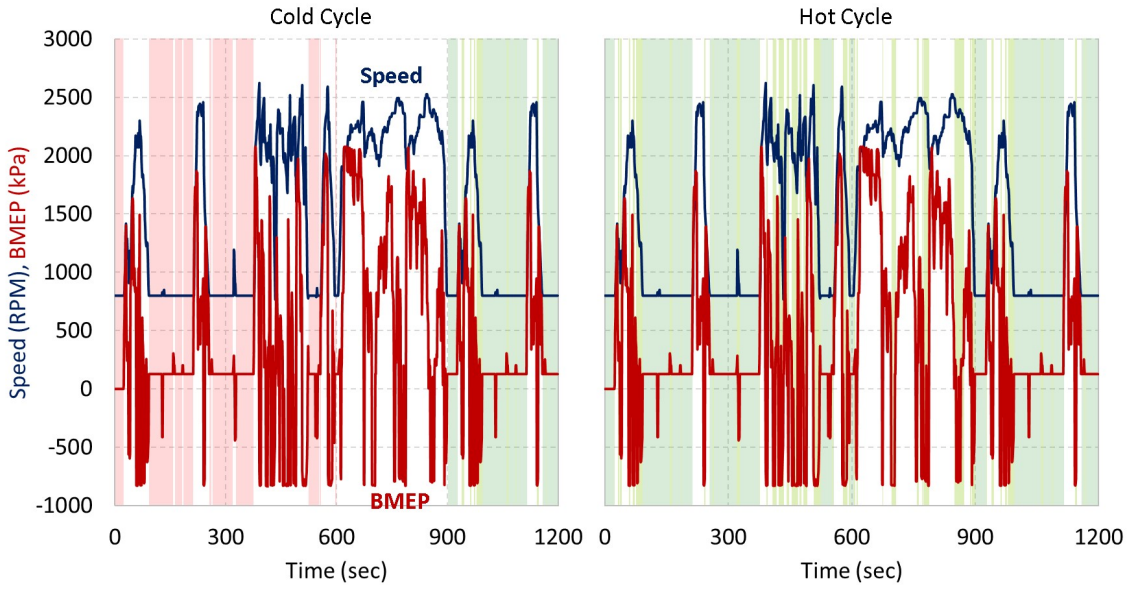

Figure 4.23. HD-FTP drive cycle speed and torque with 'warm-up' and 'stay-warm' idle and low-load regions shaded in red and green respectively

The various drive cycles compared in this section and strategies implemented during their 'stay-warm' periods are described below, and tabulated in Table 4.2.

1. **CDA stay-warm idle cycle** - The 3-cylinder strategy for aftertreatment 'stay-warm' is used during the 'stay-warm' idle regions of the HD-FTP. The 'TM Baseline' engine calibration is implemented at all off-idle conditions over both the cold and hot cycles. This drive cycle demonstrates the fuel savings possible through use of CDA during idle for maintaining elevated aftertreatment component temperatures.

2. **CDA stay-warm low-loads cycle** - In addition to idle operation, CDA is also implemented during low-load engine operation up to 3 bar BMEP during the aftertreatment 'stay-warm' period. At idle, the 3-cylinder strategy for aftertreatment 'stay-warm' is used, while at other low loads, the 3-cylinder operation is controlled by the engine control module (ECM) with charge flow and

EGR fraction targets appropriately modified. This drive cycle demonstrates a further improvement in fuel savings and aftertreatment thermal management due to additional low-load CDA operation.

3. **6-cylinder 'stay-warm' idle cycle** - This drive cycle demonstrates the lowest fuel consumption possible with 6-cylinder operation while meeting the current on-highway emissions limits. The 6-cylinder strategy for aftertreatment 'stay-warm' is used during the 'stay-warm' idle regions of the HD-FTP, while the 'TM Baseline' engine calibration is implemented at all off-idle conditions over both the cold and hot cycles. This drive cycle shows the fuel consumption increases typically required during conventional 6-cylinder engine operation in order to thermally manage the aftertreatment in a way consistent with meeting current emissions limits.

In addition, the 'TM Baseline' drive cycle from Chapter 3 is plotted on Figures 4.24- 4.29 to provide a baseline for aftertreatment thermal management and lowest tailpipe-out emissions possible via conventional 6-cylinder operation. The 'FE Baseline' strategy is also shown on Figure 4.29 to illustrate the best BSFC 6-cylinder operation possible over the HD-FTP.

4.4.2 Results

Figures 4.24 - 4.28 show results from running the three aforementioned strategies over the HD-FTP. The turbine-outlet temperature, the SCR outlet gas temperature and fuel flow rate are experimentally measured, while the SCR efficiency and tailpipe-out NOx emissions are estimated using the method described in Chapter 2, and illustrated by Figure 2.8. Strategies are compared by taking a weighted mean of the fuel consumption and predicted tailpipe-out NOx of the cold and hot drive cycles.

Figure 4.24 illustrates that the TOT for all the cycles are the same during the aftertreatment warm-up period, as all the cycles implement the same 6-cylinder warm-up strategy. The TOT is lower for the 'CDA stay-warm idle cycle' as compared to the

Table 4.2. Summary of the drive cycle strategies demonstrated in this chapter.

Drive cycle	**Idle**	**Low loads (< 3 bar BMEP)**	**Other operating conditions**
CDA stay-warm idle cycle	**3-cyl strategy for A/T stay-warm**	TM baseline calibration	TM baseline calibration
CDA stay-warm low loads cycle	**3-cyl strategy for A/T stay-warm**	**3-cyl operation**	TM baseline calibration
6-cyl stay-warm idle cycle	**6-cyl strategy for A/T stay-warm**	TM baseline calibration	TM baseline calibration
TM baseline cycle	TM baseline	TM baseline calibration	TM baseline calibration
FE baseline cycle	FE baseline	FE baseline calibration	FE baseline calibration

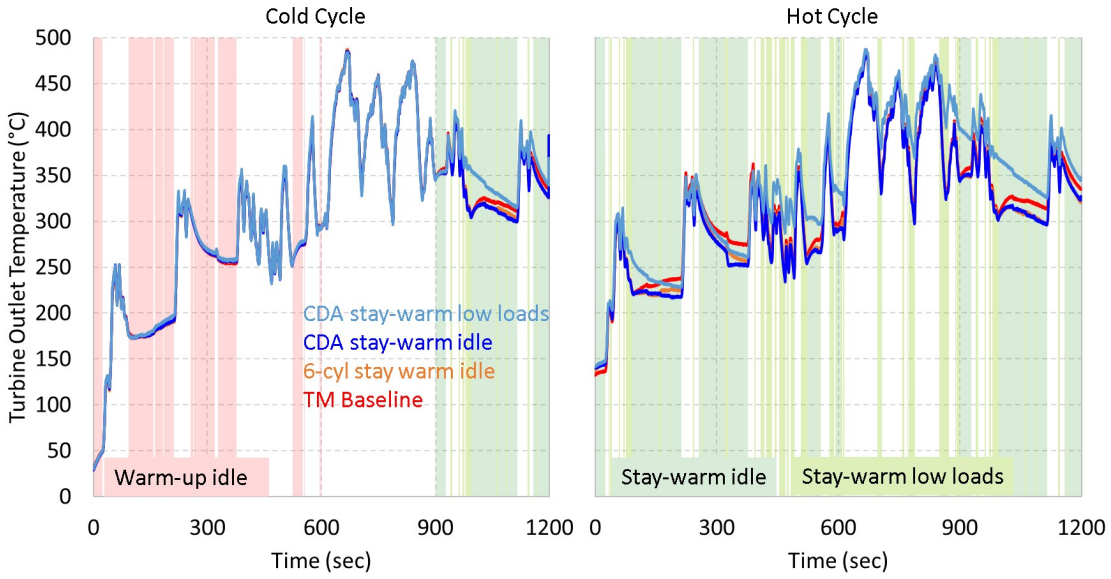

Figure 4.24. Turbine-outlet temperature over the HD-FTP for the A/T stay-warm strategies.

6-cylinder cycles, consistent with its lower TOT at steady state operation. However, the TOT with 'CDA stay-warm low-loads cycle' is highest among the four cycles, predominantly in regions where CDA is implemented at low loads below 3 bar BMEP. It may be concluded that reducing airflow through the engine wherever possible at low loads maintains elevated TOT for longer periods due to reduced cooling effect from excess airflow.

Figure 4.25 compares the SCR outlet gas temperature for the four drive cycles.The CDA stay-warm idle cycle results in nearly the same SCR temperature as the 6-cylinder stay-warm idle cycle, as the reduced exhaust flow rate for the CDA cycle compensates for the lower TOT, thereby showing nearly the same 'cool-down' effect. This is consistent with the normalized heat transfer trends shown in Figure 4.9. Running CDA at all low loads (in the CDA stay-warm low loads cycle) further enhances the 'stay-warm' operation by reducing aftertreatment cool-down and maintaining higher SCR temperatures over the cycle.

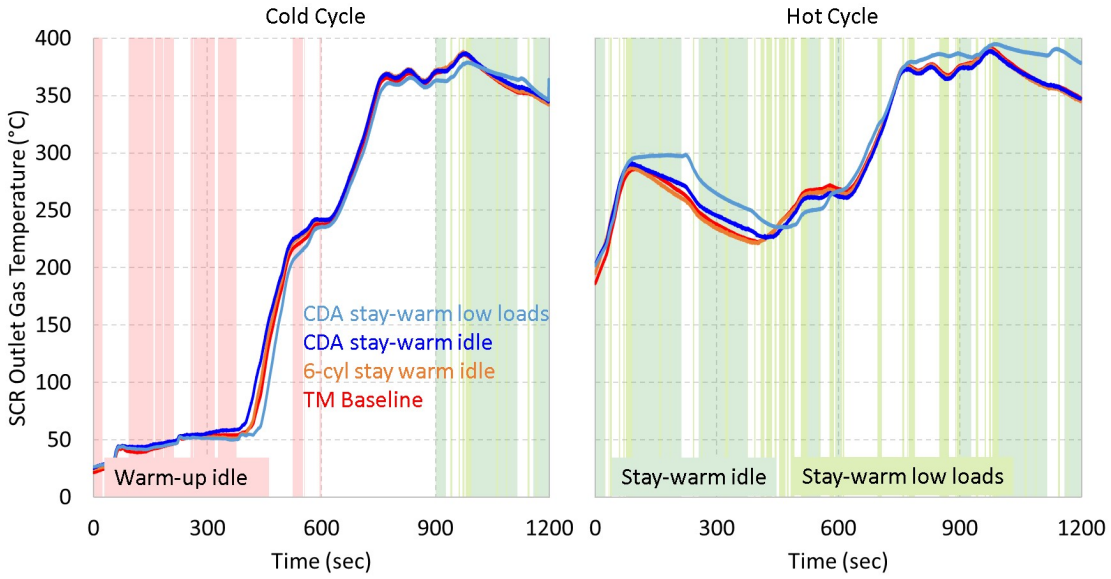

Figure 4.25. SCR outlet gas temperature over the HD-FTP for the A/T stay-warm strategies.

Figure 4.26 illustrates the predicted SCR conversion efficiency using the catalyst bed temperature-based efficiency curve shown in Figure 2.8. The CDA stay-warm low loads cycle has higher SCR efficiency than all other cycles at the beginning of the hot-cycle as a result of maintaining higher SCR temperature.

Figure 4.27 shows the predicted tailpipe-out NOx for the four drive cycles using measured engine-out NOx and predicted SCR conversion efficiency. It is shown that the CDA stay-warm low-loads cycle has lower tailpipe-out NOx during the hot cycle due to the higher SCR conversion efficiency, while the stay-warm CDA idle cycle has similar tailpipe-out NOx as the stay-warm 6-cylinder and 'TM baseline' cycles.

Figure 4.28 shows the difference in cumulative fuel consumption between the cycles, with respect to the 6-cylinder stay-warm cycle. All cycles have nearly the same fuel consumption for the first 900 seconds of the cold cycle, with minor differences occurring due to variability between experiments. The 6-cylinder stay-warm cycle has lower fuel consumption than the 'TM Baseline' cycle due to the more open VGT position it employs during the stay-warm idle regions. The stay-warm CDA idle cy-

cle shows fuel savings with respect to the 6-cylinder stay-warm cycle during the idle operation, consistent with the steady state results in Figure 4.4. It is also shown that employing CDA at low loads other than idle results in further fuel savings.

The weighted fuel consumption and predicted tailpipe-out NOx results from all the drive cycles is summarized in Figure 4.29. The 'FE Baseline' drive cycle, which is the most fuel-efficient 6-cylinder cycle, has a 53% higher tailpipe-out NOx than the 6-cylinder stay-warm and TM Baseline cycles, which meet the emissions regulations at 4.8% higher fuel consumption. Implementing CDA at stay-warm idle with the 'TM Baseline' calibration at all other operating conditions results in 2.7% fuel savings with respect to the 6-cylinder stay-warm idle cycle, while continuing to meet the emissions criteria with similar tailpipe-out NOx. Implementation of CDA at stay-warm low loads below 3 bar BMEP results in a further 0.8% fuel savings, with slightly lower tailpipe-out NOx via improved aftertreatment thermal management.

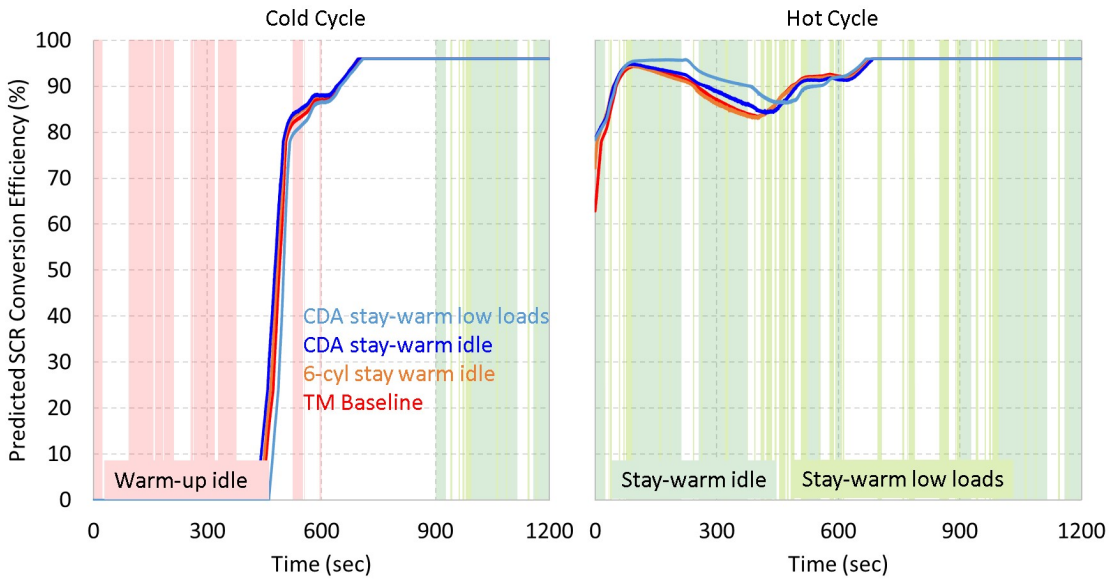

Figure 4.26. Predicted SCR conversion efficiency over the HD-FTP for the A/T stay-warm strategies.

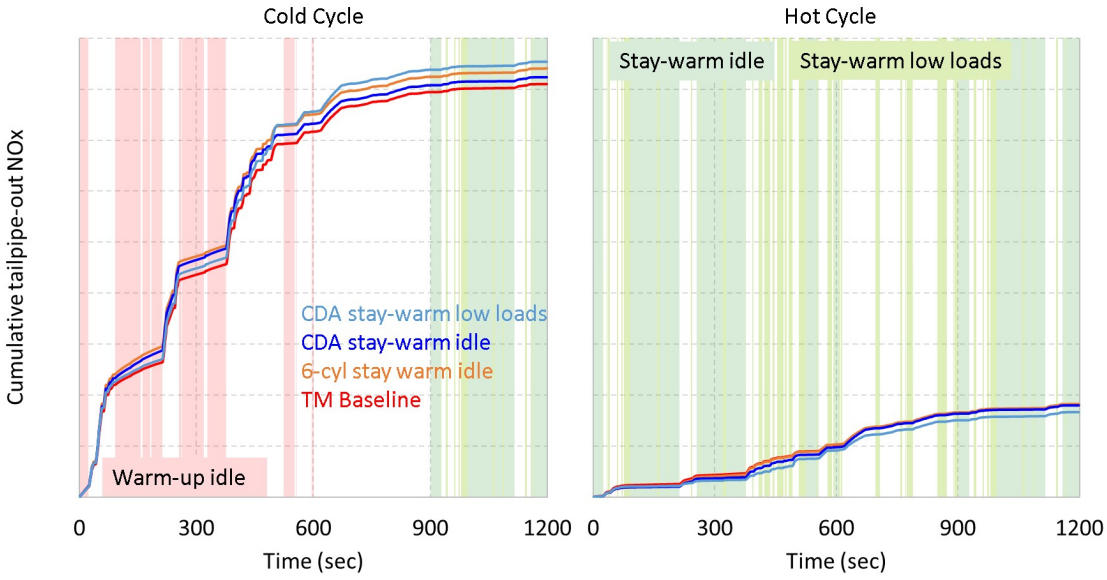

Figure 4.27. Predicted tailpipe-out NOx over the HD-FTP for the A/T stay-warm strategies.

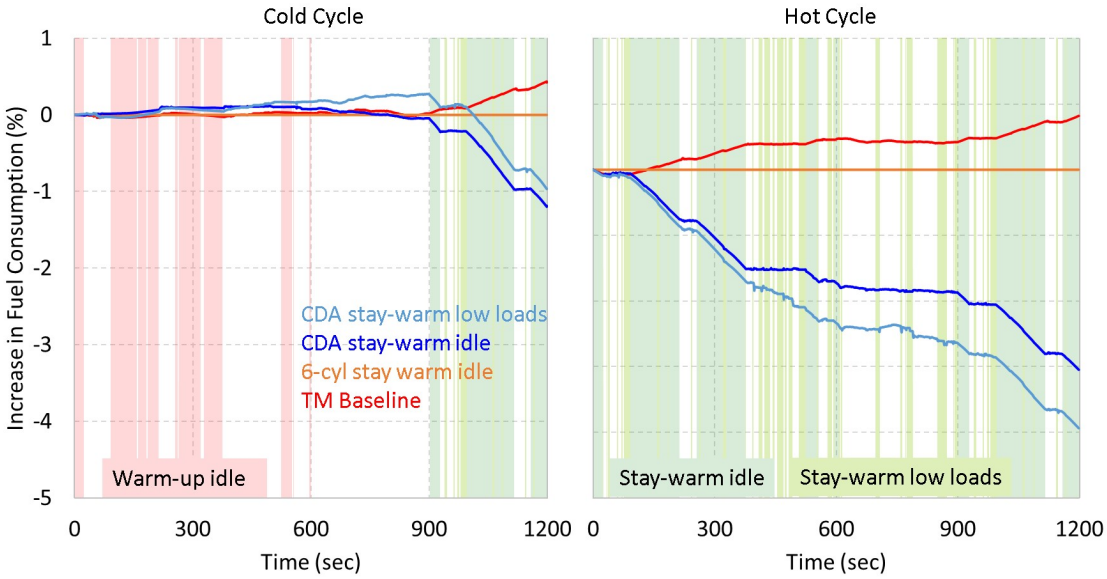

Figure 4.28. Change in fuel consumption with respect to 6-cylinder 'stay-warm' idle cycle over the HD-FTP.

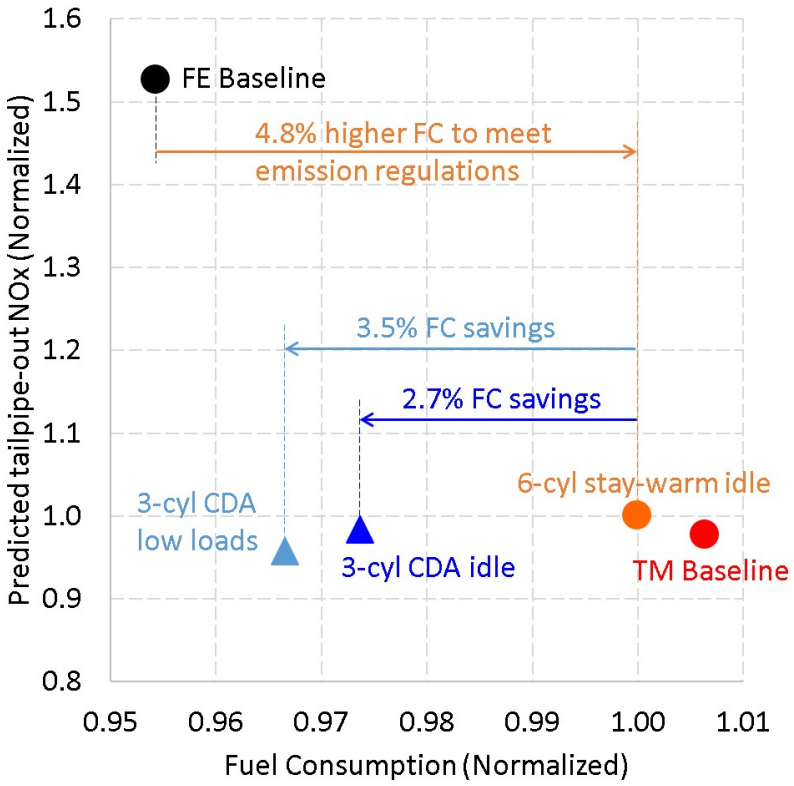

Figure 4.29. Up to 3.5% improvement in fuel consumption can be obtained by implementing CDA at curb idle sections of the HD-FTP. The ability of CDA to maintain A/T temperature is reflected in the form of nearly equal tail pipe out NOx as six-cylinder thermal management mode.

In summary, the results from this section show that implementation of 3-cylinder CDA at low-load and idle operation can result in notable fuel savings while maintaining tailpipe-out NOx emissions consistent with current emission standards.

5. DYNAMIC CYLINDER ACTIVATION FOR MANIPULATION OF ENGINE VIBRATION CHARACTERISTICS

5.1 Introduction and Motivation

This chapter discusses dynamic cylinder activation (DCA) as a manifestation of CDA during which a different set of cylinders are deactivated every cycle, as opposed to a conventional form of CDA, wherein a fixed set of cylinders are deactivated for all the cycles. Figure 5.1 illustrates the difference between the fixed diesel-engine CDA and DCA for the same fraction of overall active/firing events. This chapter

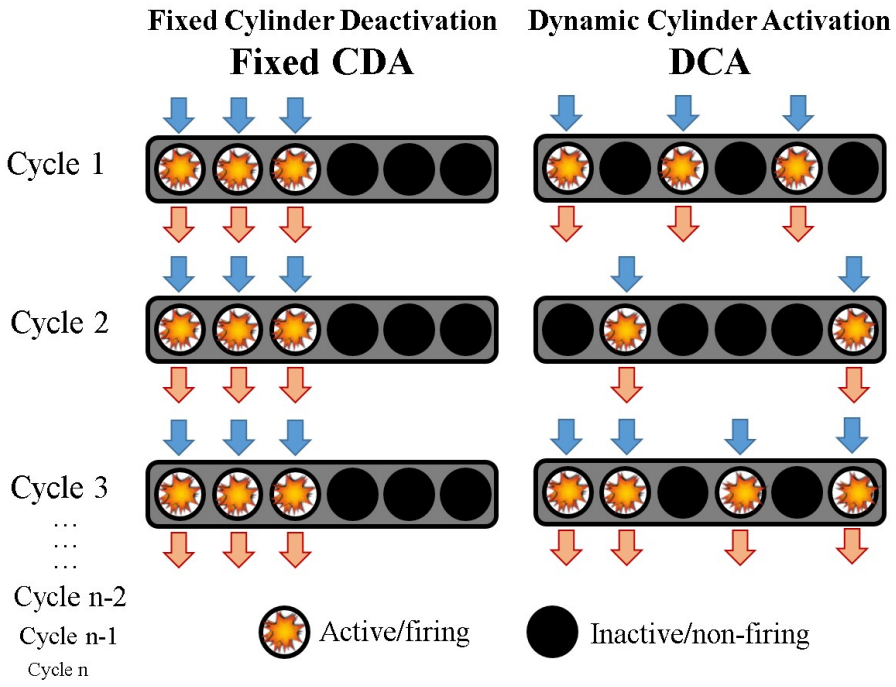

Figure 5.1. Dynamic cylinder activation involves activation of a different set of cylinders every cycle, such that every cylinder is periodically activated and deactivated, and can be implemented in a number of firing patterns.

demonstrates that DCA enables greater control over the torsional vibrational excitations from the engine than fixed CDA, thereby making it possible to move the forcing frequency of the engine away from the drivetrain resonant frequency at all engine speeds, through selection of appropriate firing patterns, while achieving the same fuel savings and thermal management benefits as fixed CDA.

While this is the first study the author is aware of for diesel engines, similar techniques have been studied, in various forms, on gasoline engines. Wilcutts et al. [56], and Eisazadeh-Far and Younkins [57], investigated 'dynamic skip fire (DSF)' as a fuel-efficient alternative to conventional eight-cylinder gasoline engine operation and demonstrated 14-21% fuel savings on a General Motors V8 engine. Fuel efficiency benefits over fixed gasoline engine CDA was hypothesized as a result of a greater number of firing patterns allowing reduced usage of throttling to maintain a stoichiometric air-to-fuel ratio.

Schaeffler implemented 'rolling cylinder deactivation (RCD)' on 3-cylinder gasoline engines, wherein every cylinder is deactivated during each alternate cycle to maintain a uniform firing pattern [58, 59]. This "1.5" cylinder operation is analogous to half-engine CDA and provides higher fuel savings than a form of CDA where two of the three cylinders were active as a result of lower pumping losses. Consistent firing intervals for the RCD approach was also shown to be more favorable with regard to torsional vibration and harshness. In addition, RCD prevented the deactivated cylinders from cooling down, thereby reducing heat-related cylinder distortion, while also preventing oil accumulation in the deactivated cylinders due to absence of prolonged inactive periods of deactivation for a given cylinder.

DSF and RCD in gasoline engines are more efficient than conventional gasoline engine CDA as a result of reduced implementation of the intake throttle. However, as diesel engines are typically unthrottled, it is predicted that DCA would maintain the performance and emissions characteristics of fixed CDA, while providing more flexibility to control the firing frequencies and cylinder usage patterns. Experimental results for each of these DCA characteristics – performance, emissions, firing frequen-

cies, and usage patterns – are compared to fixed CDA experimental results in this chapter.

Archer and McCarthy, Jr., [46] concluded that fixed CDA with a different number of active cylinders must be implemented at different engine speeds to enable resonance-free engine operation. However, in doing so, a compromise has to be made with engine performance, as the optimal CDA strategy cannot be implemented at all engine speeds. It will be shown in this chapter that DCA enables greater control over the firing frequencies than fixed CDA while operating with the same effective number of cylinders, which can be used to tune the torsional vibration characteristics during CDA to be better suited for a given drivetrain across the full range of engine speeds. This flexibility is particularly useful at low engine speed operating conditions, where (i) firing frequencies lie closer to typical drivetrain resonance frequencies and (ii) humans are more likely to be bothered by any resulting vehicle vibration [44].

DCA also reduces the continuous time for which a cylinder is deactivated, and enables intermittent utilization of all cylinders, while reducing the effective displaced volume of the engine.

5.2 Methodology

A fixed quantity of fuel is injected in each firing cylinder to realize an engine BMEP of 1.3 bar at 800 RPM, corresponding to curb idle operation, with a cylinder firing density of 50%. Fuel injection includes pilot and main injections. Rail pressure and VGT position were held constant at 600 Bar and 79% open, respectively. EGR valve position was modulated to achieve adequate EGR fraction to constrain NOx emissions to those of the conventional six-cylinder operation. The VGT nozzle was closed to increase exhaust manifold pressure in cases where adequate EGR fraction was not achieved even with a fully open EGR valve. The operating set points are summarized in Table 5.1.

Table 5.1. Engine set points for DCA operation.

Speed	800 r/min
BMEP	1.3 bar
Injection profile	2 injections (pilot + main)
Rail pressure	600 bar
VGT position	79% closed*
EGR valve	Modulated to achieve adequate EGR fraction to constrain NOx

**VGT nozzle was closed further, to increase exhaust manifold pressure, in cases where adequate EGR fraction was not achieved with fully open EGR valve.*

Friction and parasitic losses associated with the valvetrain are not accounted for any of the operating conditions during analysis, as the VVA system is powered by an external hydraulic pump. It is expected that the fuel savings for fixed CDA and DCA will be higher in production systems, as actuation of fewer valves in fixed CDA and DCA leads to lower parasitic losses than 6-cylinder operation [60].

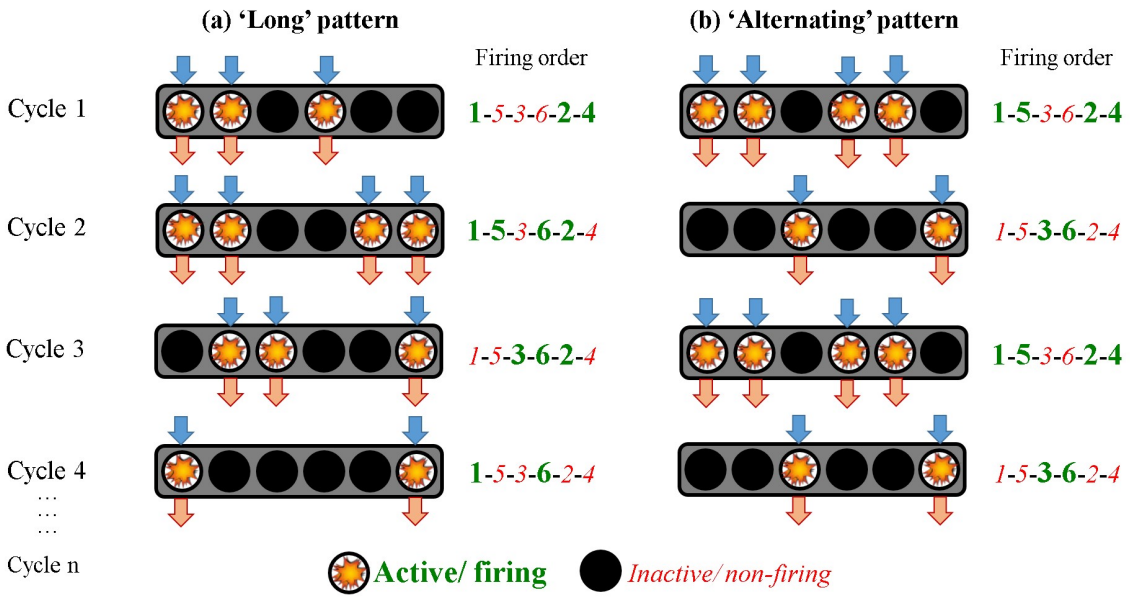

Figure 5.2. DCA is implemented using two firing patterns, in this work.

5.2.1 Firing Pattern

Two firing patterns, both with a firing density of 50%, are implemented in DCA. One of the patterns repeated every 100 cycles, with a constraint of meeting 50% firing density at the end of every ten cycles. This pattern is illustrated in Figure 5.2(a) and is hereafter referred to as the "long pattern". The other firing pattern involves two successive firing (active) events followed by two successive non-firing (inactive) events, such that the pattern repeats every two cycles. Specifically, each cylinder is activated every alternate cycle, as illustrated by Figure 5.2(b), and is hereafter referred to as the "alternating pattern". As the firing density is 50%, analogous to half-engine fixed CDA, the quantity of fuel injected in each firing cylinder is similar to that injected during half-engine fixed CDA.

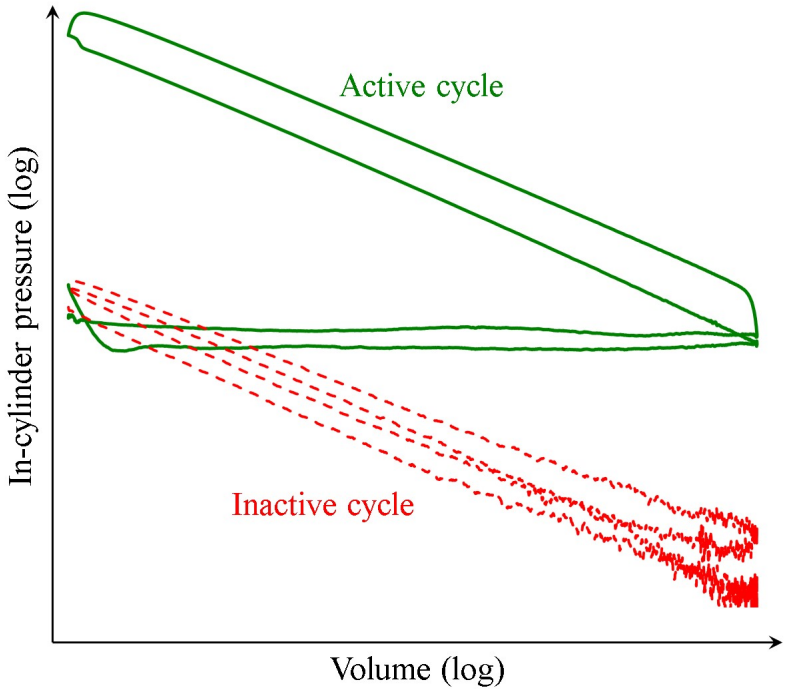

Figure 5.3. In-cylinder pressures during active and inactive cycles in low-pressure charge trapping.

5.2.2 Charge Trapping Strategy

The charge trapping and release strategies implemented during deactivation and reactivation of cylinders has a significant impact on the brake thermal efficiency of the engine. Options include fresh charge trapping (deactivation of a cylinder after its intake event [47, 49, 50, 56, 58, 59, 61]), combusted charge trapping (deactivation of a cylinder after fuel injection [37, 47, 58, 59]) and low-pressure charge trapping (deactivation of a cylinder after its exhaust event [56,58,59]). Rebbert et al. [61] advise trapping higher pressure exhaust gas, either by fresh charge trapping or combusted charge trapping, in the cylinder to reduce oil consumption. A comparative analysis of fresh charge trapping and combusted charge trapping strategies on a diesel engine during fixed CDA was performed by Allen et al. [47], and found that the pressure

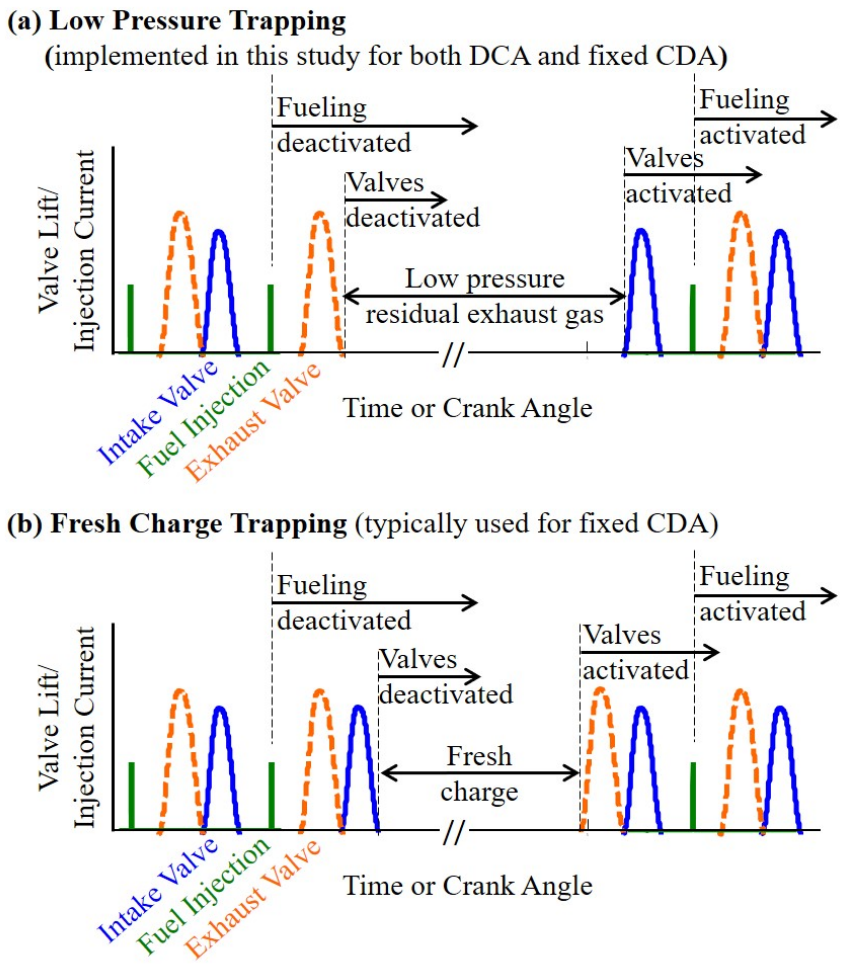

Figure 5.4. (a) The intake valve is the first to be deactivated and reactivated during low-pressure trapping, which is implemented for both DCA and fixed CDA in this study (b) The exhaust valve is the first to be deactivated and reactivated in fresh charge trapping, which is typically implemented for fixed CDA.

of the trapped charge in the deactivated cylinders decayed quite rapidly due to heat and mass loss via gas blowby.

The charge trapping and release strategy selection is especially important during DCA, as cylinders continuously undergo deactivation and reactivation, and therefore, any losses experienced as a part of the charge trapping and release strategy will be magnified. The work demonstrated by Wilcutts et al. [56] implemented low-pressure

trapping during gasoline engine dynamic skip fire operation, in order to reduce frictional losses. Schaeffler studied various charge trapping strategies for 'alternating cylinder deactivation' in a three-cylinder gasoline engine and concluded that low-pressure trapping provided the best fuel economy benefits, without noticeable loss in engine oil due to the short period of deactivation for a given cylinder [58, 59].

The exhaust valve event is the last to occur before cylinder deactivation in low-pressure charge trapping, following which the intake valve is the first to be deactivated. Therefore, the cylinder contains only the residual exhaust gases at exhaust manifold pressure (EMP) at top dead center (TDC). The intake valve is the first to be deactivated following a conventional exhaust stroke. The trapped gases expand to a lower pressure, well below atmospheric pressure, as the piston moves towards bottom dead center (BDC), and are compressed back to the EMP as the piston travels from BDC to TDC. The intake valve is the first to be reactivated, thus inducting fresh charge into the cylinder before injection of fuel, followed by reactivation of the exhaust valve. Figure 5.3 shows the variation of pressure with volume during active and inactive cycles for a given cylinder undergoing low-pressure trapping. Figure 5.4(a) illustrates the sequence of valve and fuel injection deactivation and reactivation for low-pressure trapping.

The sequence of valve and fuel injection events for fresh charge trapping, which is typically used for fixed CDA, is shown in Figure 5.4(b) for comparison. An intake valve event occurs in the first inactive cycle, inducting fresh charge into the cylinder, following which the exhaust valve is deactivated. Fresh charge is therefore retained inside the deactivated cylinder. The exhaust valve is the first to be reactivated, thereby releasing the trapped charge into the exhaust manifold, following which the intake valve and fuel injection are reactivated.

Low-pressure charge trapping is implemented for both DCA and half-engine fixed CDA modes of operation in this study. It is demonstrated later in section 5.5 that while the choice of charge trapping strategy does not affect steady state performance

in fixed CDA operation, low-pressure charge trapping is preferred over fresh charge trapping for DCA.

The performance and torsional characteristics of DCA over both the 'long' and 'alternating' patterns are compared with half-engine fixed CDA at steady state as described in the following sections.

5.3 Torsional Vibration Analysis

Figure 5.5 compares the instantaneous flywheel angular velocity of the two modes of DCA operation with half-engine fixed CDA operation and baseline six-cylinder operation at loaded idle (800 RPM, 1.3 Bar BMEP), over five engine cycles, or ~ 0.75 seconds. Figure 5.5(a) shows the angular velocity of conventional six-cylinder operation. Figure 5.5(b) shows that half-engine fixed CDA shows less periodic oscillations, consistent with only half the number of cylinders firing, and higher peak-to-peak amplitudes, consistent with the greater quantity of fuel combusted in each active cylinder. Figure 5.5(c) demonstrates that the flywheel velocity of DCA with the 'long' pattern does not appear to be periodic. Figure 5.5(d) shows the flywheel velocity of DCA with the 'alternating' pattern. The signal is clearly periodic, with a period twice that of half-engine fixed CDA, as expected. Greater peak-to-peak amplitudes in flywheel velocity correspond to the nature of the pattern where two consecutive firing events are followed by two consecutive non-firing events, thereby resulting in a greater deviation in angular velocity.

Angular acceleration of the flywheel is obtained from the flywheel velocity shown in Figure 5.5. The excitation frequencies at the flywheel are obtained by performing a fast-fourier transform (FFT) on the flywheel acceleration signal, which is proportional to the instantaneous torque produced by the engine.

Figure 5.6 shows the FFT of the flywheel acceleration over 100 cycles for DCA, compared with half-engine fixed CDA and baseline six-cylinder operation at loaded idle. The FFT shows the amplitude of flywheel acceleration as a function of frequency and engine order. An engine order analysis normalizes the frequency content of the vibration signal to the rotational speed of the engine. A first engine order corresponds to frequency of rotation of the crankshaft. Events occurring n times during each engine crankshaft rotation are said to have an n^{th} order. As an example, an engine rotating at 800 RPM has a first order at 13.33 Hz, and any frequency f Hz has an order of $\frac{f}{13.33}$.

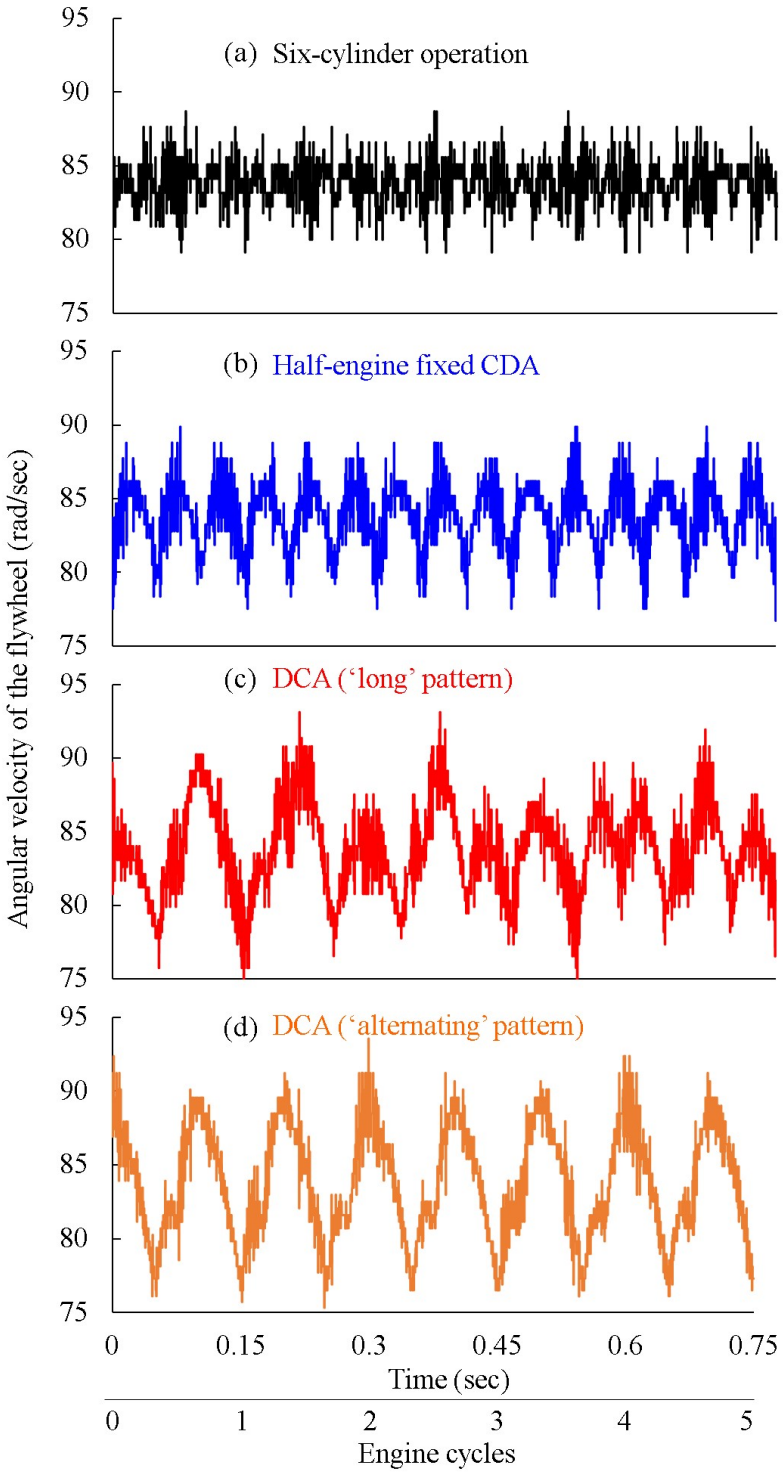

Figure 5.5. Instantaneous flywheel velocity during (a) conventional six-cylinder operation, (b) half-engine fixed CDA, (c) DCA with 'long' firing pattern, and (d) DCA with 'alternating' firing pattern.

Figures 5.6(a) and 5.6(b) show that the first harmonic of the flywheel acceleration during six-cylinder operation and half-engine fixed CDA occur at 40 Hz (3rd order) and 20 Hz (1.5 order) respectively, corresponding to the respective firing frequencies at 800 RPM. The inertial torque of the engine also occurs at 40 Hz (3rd order) as a result of the motion of the pistons in all cylinders.

Figure 5.6(c) shows that DCA with the 'long' firing pattern eliminates the vast majority of the energy content at 20 Hz (1.5 order), and "spreads out" low energy content across a range of frequencies, each with significantly smaller amplitudes. This is a result of the less periodic nature of the 'long' firing pattern where engine firing does not repeat over short intervals, as also shown in Figure 5.5(c), and therefore, elevated energy content is not concentrated at a single or few discrete frequencies. Energy content at 40 Hz corresponding to the flywheel inertia, is also observed.

Figure 5.6(d) shows the FFT of the flywheel acceleration for DCA with the 'alternating' pattern. As shown, the vast majority of the energy content at 20 Hz is replaced by distinct peaks at 10 Hz and 30 Hz. The 10 Hz peak, which has a higher amplitude than the peak at 20 Hz in half-engine fixed CDA, corresponds to the fundamental frequency of the firing pattern, or two-thirds of an engine cycle. While this firing pattern does not eliminate the concentration of energy at a few distinct frequencies, it demonstrates, together with Figures 5.6(b) and 5.6(c), that the frequencies at which energy is concentrated can be manipulated using DCA.

Therefore, it may be concluded that DCA offers the ability to either significantly reduce the amplitude of forcing frequencies at, or move the forcing frequencies of the engine away from, the drivetrain resonant frequency at all speeds, via selection of appropriate firing patterns.

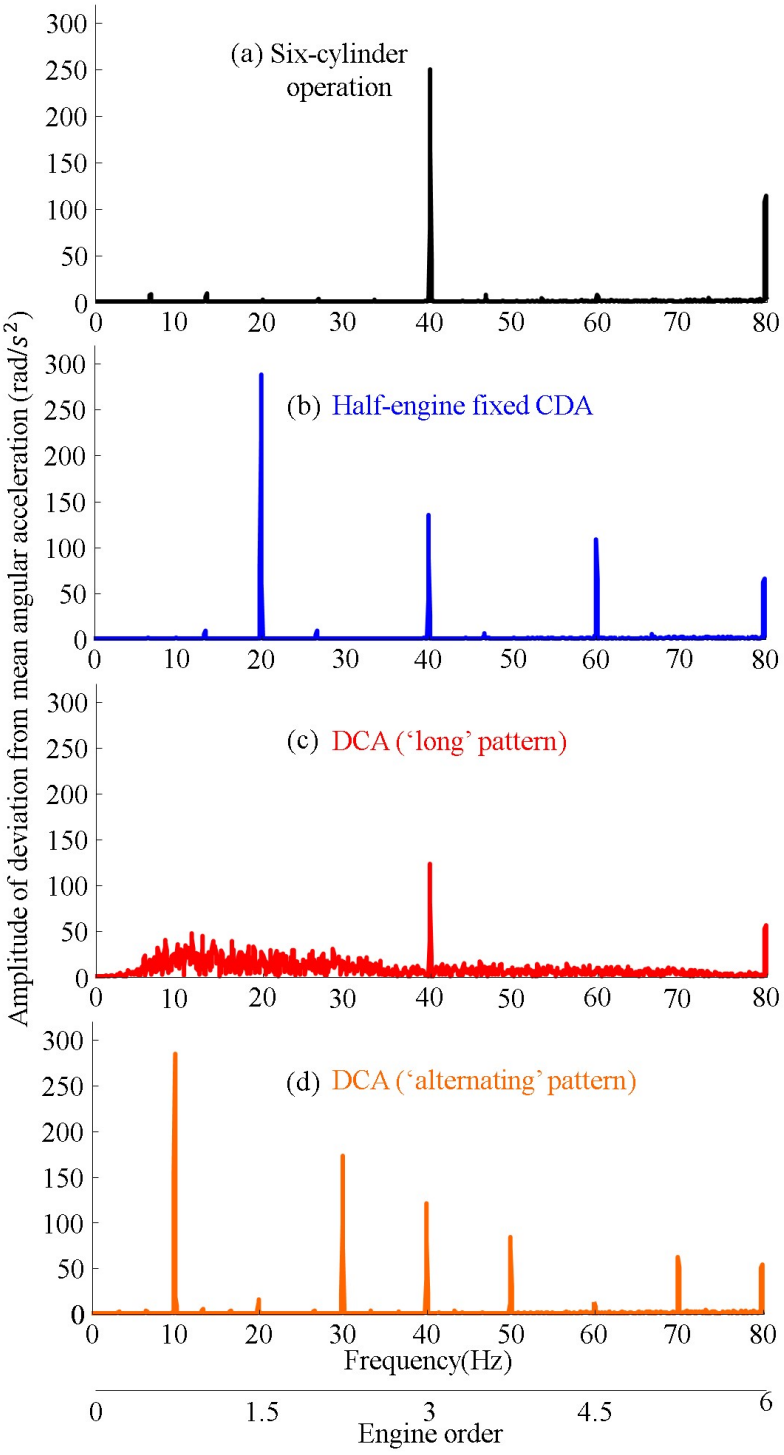

Figure 5.6. FFT of flywheel acceleration during (a) conventional six-cylinder operation, (b) half-engine fixed CDA, (c) DCA with 'long' firing pattern, and (d) DCA with 'alternating' firing pattern.

5.4 Performance Analysis

DCA with a 50% firing density is expected to show nearly the same performance and emissions behavior as half-engine fixed CDA, due to similarities in the gas exchange and combustion processes between DCA and half-engine fixed CDA, specifically, the same effective displaced volume, intake and exhaust manifold pressures, quantity and timing of fuel injection in each cylinder, and inducted in-cylinder air mass. The experimental results described below support this hypothesis.

Figure 5.7(a) shows that the brake specific fuel consumption (BSFC) is similar for DCA with both firing patterns and conventional half-engine fixed CDA, indicating that DCA is as efficient as half-engine fixed CDA. DCA and half-engine fixed CDA have 6% lower BSFC than six-cylinder operation, as expected. Figure 5.7(b) shows that nearly the same turbine-outlet temperature, between $\sim 205°C$ and $\sim 210°C$, is achieved by half-engine fixed CDA and both modes of DCA, $\sim 50°C$ higher than six-cylinder operation. Similar turbine outlet temperature can be attributed to similar air-to-fuel ratios between DCA and half-engine fixed CDA, because of similar airflows and the same quantity of fuel being injected in each cylinder. Figure 5.7(c) shows that DCA and half-engine fixed CDA have nearly the same airflow rate, slightly over half that of six-cylinder operation, as expected.

Figure 5.7(d) shows that the NOx emissions with half-engine fixed CDA and DCA with both firing patterns are approximately the same as six cylinder operation, as NOx emissions from the engine are constrained via use of EGR. Figures 5.7(e)-(f) indicate that the PM and UHC emissions are nearly the same for both modes of DCA and half-engine fixed CDA, and lower than the emissions of six-cylinder operation. This can be attributed to better combustion efficiencies in the active cylinders at loaded idle operation in fixed CDA and DCA (as also shown below), combined with lower exhaust flow rates from the engine.

Figure 5.8 shows that the in-cylinder pressures in the active cylinders are similar among both modes of DCA and half-engine fixed CDA, as a result of similar

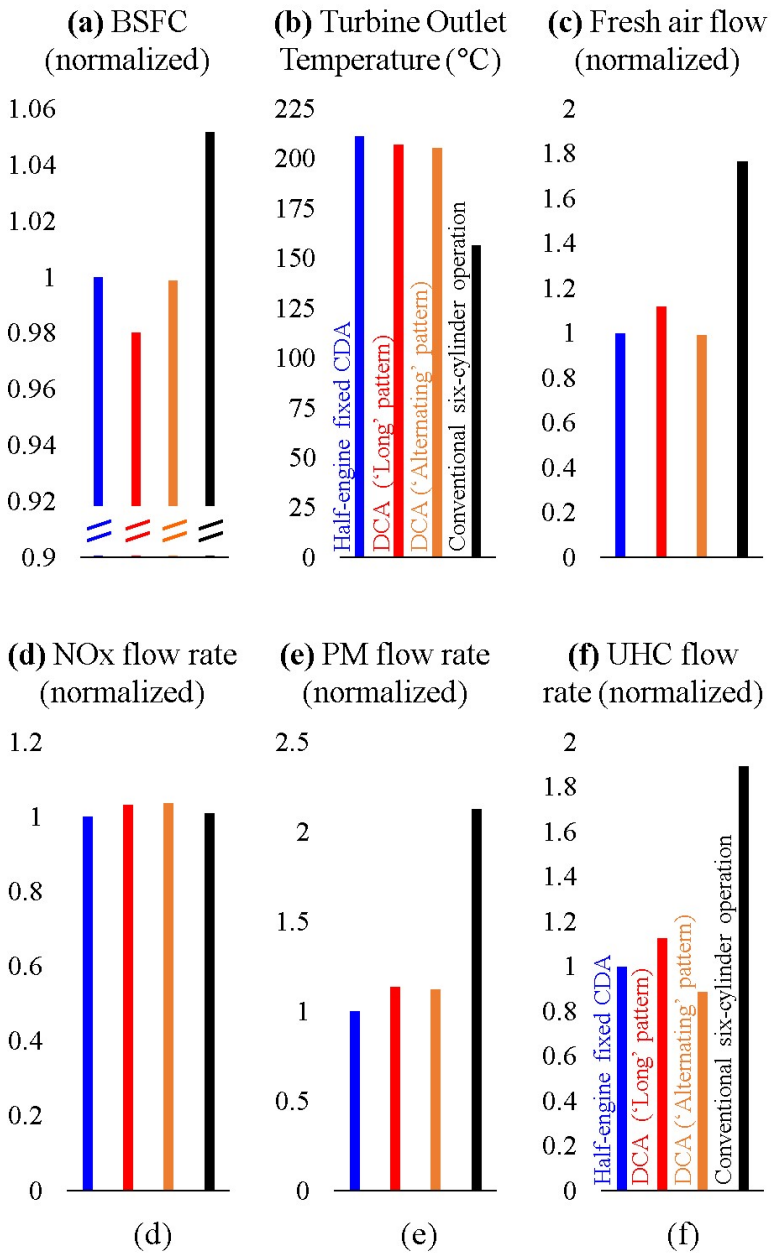

Figure 5.7. DCA at steady state loaded idle operation (800 RPM/ 1.3 Bar BMEP) shows similar fuel efficiency, fresh airflow, TOT and emissions as half-engine fixed CDA

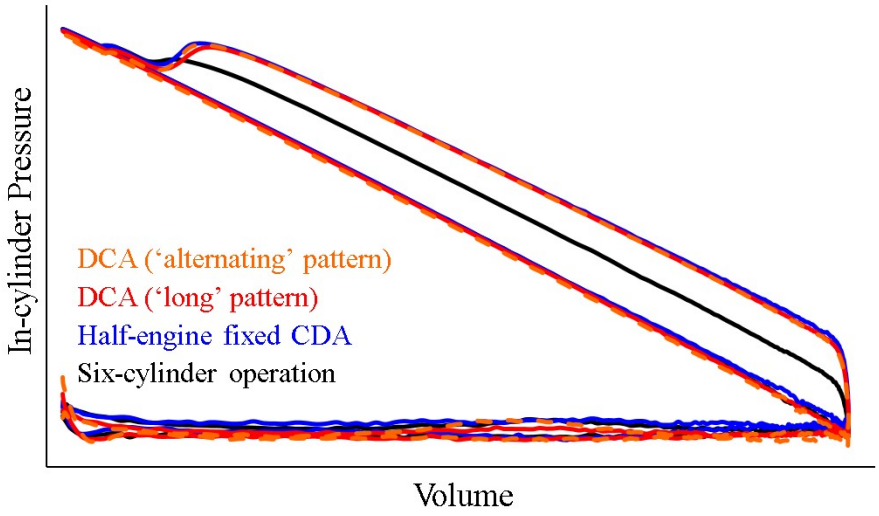

Figure 5.8. DCA at steady state loaded idle operation (800 RPM/ 1.3 Bar BMEP) shows similar in-cylinder pressures in the active cylinders as half-engine fixed CDA

gas exchange and combustion processes inside the cylinder. Figure 5.9 shows the representative heat release rates inside the active cylinders. DCA and half-engine fixed CDA have a similar heat release rate, indicating a similar in-cylinder combustion process because of similar air-to-fuel ratios, fuel injection quantities and timings. Six-cylinder operation injects a smaller quantity of fuel in each active cylinder, and therefore has a smaller heat release rate.

Figure 5.10 compares the open cycle efficiency (OCE) and closed cycle efficiency (CCE) of six-cylinder operation with half-engine fixed CDA and DCA. The OCE of DCA using both the 'long' and 'alternating' firing patterns is nearly the same as half-engine fixed CDA, as a result of similar gas exchange processes, as shown in Figure 5.8. The CCE of both modes of DCA is also comparable to half-engine fixed CDA as a result of similar heat release rate profiles, as also shown in Figure 5.9.

While these results are consistent with expectations, they are profound as they prove that DCA can achieve similar fuel efficiency, emissions, and thermal management benefits resulting from half-engine fixed CDA.

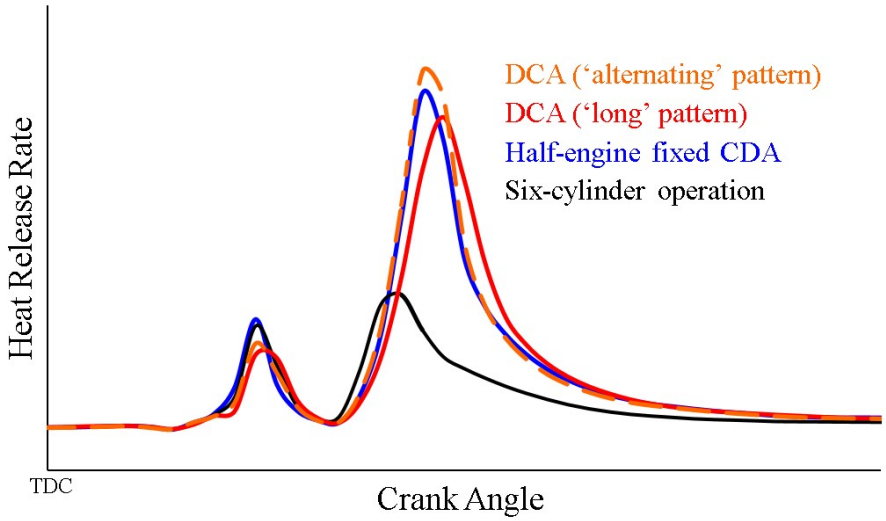

Figure 5.9. DCA at steady state loaded idle operation (800 RPM/ 1.3 Bar BMEP) shows similar heat release rates in the active cylinders as half-engine fixed CDA

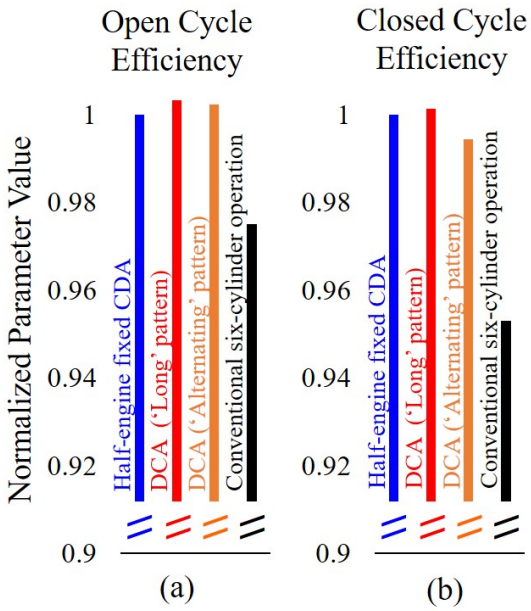

Figure 5.10. DCA at steady state loaded idle operation (800 RPM/ 1.3 Bar BMEP) shows similar open and closed cycle efficiencies as half-engine fixed CDA

5.4.1 Combustion Stability in DCA

Combustion stability is assessed by evaluating the cyclic variation of the crank angle at which 50% of the total energy is released (CA50), for the same injection timing. Stable combustion is expected to achieve similar rates of heat (energy) release from each engine cycle, and therefore, similar CA50. On the other hand, higher standard deviation indicates that the rate of heat release is not consistent in that cylinder, thereby corresponding to less stable combustion. Figure 5.11 shows the cyclic variation and standard deviation in CA50 for each cylinder over 100 cycles for DCA, half-engine fixed CDA and conventional six-cylinder operation at loaded idle. Figures 5.11(a) and 5.11(b) show that the standard deviation of CA50 during six-cylinder operation is between 0.16 CA° and 0.22 CA°, while a standard deviation between 0.1 CA° and 0.17 CA° is observed in half-engine fixed CDA. Figure 5.11(c) shows that DCA operation with the 'long' pattern has a higher standard deviation, between 0.37 CA° and 0.69 CA°, indicating relatively less consistent combustion. This can be attributed to the different, and varying, number of cycles for which each cylinder is deactivated, in addition to expected cylinder-to-cylinder, cycle-to-cycle variation in in-cylinder air-to-fuel ratios, as described earlier. Figure 5.11(d) shows that the standard deviation for DCA operation with the shorter 'alternating' pattern is between 0.08 CA° and 0.12 CA°, indicating greater stability, within the range of half-engine fixed CDA and six-cylinder operation.

It may therefore be concluded that the combustion stability in DCA depends on the nature of the firing pattern, with higher combustion stability expected in more uniform firing patterns, where cylinders are active more frequently.

5.5 Comparison of Charge Trapping Strategies

Two charge trapping strategies - fresh charge trapping and low-pressure charge trapping - are compared in fixed CDA and DCA modes of operation. It is demonstrated that while the choice of charge trapping strategy does not affect steady state

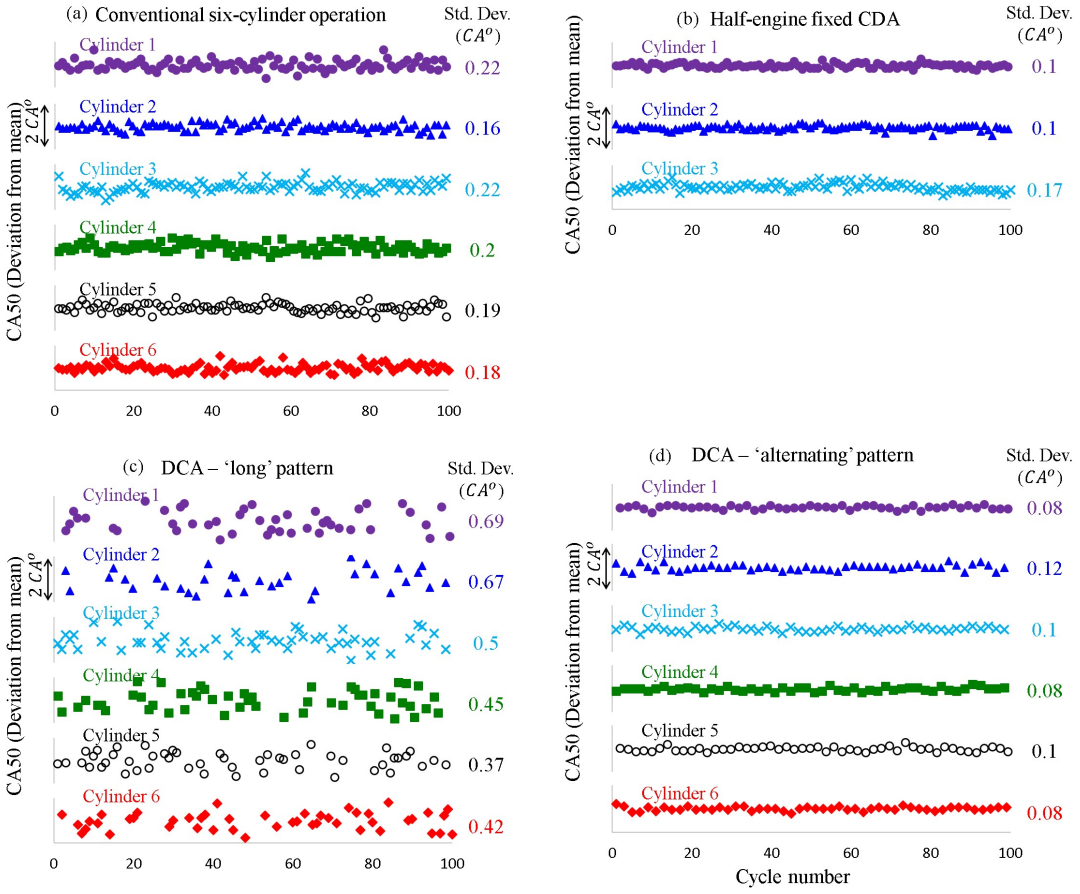

Figure 5.11. Cyclic variation in CA50 during the active cycles of (a) conventional six-cylinder operation (b) Half-engine fixed CDA with cylinders 1,2,3 active (c) DCA with the 'long' pattern, and (d) DCA with 'alternating' pattern

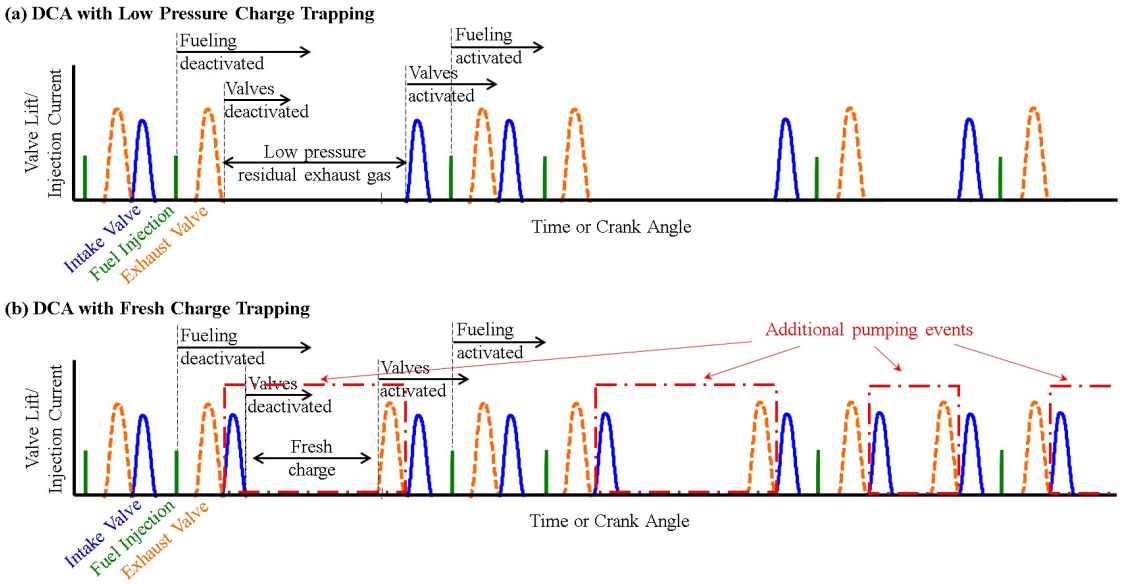

Figure 5.12. The continuous activation and deactivation of valves results in excess pumping events for DCA with fresh charge trapping, compared to DCA with low-pressure charge trapping, for the same firing pattern.

performance in fixed CDA operation, low-pressure charge trapping is more favorable for DCA in this engine configuration.

Figure 5.12 compares the low-pressure charge trapping and fresh charge trapping implementations for DCA operation over the same firing pattern. The fresh charge trapping strategy involves an additional intake valve event during the cycle immediately after deactivation and an additional exhaust valve event immediately prior to reactivation of a cylinder. Continuous activation and deactivation of a given cylinder in DCA results in a greater number of pumping events than necessary for combustion, thereby increasing the total pumping work done by the engine. Fixed CDA operation involves combustion in a fixed set of cylinders, as a result of which deactivation and reactivation of the inactive cylinders occur only once. Steady state operation in fixed

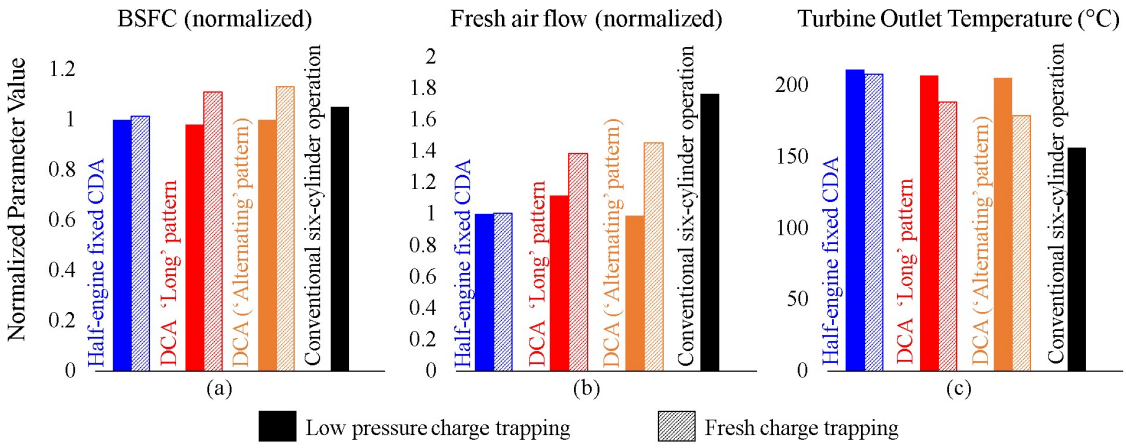

Figure 5.13. Half-engine fixed CDA shows similar BSFC, fresh airflow and TOT between fresh charge trapping and low-pressure charge trapping implementations, while DCA shows lower BSFC, lower fresh airflow and higher TOT with low-pressure charge trapping.

CDA, therefore, has the same number of gas exchange/pumping events for both fresh charge trapping and low-pressure charge trapping.

Figure 5.13(a) compares the BSFC achieved using the two trapping strategies in half-engine fixed CDA and DCA. Half-engine fixed CDA achieves similar BSFC in low-pressure charge trapping and fresh charge trapping. Both modes of DCA ('long' pattern and 'alternating' pattern) show higher BSFC with fresh charge trapping than with low-pressure charge trapping. This can be attributed to the greater number of pumping events during fresh charge trapping, which increases the total pumping work of the engine, as described above. Greater overall pumping work for DCA with fresh charge trapping increases the BSFC of the engine.

Figure 5.13(b) shows that the fresh airflow is similar in both charge trapping strategies in half-engine fixed CDA operation, as airflow occurs only through the three active cylinders during steady state operation. Fresh airflow for DCA using both the 'long' and 'alternating' firing patterns is $\sim 25\%$ and $\sim 45\%$ higher, respectively, with

fresh charge trapping, as a result of airflow through the cylinders during the additional pumping events, which is absent in low-pressure charge trapping.

Figure 5.13(c) shows that the turbine-outlet temperatures for half-engine fixed CDA are similar with both fresh charge and low-pressure charge trapping strategies. Both DCA firing pattern implementations, however, show $\sim 20° - 30°$C lower turbine-outlet temperatures with fresh-charge trapping as a result of net higher airflow, and therefore, higher overall air-to-fuel ratios, through the engine.

It can therefore be concluded that while the choice of charge trapping strategy does not affect steady state performance in fixed CDA, low-pressure charge trapping is preferred for DCA due to its lower BSFC and better thermal management characteristics than fresh charge trapping.

5.6 Recipe for Implementation of Fixed CDA and DCA

The dominant firing frequencies of the engine are directly proportional to engine speed. Figure 5.14 shows the firing frequencies of six-cylinder operation, half engine fixed CDA and DCA "alternating" pattern as a function of engine speed. Half engine fixed CDA shows half the firing frequency of six cylinder operation at all engine speeds, while DCA "Alternating" pattern displays energy content at 25% and 75% of the six cylinder firing frequency. The fixed-CDA and DCA strategies are more efficient than six-cylinder operation, and are therefore the preferred operating strategies.

A hypothetical resonance band is shown between 25 Hz and 35 Hz, to demonstrate selection of an appropriate firing pattern at various engine speeds. Half-engine CDA

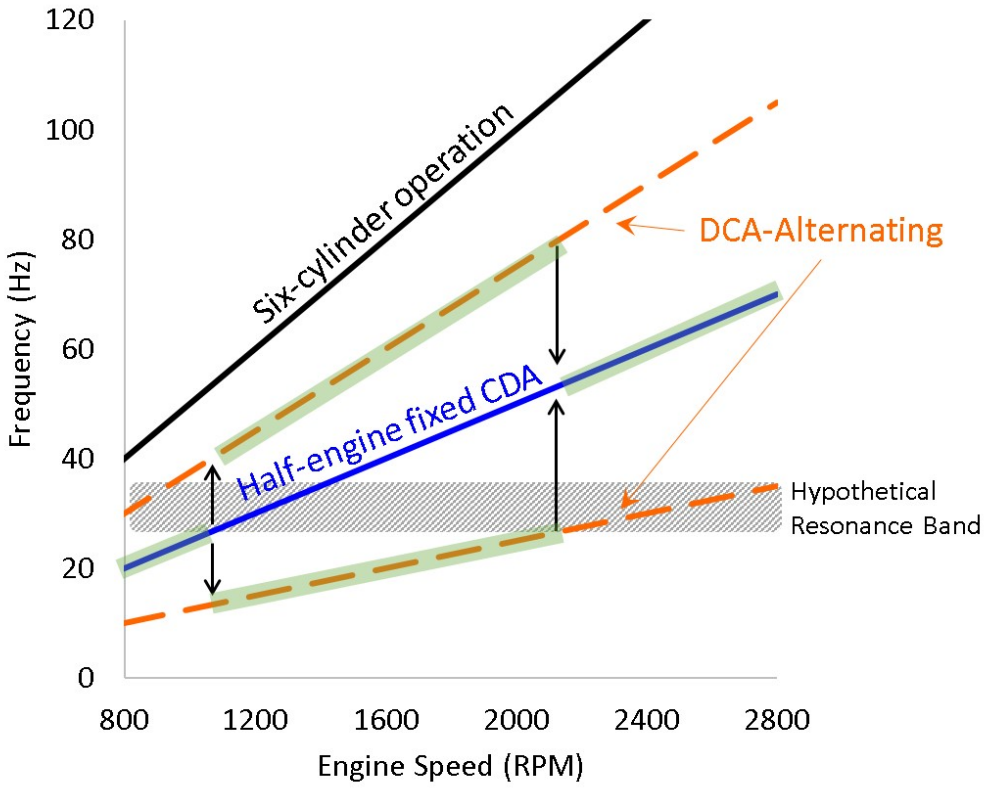

Figure 5.14. Appropriate DCA or fixed CDA strategy can be selected based on engine speed to avoid driveline resonance without compromising on performance.

can be implemented up to a speed of 1000 RPM as the dominant frequency is below the resonance band, while the second harmonic of DCA is within the resonance band. DCA "alternating" strategy can be implemented between 1000 RPM and at least 1400 RPM, as the fundamental order and second harmonic are below and above the resonance band, respectively. Either DCA or half engine fixed CDA can be implemented between 1400 RPM and 2000 RPM as all the harmonics of both strategies are outside the resonance band. Half-engine fixed CDA is the preferred strategy above 2000 RPM as the fundamental order of DCA lies within the resonance band. One such preferred recipe, as described above, is marked in green in Figure 5.14

Similar recipes can be developed using other DCA firing patterns as well, depending on the location of the resonance band. Selection of appropriate firing patterns can ensure engine operation away from the drivetrain resonance band at all engine speeds while maintaining the same performance and emissions as fixed CDA.

5.7 Summary

This chapter demonstrates that dynamic cylinder activation (DCA) can enable greater control over the forcing frequencies on the drivetrain, while achieving similar fuel efficiency and aftertreatment thermal management benefits as fixed CDA. Choice of appropriate firing patterns can ensure engine operation away from drivetrain resonant frequencies at all engine speeds. Further, intermittent activation and deactivation of every cylinder ensures that a given cylinder is not deactivated for extended periods of time and leads to a more even cylinder usage.

6. VENTILATED CYLINDER CUTOUT FOR FUEL-EFFICIENT AFTERTREATMENT THERMAL MANAGEMENT

6.1 Introduction

Cylinder deactivation provides fuel efficiency as well as aftertreatment thermal management benefits, enabling simultaneous reduction of greenhouse gases and regulated pollutant emissions, as described in detail in Chapter 4. However, oil accumulation in the non-firing (inactive) cylinders during CDA is a challenge, as described in Section 1.2.6. Oil transport to cylinders primarily occurs from the crankcase through the piston ring pack [48], and is exacerbated by low in-cylinder pressures, bore distortion, smaller ring tension, and higher piston speed. The non-firing cylinders, during CDA, experience a loss in pressure due to blowby of the trapped charge through the piston rings [47], inducing a positive pressure gradient between the crankcase and the cylinder, which is favorable for oil accumulation. Halbe et al. [49] observed an increase in oil accumulation with increasing duration of CDA at 100 ft-lbf torque, at two speeds of 800 rpm and 1200 rpm.

This chapter describes a set of alternate valvetrain strategies where the non-firing cylinders are maintained close to the intake or exhaust manifold pressures by 'ventilating' the non-firing cylinders to the manifold(s). The manifolds are typically at/above atmospheric pressure in turbocharged diesel engines due to the absence of a throttle, therefore, ventilation of the non-firing cylinders to the manifolds eliminates vacuum inside the cylinders, thereby potentially mitigating oil accumulation. These strategies will collectively be referred to as ventilated cylinder cutout (VCC). VCC, like CDA, involves deactivation of fueling from a set of cylinders, such that a greater quantity of fuel is combusted in the remaining active cylinders to meet the torque/ power demand. VCC can be implemented in three forms- (i) ventilating the non-firing

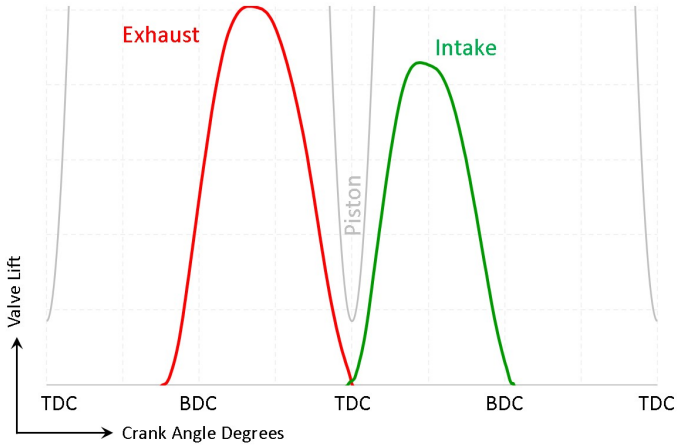

Figure 6.1. Intake and exhaust valve profiles in the active cylinders.

cylinders only to the intake manifold, (ii) ventilating the non-firing cylinders only to the exhaust manifold, and (iii) ventilating the cylinders to the intake and exhaust manifolds for two strokes each, alternately, as described in the following section.

6.1.1 Description of Strategies

All the VCC strategies described in this section have three firing cylinders (cylinders 1,2 and 3) and three non-firing cylinders (cylinders 4,5 and 6), consistent with '3-cyl strategy for A/T stay-warm' described in section 4.2. The firing order of the engine, which is 1-5-3-6-2-4 during conventional six-cylinder operation, is 1-x-3-x-2-x during CDA and VCC strategies, as combustion does not occur in cylinders 4, 5 and 6.

The intake and exhaust valve profiles in the active cylinders are kept consistent with conventional engine operation, and are shown in Figure 6.1.

1. **Cylinder deactivation**: CDA involves deactivation of both the intake and exhaust valves in the non-firing cylinders, as shown in Figure 6.2(a), and therefore, no gas exchange takes place in the non-firing (deactivated) cylinders. The

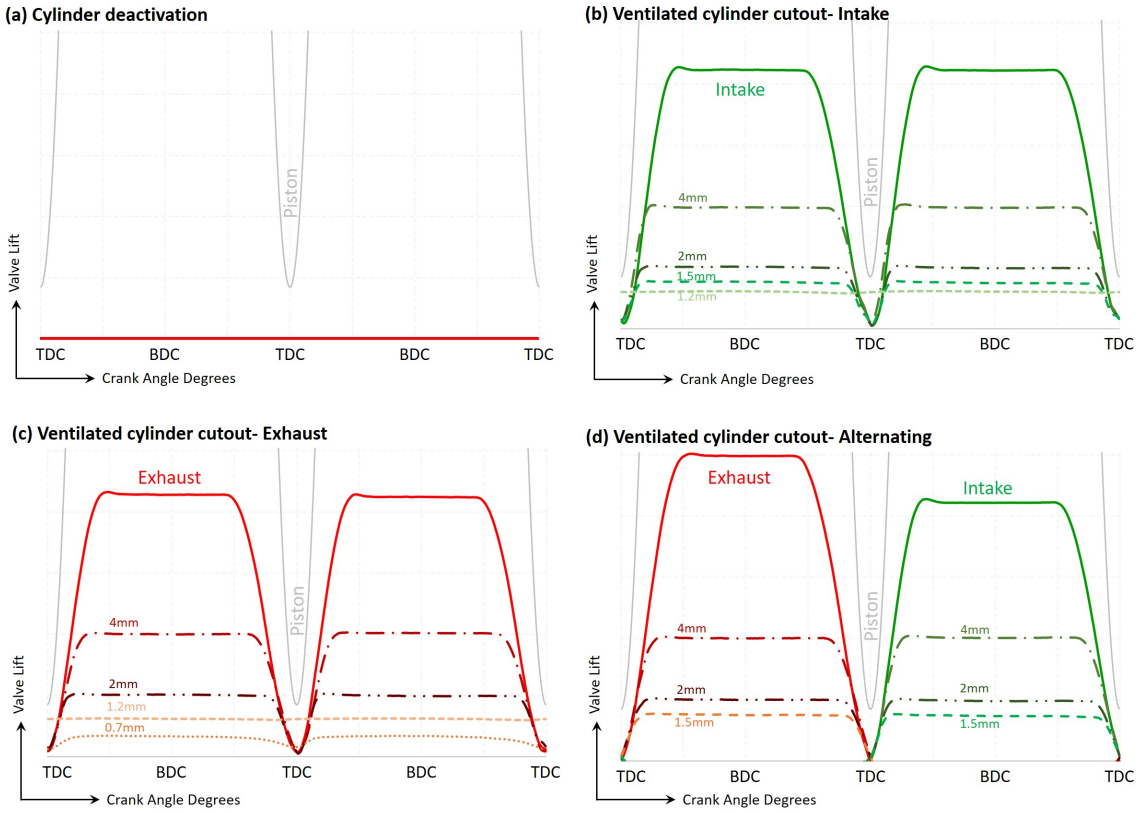

Figure 6.2. Intake and exhaust valve profiles in the non-firing cylinders during (a) CDA, (b) VCC-Intake, (c) VCC-Exhaust and (d) VCC-Alternating.

strategy for implementation of CDA at idle, as described by "3-cyl strategy for A/T stay-warm" in Table 4.1, is implemented in this work.

2. **Ventilation to intake manifold - "VCC-Intake"**: Ventilation of the cylinder to the intake manifold is achieved by keeping the intake valves open throughout the four strokes of the cycle in the non-firing cylinders, with the corresponding exhaust valves deactivated, as represented by Figure 6.2(b). In this configuration, the non-firing cylinders induct gases from the intake manifold as the pistons move towards the BDC and expel them back to the intake manifold during the piston motion towards the TDC, thereby remaining in near-equilibrium

with the intake manifold. This configuration is hereby referred to as "VCC-Intake". The strategy is implemented on this experimental setup by closing the intake valves near the top dead center (TDC) to avoid contact between the valves and the piston. This strategy may also be implemented by leaving the intake valve open at a certain height in engine configurations where a piston valve pocket is available. Typically, valve pockets are shallow and do not allow keeping the valves open at full lift. Therefore, the VCC-Intake strategy has also been experimentally demonstrated with lower valve lifts of 4mm, 2mm, 1.5mm and 1.2mm, while closing the valve to avoid the piston, where necessary, as shown in Figure 6.2(b).

3. **Ventilation to exhaust manifold - "VCC-Exhaust"**: Ventilation of the non-firing cylinders to the exhaust manifold is achieved by keeping the exhaust valves open throughout the four strokes of the cycle, with the corresponding intake valves deactivated, as represented by Figure 6.2(c). In this configuration, the non-firing cylinders induct gases from the exhaust manifold as the pistons move towards the BDC and expel them back to the exhaust manifold during the piston motion towards the TDC, thereby remaining in near-equilibrium with the exhaust manifold. This configuration is hereby referred to as "VCC-Exhaust". While VCC-Exhaust is implemented on this experimental setup by closing the exhaust valves near the TDC to avoid contact between the valves and the piston, it may also be implemented by leaving the exhaust valves open at a certain height, when piston valve pockets are present. Similar to VCC-Intake, VCC-Exhaust has also been implemented with lower valve lifts of 4mm, 2mm, 1.2mm and 0.7mm, while closing the valve to avoid the piston where necessary, as shown in Figure 6.2(c).

4. **Alternating ventilation to both intake and exhaust manifolds- "VCC-Alternating"**: Ventilation of the non-firing cylinders alternately to the intake and exhaust manifolds can be achieved by opening the intake and exhaust

valves alternately, each for two strokes of the engine cycle. Figure 6.2(d) represents the valve profiles used for this strategy. This configuration involves induction, and expulsion of gases, from/to the intake manifold during the two strokes when the intake valve is open, and induction and expulsion of gases from/to the exhaust manifold when the exhaust valve is open during the remaining two strokes. This configuration is hereby referred to as "VCC-Alternating". VCC-Alternating can be implemented through a combination of (very) late intake valve closure (LIVC) and (very) early exhaust valve opening (EEVO). Both LIVC and EEVO can be implemented using production-viable hardware, with lost motion valvetrain hardware being one such example [62]. Implementation using lost-motion valvetrain hardware results in a 'boot'-shaped valve profile, with the valve kept open at a 'dwell' lift, typically lower than peak valve lift, during the extended duration for which it is open. Dwelling at a lower valve lift results in smaller forces acting on the valves, allowing a compact and durable solution to be realized at a relatively inexpensive cost [55]. VCC-Alternating has therefore been studied with valve lifts of 4mm, 2mm and 1.5mm, to understand the impact of lower valve lifts in the non-firing cylinders on the overall engine performance.

The non-firing cylinders, which are kept in near-equilibrium with the intake or exhaust manifolds in all modes of VCC, are expected to consume negligible pumping work as gas is inducted from, and expelled to, the same manifold. Ventilation of the cylinders to one or both the manifolds ensures that elevated in-cylinder pressures are maintained in the cylinders, also mitigating potential for oil accumulation in the non-firing cylinders. Experimental data at curb idle operation (800 rpm, 1.3 bar BMEP), presented in this chapter, confirm these hypotheses.

6.2 Methodology

Experiments were performed at curb idle operation (800 rpm, 1.3 bar BMEP) to demonstrate the fuel efficiency and thermal management characteristics of the VCC strategies described above, in comparison with CDA and six-cylinder operation. All strategies (except six-cylinder operation) involved three active cylinders and three non-firing cylinders.

Fuel injection parameters like number of injections, injection timings, quantity of pilot injection and rail pressure, and air handling parameters like EGR valve position, were held constant. Quantity of main fuel injection was modulated to achieve constant torque. EGR flow rate was modulated to constrain NOx emissions by modulating the pressure difference between the exhaust and intake manifolds via the VGT nozzle. The engine set points for CDA and VCC strategies, presented in this chapter, are summarized in Table 6.1.

NOx, PM and unburnt HC emissions were constrained to remain within the emissions of both the six-cylinder baseline cases. All data presented in the following section has been normalized with the data of 'TM Baseline' six-cylinder strategy at curb idle operation.

The efficiency of the gas exchange process of the non-firing cylinders is assessed by calculating the net indicated mean effective pressure (NIMEP) of the non-firing cylinders, which is mathematically represented by Equation (6.1). Non-firing cylinders typically consume work, and therefore show negative NIMEPs. Negative NIMEPs of greater magnitude indicate a more inefficient gas exchange process in the non-firing cylinders.

$$NIMEP_{NF} = \frac{\oint P_{NF} dV}{V_{d,NF}} \tag{6.1}$$

Table 6.1. Engine set points for CDA and VCC strategies described in this chapter.

Speed	800 rpm
BMEP	1.3 bar
Number of active cylinders	3 of 6
Injection profile	2 injections (pilot + main)
Rail pressure	600 bar
EGR valve	100% open
VGT position	Modulated to achieve adequate EGR fraction to constrain NOx

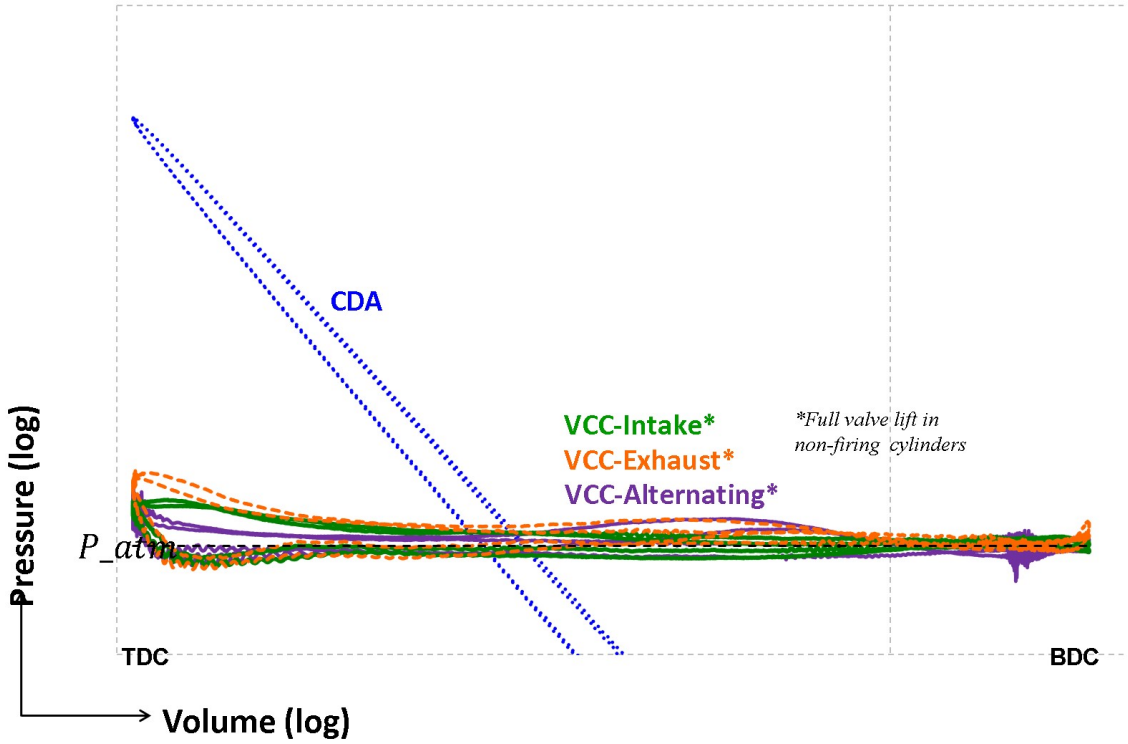

Figure 6.3. In-cylinder pressures in the non-firing cylinders remain above atmospheric pressure during VCC.

6.3 Results and Discussion

Figure 6.3 compares the in-cylinder pressures in the non-firing cylinders during CDA, VCC-Intake, VCC-Exhaust and VCC-Alternating during steady state curb idle operation. The VCC strategies shown in this plot employ full valve lift in the non-firing cylinders.

The non-firing cylinders, during CDA, undergo a near-isentropic compression-expansion process during the four strokes of the cycle, due to the gas-spring effect of the charge trapped inside the cylinder. The in-cylinder pressures are below atmospheric pressure for most of the cycle, as a result of loss of trapped gases via heat loss and blowby through the piston rings [47].

The in-cylinder pressures in the non-firing cylinders during all three modes of VCC, when the valves are open to full lift, are close to atmospheric pressure throughout the cycle. This is a result of the non-firing cylinders being ventilated to, and thereby being in near equilibrium with, the intake and/or exhaust manifolds, which are close to atmospheric pressure at this operating condition. Absence of a prominent pumping loop is a result of induction and expulsion of gases from/to the same manifold.

Figures 6.4(a), 6.4(b) and 6.4(c) compare the in-cylinder pressures in the non-firing cylinders during VCC-Intake, VCC-Exhaust and VCC-Alternating strategies, respectively, as the valve lift is reduced. The pumping loops are similar in size when the valves are open to full lift and 4mm lift, in all three cases. Valve lifts lower than 4mm result in bigger pumping loops, as the throttling effect across the valve between the cylinder and the manifold becomes more prominent. The throttling effect intensifies at, and is very sensitive to, lower valve lifts. For example, reduction of valve lift from 1.2mm to 0.7mm during the VCC-Exhaust strategy significantly increases the size of the pumping loop, as shown by Figure 6.3(b). It is also observed that the shape of the pumping loops is fairly consistent for a given valve lift across the three modes of VCC.

Figure 6.5 shows the average NIMEP in the non-firing cylinders for CDA and all three modes of VCC, against valve lift in the non-firing cylinders. As described earlier, NIMEP of the non-firing cylinders is indicative of the parasitic work consumed in the form of pumping loss, heat loss, and bleed-down of in-cylinder pressure via blowby in the non-firing cylinders. CDA shows an NIMEP of ~ -15kPa in the non-firing cylinders, as a result of losses involved in compression and expansion of the trapped gases. VCC-Intake, VCC-Exhaust and VCC-Alternating strategies show a nearly identical variation in non-firing NIMEP with varying valve lifts, consistent with the observation from the pressure-volume plots from Figure 6.3 and Figure 6.4. VCC strategies with valve lifts of 4mm and above in the non-firing cylinders show similar NIMEP as CDA, indicating that the gas exchange work done by the non-

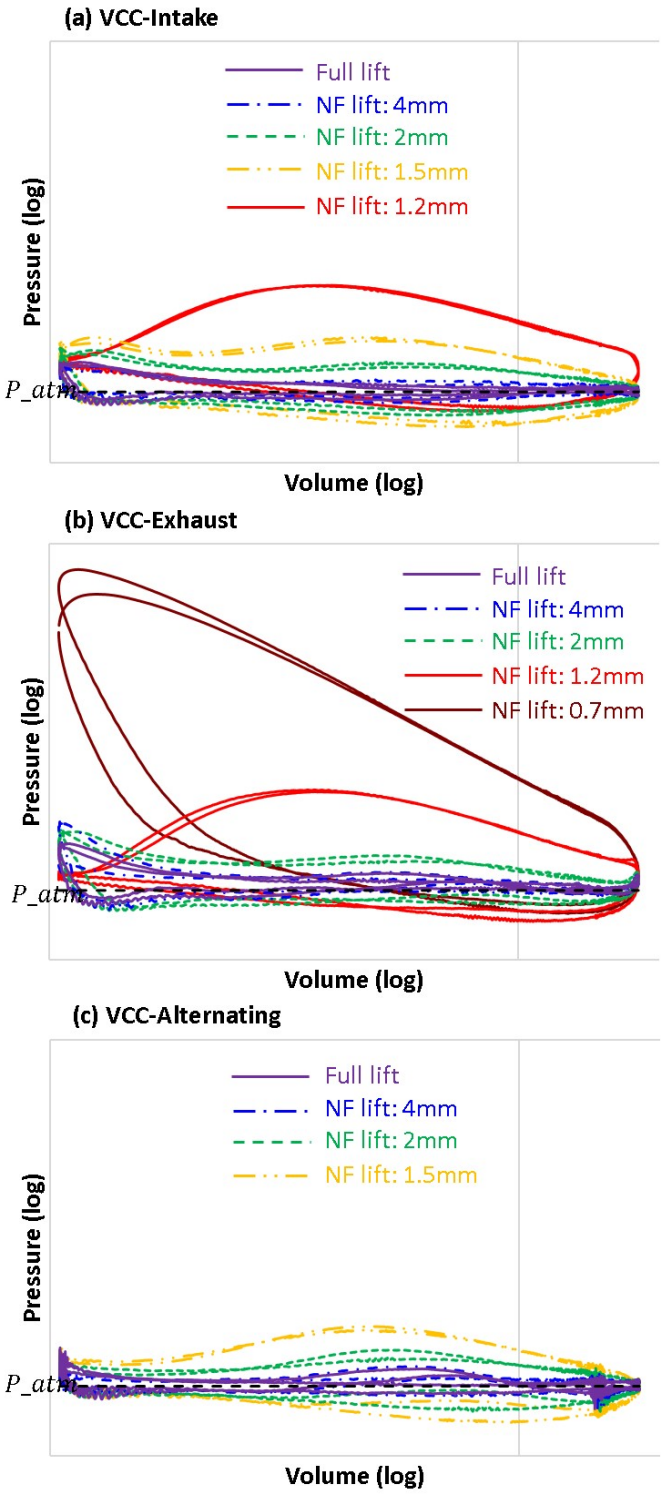

Figure 6.4. Larger pumping loops are observed in the non-firing cylinders when VCC with lower non-firing valve lifts is implemented.

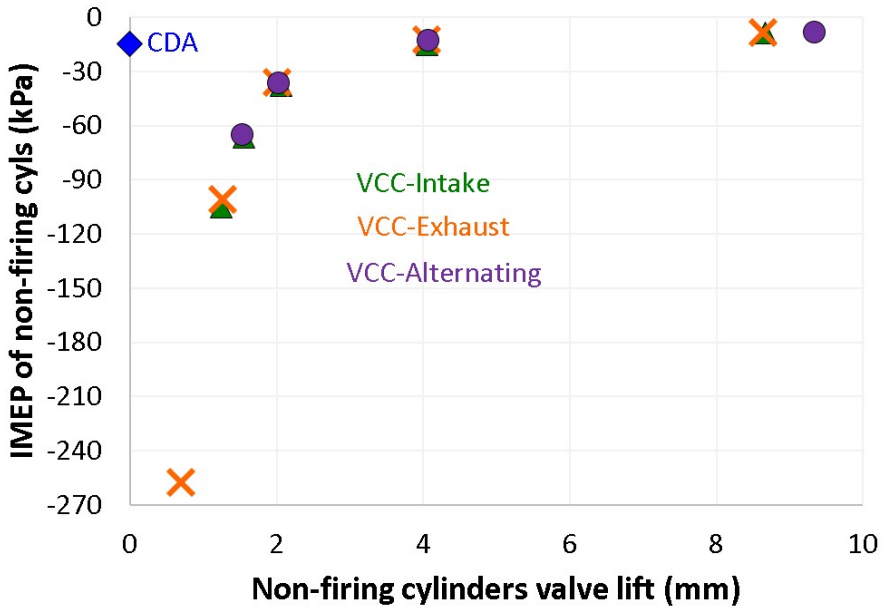

Figure 6.5. NIMEP of the non-firing cylinders becomes more negative during VCC with lower non-firing valve lifts.

firing cylinders is identical to CDA, and nearly negligible. Reduction in valve lift in the non-firing cylinders results in a more negative NIMEP, as a result of greater throttling losses across the valves, consistent with the bigger pumping loops observed in Figure 6.3. Valve lift of 0.7mm, implemented here only for the VCC-Exhaust case, results in an NIMEP of ~ -260kPa in the non-firing cylinders, almost 17 times higher than CDA.

Figure 6.6 shows the trade-off between fuel consumption and TOT for CDA, all three modes of VCC and the two baseline six-cylinder strategies. The 'TM Baseline' strategy shows a TOT of ~ 255°C, over 100°C higher than the 'FE Baseline' strategy, but at a significant fuel penalty of $\sim 60\%$ with respect to FE Baseline. CDA, with three cylinders firing, shows a TOT of ~ 205°C, with fuel savings of $\sim 42\%$ with respect to the 'TM Baseline' strategy, as also shown earlier in Chapters 3 and 4. VCC-Intake, VCC-Exhaust and VCC-Alternating strategies with valve lifts greater than 4mm in the non-firing cylinders show the same fuel consumption and TOT

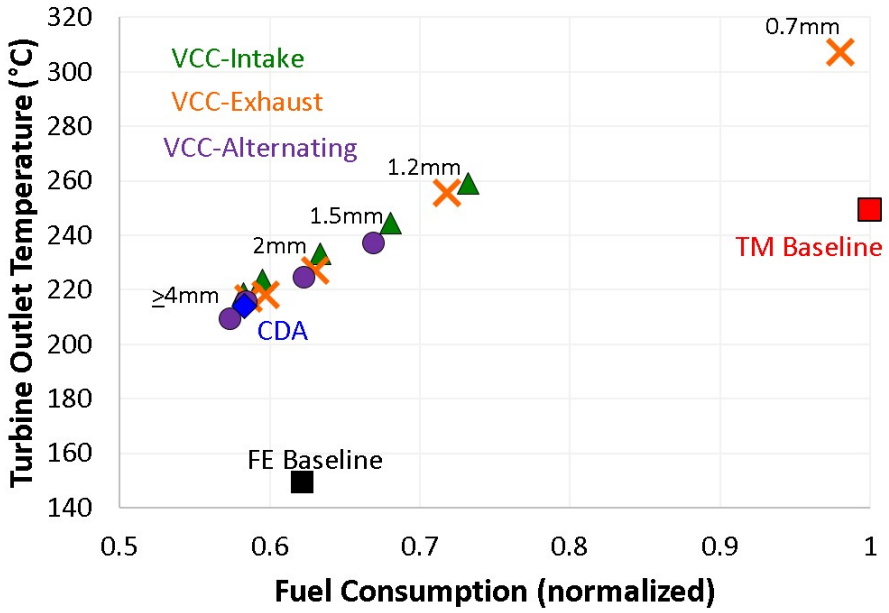

Figure 6.6. TOT vs normalized fuel consumption at steady state curb idle operation.

as CDA. This is expected because the in-cylinder processes in the active cylinders is maintained to remain identical, as will be shown in Figure 6.7, and the work consumed by the non-firing cylinders is similar, as shown in Figure 6.5. Reducing the valve lift in the non-firing cylinders below 4mm results in higher fuel consumption and higher TOT, as a result of greater gas-exchange work in the non-firing cylinders. The resulting trade-off curve is nearly parallel to that of six-cylinder operation, with VCC strategies showing $\sim 75°C$ higher TOT at fuel-neutral conditions and $\sim 30-35\%$ fuel savings at similar TOT.

Figure 6.7 compares the open cycle efficiency (OCE), closed cycle efficiency (CCE) and mechanical efficiency (ME) in the active/firing cylinders for all the strategies, against brake thermal efficiency (BTE). Figure 6.7(a) shows that OCE is the lowest for TM Baseline six-cylinder operation, as a result of high pumping work in the active cylinders, due to increased back-pressure upon maximally closing the VGT nozzle. FE Baseline has $\sim 48\%$ higher OCE due to a more efficient gas exchange

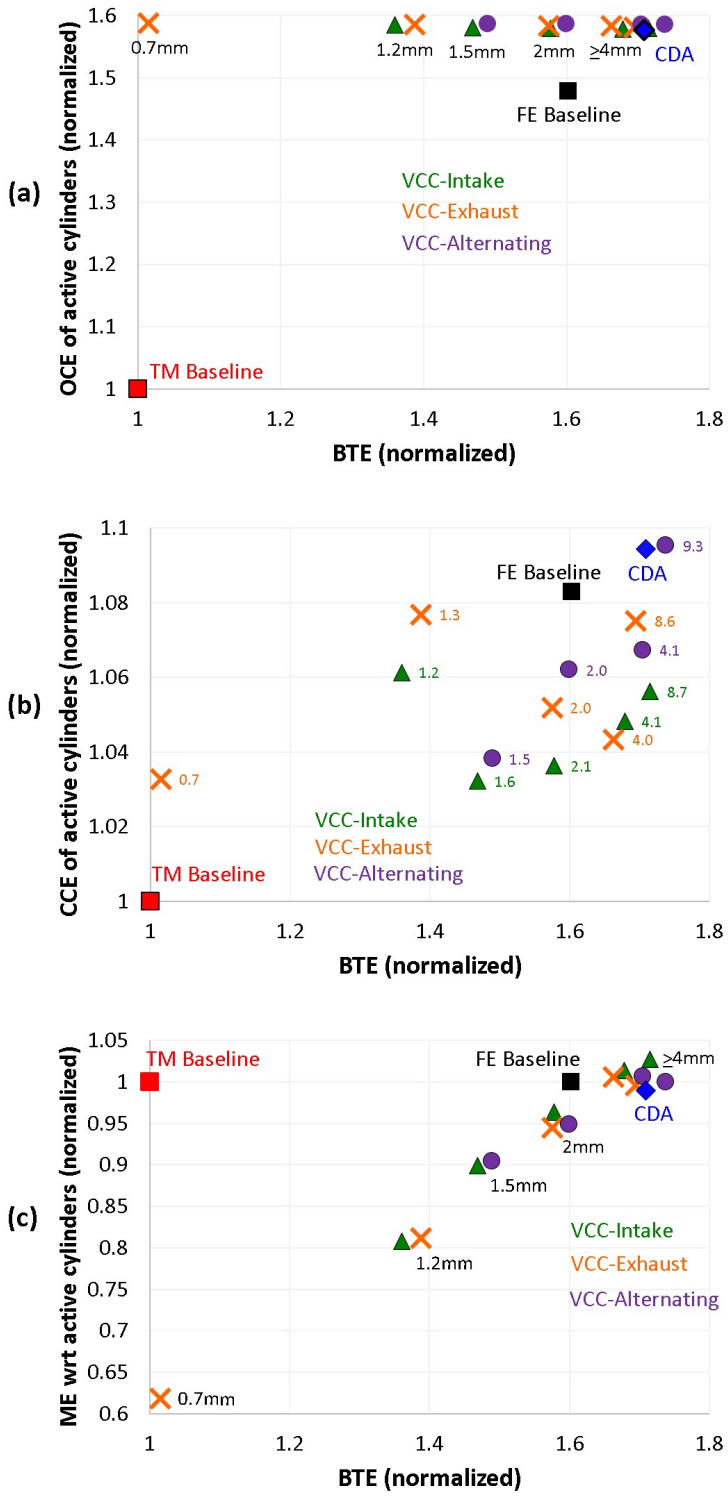

Figure 6.7. OCE, CCE, ME and BTE of VCC at steady state curb idle operation.

process. CDA and all VCC strategies show identical OCE, $\sim$ 60% higher than TM Baseline operation, as a result of airflow occurring in fewer cylinders, resulting in lower pumping work in the active cylinders. The valve profiles in the non-firing cylinders have no effect on OCE, as the gas exchange process of the active cylinders is unaffected by the gas exchange in the non-firing cylinders. Figure 6.7(a) also demonstrates that differences in BTE upon reducing the valve lift during VCC is not driven by changes in OCE of the active cylinders, as expected.

Figure 6.7(b) compares the CCE of the described strategies, with the labels indicating the valve lift of the non-firing cylinders during VCC. CCE of TM Baseline is 8% lower than the FE Baseline six-cylinder strategy, as a result of late fuel injections incorporated as a part of the TM Baseline strategy. There is no clear trend in the CCE of CDA and VCC with different valve lifts. The differences in CCE can be attributed to variations in EGR fraction and quantity of fuel combusted in the active cylinders. The relative variation between the strategies is 6%, which is minor compared to the differences in BTE between the strategies. It can therefore be inferred that CCE is nearly similar between CDA and all modes and valve lifts with VCC, and does not drive differences in BTE.

Figure 6.7(c) shows the ME of all the strategies, which not only captures the friction and accessory loads but also the work done and losses incurred in the non-firing cylinders for CDA and VCC. ME of both the six-cylinder baseline strategies, CDA and VCC with higher non-firing valve lifts are similar. A reduction in ME is observed for VCC strategies with lower valve lifts, consistent with higher work consumed in the non-firing cylinders, as shown by Figure 6.5. Figure 6.7(c) demonstrates that lower BTE observed for VCC strategies with lower valve lifts is strongly driven by reduction in ME as a result of greater work done by the non-firing cylinders.

Figure 6.8 compares the TOT and exhaust flow rate of all the strategies. The TM Baseline six-cylinder strategy, which implements late fuel injections as a means to mitigate engine-out NOx with low external EGR, shows the highest exhaust flow rate. The FE Baseline strategy shows $\sim$ 35% lower exhaust flow rate as a result of

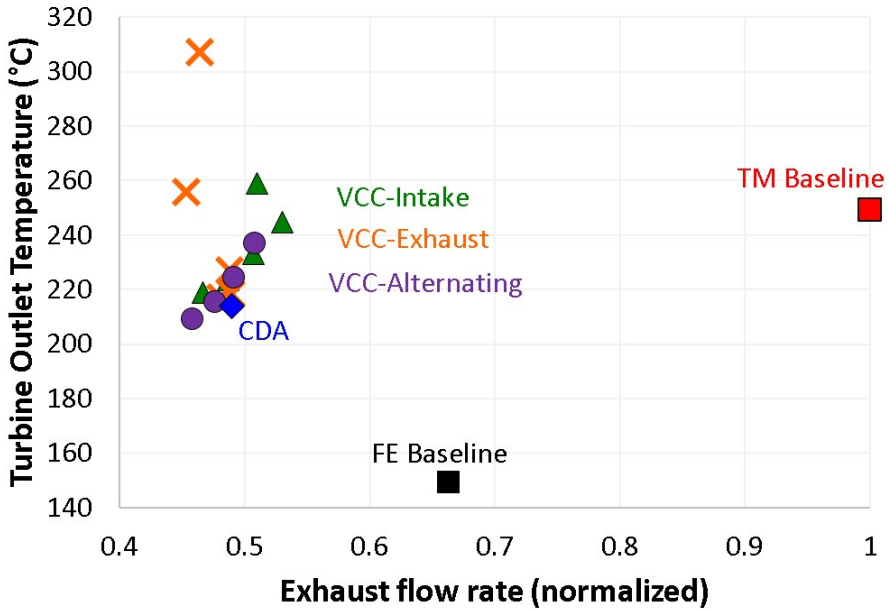

Figure 6.8. TOT vs exhaust flow rate of VCC at steady state curb idle operation.

high external EGR used to mitigate NOx. CDA and VCC strategies show similar exhaust flow rates, between 45% and 55% of the TM Baseline operation, as there is no net airflow occurring through the three non-firing cylinders in all these cases. Minor differences in exhaust flow rates between these strategies are a result of minor variations in EGR fraction, to constrain NOx emissions. All three modes of VCC with valve lifts greater than 4mm show similar TOT and exhaust flow rate as CDA, indicating similar thermal management performance to maintain elevated aftertreatment component temperatures. VCC strategies with lower valve lifts show higher TOT at similar exhaust flow rates as CDA, thereby showing better aftertreatment 'stay-warm' characteristics than CDA, but at higher fuel consumption, as shown earlier in Figure 6.6.

Figure 6.9 demonstrates that the NOx, PM and UHC emissions for all the VCC strategies are lower than the emissions of the corresponding six-cylinder baseline strategies at curb idle operation. More specifically, Figure 6.9(a) shows that the NOx emissions of CDA and all VCC strategies have been maintained similar to, or lower

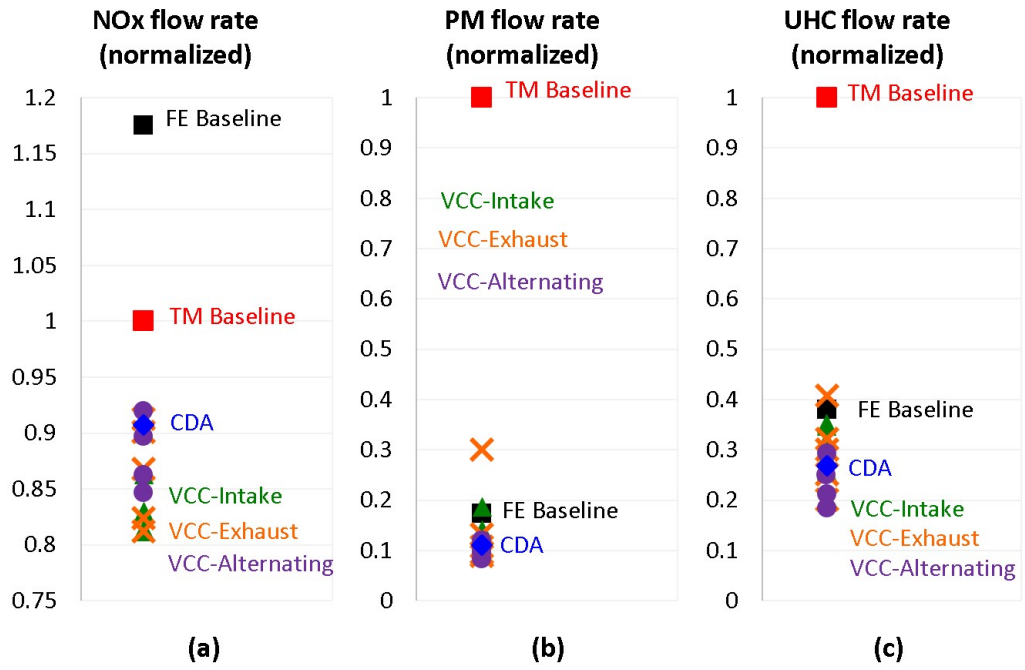

Figure 6.9. NOx, PM and UHC emissions of VCC at steady state curb idle.

than, the baseline six-cylinder strategies through modulation of VGT position with a fully open EGR valve. Figure 6.9(b) shows that PM emissions of all strategies are at least 60% lower than the TM baseline six-cylinder strategy. CDA and most of the VCC strategies show similar, or lower, PM than the FE Baseline six-cylinder strategy. Figure 6.9(c) shows that the FE Baseline strategy shows 60% lower UHC emissions than TM Baseline, with CDA and VCC strategies showing similar, or lower, UHC emissions than FE Baseline strategy.

It may therefore be concluded, from Figures 6.6-6.9, that choice of an appropriate VCC strategy can enable fuel-efficient maintenance of elevated aftertreatment component temperatures, with the choice of the strategy depending on the desired TOT, acceptable fuel penalty with respect to CDA, and ease of hardware implementation.

6.4 Summary

The following conclusions may be drawn based on the results presented in this chapter:

- Ventilated cylinder cutout (VCC) is a strategy by which similar engine performance as CDA may be obtained, while maintaining the non-firing cylinders close to the manifold pressures to avoid oil accumulation in the cylinders.

- VCC shows similar fuel efficiency, thermal management and emissions characteristics as CDA when the valves of the inactive cylinders are open by at least 4mm. Lower valve lifts result in relatively higher fuel consumption and higher TOT than CDA, while continuing to achieve $\sim 60°C$ higher TOT at fuel neutral conditions, or $\sim 30\%$ fuel savings at similar TOT, compared to six-cylinder operation.

- The choice of VCC strategy to be implemented on an engine depends on the desired TOT, acceptable fuel penalty with respect to CDA at curb idle, and ease of hardware implementation.

- VCC can be implemented via production-viable valvetrain technology. Specifically, VCC-Intake and VCC-Exhaust may be implemented by leaving the intake and exhaust valves, respectively, open throughout the cycle if a valve pocket is present in the piston. VCC-Alternating may be implemented using a combination of EEVO and LIVC hardware.

7. SUMMARY

This dissertation presents the potential of implementation of advanced gas exchange management in diesel engines, via variable valve actuation, for reduction of greenhouse gases and regulated pollutants. Although diesel engine aftertreatment systems are highly effective in reducing engine-out emissions before releasing them into the atmosphere, their peak efficiency lies at component temperatures in excess of 200°C, which is difficult to achieve during cold start and maintain at low-load engine operation in a fuel-efficient manner.

The aftertreatment warm-up potential of the combination of EEVO and iEGR at idle operation, and EEVO and LIVC at off-idle operation, was demonstrated in Chapter 3. Specifically, the combination of EEVO and iEGR resulted in turbine-outlet temperatures in excess of 400°C at steady state idle operation, with a 42% fuel penalty with respect to the baseline thermal management operation. Implementation of this strategy at idle over the HD-FTP drive cycle resulted in 7.9% lower predicted tailpipe-out NOx with 2.1% fuel penalty. Implementation of EEVO and LIVC at off-idle operation below 7.6 bar BMEP resulted in 10.1% lower predicted tailpipe-out NOx with a fuel penalty of 3.1% over the HD-FTP.

Chapter 4 demonstrated the use of half-engine cylinder deactivation to achieve fuel savings while maintaining higher aftertreatment component temperatures during both the HD-FTP drive cycle. Fuel savings of 3.5% were demonstrated over the HD-FTP drive cycle, at similar tailpipe-out NOx levels. It was also demonstrated that the transient response of the engine remained unaffected when CDA was implemented at and near idle operation - a key finding for enabling practical implementation of CDA.

Dynamic cylinder activation (DCA), a variant of CDA where a different set of cylinders are deactivated each cycle, was introduced in Chapter 5. It was demon-

strated that DCA enabled greater control over the forcing frequencies on the driveline while achieving the same fuel efficiency, thermal management and emissions as fixed CDA. It was demonstrated that the charge trapping strategy during deactivation played an important role during DCA, unlike fixed CDA, with low-pressure trapping being the favorable strategy. Further, periodic activation of all cylinders in DCA ensured that a given cylinder was not deactivated for extended periods of time.

Chapter 6 introduced ventilated cylinder cutout (VCC) as a variant of CDA where the non-firing cylinders are ventilated to one or both of the intake and exhaust manifolds, to mitigate oil accumulation concerns with CDA. VCC maintained the pressures of non-firing cylinders close to intake/exhaust manifold pressures by keeping the intake/exhaust valves open throughout the cycle, eliminating vacuum in the cylinders. It was demonstrated that opening the valves of the non-firing cylinders to a lift of 4mm or higher resulted in the same performance, emissions and vibration characteristics as CDA, while lower valve lifts in the non-firing cylinders resulted in higher fuel consumption and higher TOT.

From chapters 4-6, it may be concluded that implementation of fixed CDA, in tandem with DCA, and/or VCC, can ensure fuel-efficient "stay warm" aftertreatment thermal management of the diesel engine, while better managing potential challenges associated with CDA such as transient response, torsional vibration and oil accumulation.

8. RECOMMENDATIONS

Future work may focus on implementation of other alternate valvetrain strategies to improve cold start aftertreatment warm-up of the diesel engine aftertreatment system. Potential valvetrain strategies, to this end, include (i) exhaust valve throttling via late exhaust valve opening to increase TOT, while allowing adequate time for soot oxidation inside the cylinders, and (ii) two-stroke operation in a select set of cylinders to increase exhaust flow rates. Two-stroke operation may also be leveraged to improve transient response of the engine by enabling faster "spool-up" of the turbocharger.

The transient response of CDA at off-idle low-load operation, where boost pressures are typically high, can be improved by optimizing the air handling controller. Effective air handling control of CDA will also help during implementation of CDA in turbocharged spark-ignited engines, which employ CDA at low loads at all engine speeds. Implementation of look-ahead controls in next-generation heavy-duty vehicles can also be leveraged to further expand the use of CDA.

DCA has been demonstrated as a means to enable greater control over the forcing frequencies on the driveline, while achieving similar performance as fixed CDA. Future work could explore the potential of DCA to operate at firing densities not achievable by fixed CDA, thereby enabling improvements in fuel efficiency and thermal management beyond what is achievable by fixed CDA, by operating the firing cylinders at their peak combustion and gas exchange efficiencies at all speeds and loads. DCA, when implemented with fully continuous options of firing densities, can enable significant fuel savings on a spark-ignited engine, via reduced use of the intake air throttle to maintain stoichiometric air-to-fuel ratios.

Lastly, the potential of production-viable variants of the valvetrain strategies described in this dissertation, and the trade-offs involved to achieve fuel-efficient aftertreatment thermal management, can be studied in detail.

REFERENCES

REFERENCES

[1] *WHO - Priority environment and health risks*, 2018 (accessed August 19, 2018).

[2] United States Environmental Protection Agency. Air pollutant emissions trends data, 2015.

[3] J. Hansen, R. Ruedy, M. Sato, and K. Lo. Global surface temperature change. *Reviews of Geophysics*, 48(4):n/a–n/a, 2010. RG4004.

[4] United States Environmental Protection Agency. Inventory of u.s. greenhouse gas emissions and sinks: 1990-2015, 2017.

[5] United States Environmental Protection Agency. Final rule for phase 1 greenhouse gas emissions standards and fuel efficiency standards for medium- and heavy-duty engines and vehicles, 2011.

[6] United States Environmental Protection Agency. Final rule for greenhouse gas emissions and fuel efficiency standards for medium- and heavy-duty engines and vehicles - phase 2, 2016.

[7] D.W. Stanton. L. Ray Buckendale Lecture 2013-01-2421 2013. 2015.

[8] European Automobile Manufacturers Association. Reducing CO2 emissions from heavy-duty vehicles, 2016.

[9] D.W. Stanton. Systematic development of highly efficient and clean engines to meet future commercial vehicle greenhouse gas regulations. *Diesel Engine*, 2013:05–16, 2013.

[10] S. Stadlbauer, H. Waschl, A. Schilling, and L. del Re. DOC temperature control for low temperature operating ranges with post and main injection actuation. Technical report, SAE Technical Paper, 2013.

[11] X. Song, H. Surenahalli, J. Naber, G. Parker, et al. Experimental and modeling study of a diesel oxidation catalyst (DOC) under transient and CPF active regeneration conditions. *SAE International*, 2007:10–01.

[12] X. Hou, Y. Ma, F. Peng, F. Yan, and X. Zhang. Research on temperature characteristics of dpf regeneration technology based on catalytic combustion of fuel injection. In *Power and Energy Engineering Conference (APPEEC), 2010 Asia-Pacific*, pages 1–4. IEEE, 2010.

[13] A.P. Walker. Controlling particulate emissions from diesel vehicles. *Topics in catalysis*, 28(1-4):165–170, 2004.

[14] R. Allanson, P. Blakeman, B. Cooper, H. Hess, P. Silcock, and A. Walker. Optimising the low temperature performance and regeneration efficiency of the continuously regenerating diesel particulate filter (CR-DPF) system. 2002.

[15] M. Koebel, M. Elsener, and M. Kleemann. Urea-SCR: a promising technique to reduce NOx emissions from automotive diesel engines. *Catalysis Today*, 59(3):335–345, 2000.

[16] S. Charlton, T. Dollmeyer, and T. Grana. Meeting the US heavy-duty EPA 2010 standards and providing increased value for the customer. *SAE International Journal of Commercial Vehicles*, 3(1):101–110, 2010.

[17] J. Girard, G. Cavataio, R. Snow, and C. Lambert. Combined fe-cu SCR systems with optimized ammonia to NOx ratio for diesel NOx control. *SAE International Journal of Fuels and Lubricants*, 1(1):603–610, 2009.

[18] C. Lambert, R. Hammerle, R. McGill, M. Khair, and C. Sharp. Technical advantages of urea SCR for light-duty and heavy-duty diesel vehicle applications. *SAE transactions*, 113(4):580–589, 2004.

[19] M. Ruth and G. Salemme. Engine system technologies for reducing GHG and NOx. ERC UW-Madison Symposium, 06 2015.

[20] M. Naseri, R. Conway, H. Hess, and C. Aydin. Development of emission control systems to enable high NOx conversion on heavy duty diesel engines. 2014.

[21] D. Stanton, S. Charlton, and P. Vajapeyazula. Diesel engine technologies enabling powertrain optimization to meet US greenhouse gas emissions. *SAE International Journal of Engines*, 6(3):1757–1770, 2013.

[22] S. Gehrke, D. Kovács, P. Eilts, A. Rempel, and P. Eckert. Investigation of VVA-based exhaust management strategies by means of a HD single cylinder research engine and rapid prototyping systems. *SAE International Journal of Commercial Vehicles*, 6(1):47–61, 2013.

[23] A. Mayer, T. Lutz, C. Lämmle, M. Wyser, and F. Legerer. Engine intake throttling for active regeneration of diesel particle filters. 2003.

[24] J.P. Zammit, M.J. McGhee, P.J. Shayler, and I. Pegg. The influence of cylinder deactivation on the emissions and fuel economy of a four-cylinder direct-injection diesel engine. *Proceedings of the Institution of Mechanical Engineers, Part D: Journal of Automobile Engineering*, 228(2):206–217, 2014.

[25] J.P. Zammit, M.J. McGhee, P.J. Shayler, T. Law, and I. Pegg. The effects of early inlet valve closing and cylinder disablement onfuel economy and emissions of a direct injection diesel engine. *Energy*, 2015.

[26] C. Ding, L. Roberts, D.J. Fain, A.K. Ramesh, G.M. Shaver, J. McCarthy, M. Ruth, E. Koeberlein, E.A. Holloway, and D. Nielsen. Fuel efficient exhaust thermal management for compression ignition engines during idle via cylinder deactivation and flexible valve actuation. *International Journal of Engine Research*, 2015.

[27] K.J. Douglas, N. Milovanovic, J. Turner, and D. Blundell. Fuel Economy Improvement Using Combined CAI and Cylinder Deactivation (CDA)-An Initial Study. *Sae Technical Paper Series 2005-01-0110*, 2005(724):1–3, 2005.

[28] A. Garg, M. Magee, C. Ding, L. Roberts, G. Shaver, E. Koeberlein, R. Shute, D. Koeberlein, J. McCarthy, and D. Nielsen. Fuel-efficient exhaust thermal management using cylinder throttling via intake valve closing timing modulation. *Proceedings of the Institution of Mechanical Engineers, Part D: Journal of Automobile Engineering*, 230(4):470–478, 2016.

[29] T.G. Leone and M. Pozar. Fuel Economy Benefit of Cylinder Deactivation - Sensitivity to Vehicle Application and Operating Constraints. *SAE Technical Paper Series*, 1645(724):10–11, 2001.

[30] M. Bouchez and J.B. Dementhon. Strategies for the control of particulate trap regeneration. Technical report, SAE technical paper, 2000.

[31] J. Parks, S. Huff, M. Kass, and J. Storey. Characterization of in-cylinder techniques for thermal management of diesel aftertreatment. *SAE International*, 10:11, 2007.

[32] P. Singh, A.M. Thalagavara, J.D. Naber, J.H. Johnson, and S.T. Bagley. *An experimental study of active regeneration of an advanced catalyzed particulate filter by diesel fuel injection upstream of an oxidation catalyst*. PhD thesis, Michigan Technological University, 2006.

[33] A. Joshi, S. Chatterjee, A. Sawant, C. Akerlund, S. Andersson, M. Blomquist, J. Brooks, and S. Kattan. Development of an actively regenerating dpf system for retrofit applications. In *SAE Technical Paper*. SAE International, 10 2006.

[34] L. Roberts, M. Magee, G. Shaver, A. Garg, J. McCarthy, E. Koeberlein, E. Holloway, R. Shute, D. Koeberlein, and D. Nielsen. Modeling the impact of early exhaust valve opening on exhaust aftertreatment thermal management and efficiency for compression ignition engines. *International Journal of Engine Research*, 16(6):773–794, 2015.

[35] A.N. Bharath, Y. Yang, R.D. Reitz, and C. Rutland. Comparison of Variable Valve Actuation , Cylinder Deactivation and Injection Strategies for Low-Load RCCI Operation of a Light Duty Engine. *SAE Technical Paper*, 2015.

[36] K. Blumenroder, G. Buschmann, J. Kahrstedt, A. Sommer, and O. Maiwald. Variable valve trains for passenger car diesel engines-potentials, limits and ways of realisation. *Fortschritt Berichte-VDI Reihe 12 Verkehrstechnik Fahrzeugtechnik*, 622(2):280, 2006.

[37] A. Radulescu, J. McCarthy, and S. Brownell. Development of a Switching Roller Finger Follower for Cylinder Deactivation in Gasoline Engine Applications. *SAE Technical Paper 2013-01-0589*, 91:347–360, 2013.

[38] J.B. Heywood and O.Z. Welling. Trends in performance characteristics of modern automobile SI and diesel engines. *SAE Technical Paper*, 2(1):1650, 2009.

[39] J. McCarthy. Cylinder Deactivation for Optimizing Conventional Engines. *Driving Automotive Innovation Conference*, 2016.

[40] A. Ramesh, G. Shaver, C. Allen, D. Gosala, S. Nayyar, D. Caicedo, E. Koberlein, L. Kocher, M. Ruth, J. McCarthy, D. Nielsen, and E. Holloway. Utilizing low airflow strategies, including cylinder deactivation, to improve fuel efficiency and aftertreatment thermal management. *International Journal of Engine Research*, 18:1005–1016, 2017.

[41] X. Lu, C. Ding, A. Ramesh, G. Shaver, E. Holloway, J. McCarthy, M. Ruth, E. Koeberlein, and D. Nielsen. Impact of cylinder deactivation on active diesel particulate filter regeneration at highway cruise conditions. *Frontiers in Mechanical Engineering*, 1(9), 2015.

[42] R. Kitabatake, A. Minato, N. Inukai, and N. Shimazaki. Simultaneous Improvement of Fuel Consumption and Exhaust Emissions on a Multi-Cylinder Camless Engine. *SAE Technical Paper*, 4(1):1225–1234, 2012.

[43] J. Yang, L. Quan, and Y. Yang. Excavator energy-saving efficiency based on diesel engine cylinder deactivation technology. *Chinese Journal of Mechanical Engineering*, 25(5):897–904, 2012.

[44] J. Serrano, G. Routledge, N. Lo, M. Shost, V. Srinivasan, and B. Ghosh. Methods of evaluating and mitigating nvh when operating an engine in dynamic skip fire. *SAE Int. J. Engines*, 7:1489–1501, 04 2014.

[45] S. Brandl, B. Graf, and A. Rust. NVH Challenges and Solutions for Vehicles with Low CO2 Emission. *SAE Int. J. Passeng. Cars - Mech. Syst.*, 5(3):1084–1090, 2012.

[46] A. Archer and J. McCarthy. Quantification of diesel engine vibration using cylinder deactivation for exhaust temperature management and recipe for implementation in commercial vehicles. In *WCX World Congress Experience*. SAE International, apr 2018.

[47] C.M. Allen, D.B. Gosala, G.M. Shaver, and J. McCarthy. Comparative study of diesel engine cylinder deactivation transition strategies. *International Journal of Engine Research*, 0(0):1468087418768117, 0.

[48] Z. Ma. Oil transport analysis of a cylinder deactivation engine. In *SAE 2010 World Congress & Exhibition*. SAE International, apr 2010.

[49] M. Halbe, B. Pietrzak, D. Fain, A. Ramesh, G. Shaver, J.E. McCarthy, M. Ruth, and E. Koeberlein. Oil accumulation and first fire readiness analysis of cylinder deactivation. *Frontiers in Mechanical Engineering*, 3:1, 2017.

[50] W. Gottschalk, R. Fink, and M. Schultalbers. Investigations on ventilation strategies for si cylinder deactivation based on a variable valve train. In *SAE 2016 International Powertrains, Fuels and Lubricants Meeting*. SAE International, 10 2016.

[51] E.D. Marquez, J. Stevenson, E. Dietrich, D. Nelson, C. Flake, A. Neblett, and S. Reinsel. Simulation and bench testing of a gm 5.3l v8 engine. In *SAE Technical Paper*. SAE International, 03 2017.

[52] M. Joshi, D. Gosala, C. Allen, S. Srinivasan, A. Ramesh, M. VanVoorhis, A. Taylor, K. Vos, G. Shaver, J. McCarthy, L. Farrell, and E. Koeberlein. Diesel engine cylinder deactivation for improved system performance over transient real-world drive cycles. In *WCX World Congress Experience*. SAE International, apr 2018.

[53] Environmental Protection Agency. 40 CFR 86.1342-90 - calculations; exhaust emissions, July 2002. 54 FR 14605, Apr. 11, 1989, as amended at 62 FR 47135, Sept. 5, 1997.

[54] K.R. Vos, G.M. Shaver, X. Lu, C.M. Allen, J. McCarthy, and L. Farrell. Improving diesel engine efficiency at high speeds and loads through improved breathing via delayed intake valve closure timing. *International Journal of Engine Research*, 0(0):1468087417743157, 0.

[55] K.R. Vos, G.M. Shaver, J. McCarthy, and L. Farrell. Utilizing production viable valve strategies at elevated speeds and loads to improve volumetric efficiency via intake valve modulation. *Frontiers in Mechanical Engineering*, 4:2, 2018.

[56] M. Wilcutts, J. Switkes, M. Shost, and A. Tripathi. Design and benefits of dynamic skip fire strategies for cylinder deactivated engines. *SAE Int. J. Engines*, 6:278–288, 04 2013.

[57] K. Eisazadeh-Far and M. Younkins. Fuel economy gains through dynamic-skip-fire in spark ignition engines. In *SAE Technical Paper*. SAE International, 04 2016.

[58] Schaeffler Technologies GmbH & Co. KG, editor. *Cylinder Deactivation*, pages 172–186. Springer Fachmedien Wiesbaden, Wiesbaden, 2014.

[59] Schaeffler Technologies GmbH & Co. KG, editor. *Powertrain Systems of the Future*, pages 24–40. Springer Fachmedien Wiesbaden, Wiesbaden, 2014.

[60] J. McCarthy. Cylinder deactivation improves diesel aftertreatment and fuel economy for commercial vehicles. In *17. Internationales Stuttgarter Symposium*, pages 1013–1039, Wiesbaden, 2017. Springer Fachmedien Wiesbaden.

[61] M. Rebbert, G. Kreusen, and S. Lauer. A New Cylinder Deactivation by FEV and Mahle. *SAE Technical Paper*, 2008-01-1354, 2008.

[62] J.A. Schwoerer, K. Kumar, B. Ruggiero, and B. Swanbon. Lost-motion vva systems for enabling next generation diesel engine efficiency and after-treatment optimization. In *SAE Technical Paper*. SAE International, 04 2010.

VITA

VITA

EDUCATION

Ph.D., Mechanical Engineering *December 2018*

Purdue University, West Lafayette, IN

- Dissertation- *Fuel-efficient emissions reduction from diesel engines via advanced gas exchange management*

B.Tech.(Honors), Mechanical Engineering *July 2014*

Indian Institute of Technology Madras, Chennai, India

- Undergraduate thesis- *Development of standalone controller to switch between DI Diesel, dual fuel and HCCI modes of a generator set engine*

ACADEMIC EMPLOYMENT

Graduate Research Assistant

- Variable valve actuation in ultra-high efficiency compression-ignition engines
  August 2014 - May 2018
- Control architecture analysis for high BMEP spark-ignited engines
  May 2018 - October 2018

Graduate Teaching Assistant

- ME540: Advanced IC Engine Systems and Modeling
  August 2016 - December 2016
- ME365: Systems, Measurements and Control
  August 2017 - December 2017

- ME675: Multivariable Control Systems Design
  January 2018 - May 2018

INVITED TALKS AND PRESENTATIONS

- SAE Commercial Vehicles Conference - Powertrain Technical Panel
  September 12, 2018
- International Combustion Institute Winter School (Poster)
  December 22, 2015

AWARDS AND FELLOWSHIPS

- Ross Fellowship, Purdue University (2014-2015)
- Sivasailam Merit Prize, IIT Madras (2014)
- Bhagyalakshmi and Krishna Ayengar Award, IIT Madras (2014)

PUBLICATIONS

- Aswin K Ramesh, Troy E Odstrcil, **Dheeraj B Gosala**, Gregory M Shaver, Soumya Nayyar, Edward Koeberlein and James McCarthy, Jr., **Reverse Breathing in Diesel Engines for Aftertreatment Thermal Management**, International Journal of Engine Research, 2018
- **Dheeraj B Gosala**, Cody M Allen, Gregory M Shaver, Lisa Farrell, Edward Koeberlein, Brian Franke, Dale Stretch, James McCarthy, Jr., **Dynamic cylinder activation in diesel engines**, International Journal of Engine Research, 2018
- Cody M Allen, **Dheeraj B Gosala**, Gregory M Shaver and James McCarthy, Jr., **Comparative study of diesel engine cylinder deactivation transition strategies**, International Journal of Engine Research, 2018

- Mrunal Joshi, **Dheeraj B Gosala**, Cody M Allen, Sirish Srinivasan, Aswin K Ramesh, Matthew VanVoorhis, Alexander Taylor, Kalen Vos, Gregory Shaver, James McCarthy, Jr., Lisa Farrell and Edward Koeberlein, **Diesel Engine Cylinder Deactivation for Improved System Performance over Transient Real-World Drive Cycles**, SAE Technical Paper 2018-01-0880, 2018

- Aswin K Ramesh, **Dheeraj B Gosala**, Cody M Allen, Mrunal Joshi, Lisa Farrell, Edward Koeberlein, James McCarthy, Jr. and Gregory M Shaver, **Cylinder Deactivation for Increased Engine Efficiency and Aftertreatment Thermal Management in Diesel Engines**, SAE Technical Paper 2018-01-0384, 2018

- **Dheeraj B Gosala**, Aswin K Ramesh, Cody M Allen, Mrunal C Joshi, Alexander H Taylor, Matthew Van Voorhis, Gregory M Shaver, Lisa Farrell, Edward Koeberlein, James McCarthy, Jr. and Dale Stretch, **Diesel engine aftertreatment warm-up through early exhaust valve opening and internal exhaust gas recirculation during idle operation**, International Journal of Engine Research, 2017

- Mrunal Joshi, **Dheeraj B Gosala**, Cody M Allen, Kalen Vos, Matthew Van Voorhis, Alexander Taylor, Gregory M Shaver, James McCarthy, Jr., Dale Stretch, Edward Koeberlein and Lisa Farrell, **Reducing Diesel Engine Drive Cycle Fuel Consumption through Use of Cylinder Deactivation to Maintain Aftertreatment Component Temperature during Idle and Low Load Operating Conditions**, Frontiers in Mechanical Engineering, 2017

- Aswin K Ramesh, Gregory M Shaver, Cody M Allen, Soumya Nayyar, **Dheeraj B Gosala**, Dina Caicedo Parra, Edward Koeberlein, James McCarthy, Jr and Doug Nielsen **Utilizing Low Airflow Strategies, Including Cylinder De-**

activation, to Improve Fuel Efficiency and Aftertreatment Thermal Management, International Journal of Engine Research, 2017

- **Dheeraj B Gosala**, Cody M Allen, Aswin K Ramesh, Gregory M Shaver, James McCarthy, Jr., Dale Stretch, Edward Koeberlein, Lisa Farrell **Cylinder deactivation during dynamic diesel engine operation**, International Journal of Engine Research, 2017

- Venugopal Thangavel, Sai Yashwanth Momula, **Dheeraj B Gosala**, Ramesh Asvathanarayanan, **Experimental studies on simultaneous injection of ethanolgasoline and n-butanolgasoline in the intake port of a four stroke SI engine**, Renewable Energy, 2016